NUREG/CR-6801
ORNL/TM-2001/273

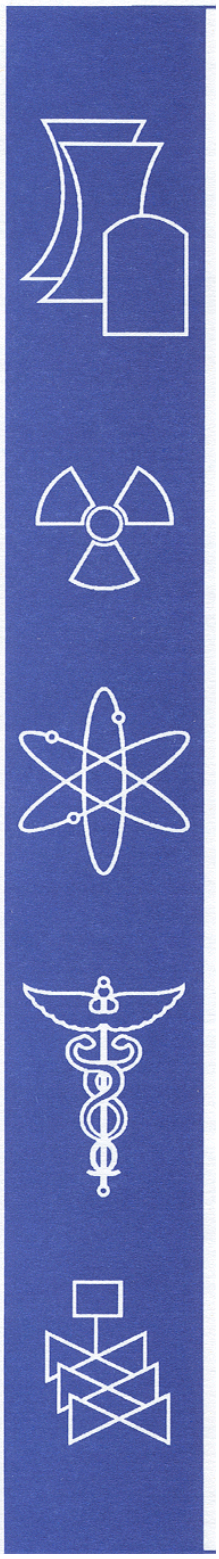

Recommendations for Addressing Axial Burnup in PWR Burnup Credit Analyses

Prepared by
J. C. Wagner, M. D. DeHart, and C. V. Parks, ORNL

Oak Ridge National Laboratory

U.S. Nuclear Regulatory Commission
Office of Nuclear Regulatory Research
Washington, DC 20555-0001

AVAILABILITY OF REFERENCE MATERIALS IN NRC PUBLICATIONS

NRC Reference Material

As of November 1999, you may electronically access NUREG-series publications and other NRC records at NRC's Public Electronic Reading Room at http://www.nrc.gov/reading-rm.html. Publicly released records include, to name a few, NUREG-series publications; *Federal Register* notices; applicant, licensee, and vendor documents and correspondence; NRC correspondence and internal memoranda; bulletins and information notices; inspection and investigative reports; licensee event reports; and Commission papers and their attachments.

NRC publications in the NUREG series, NRC regulations, and *Title 10, Energy*, in the Code of *Federal Regulations* may also be purchased from one of these two sources:

1. The Superintendent of Documents
   U.S. Government Printing Office
   P.O. Box SSOP
   Washington, DC 20402–0001
   Internet: bookstore.gpo.gov
   Telephone: 202–512–1800
   Fax: 202-512-2250
2. The National Technical Information Service
   Springfield, VA 22161–0002
   www.ntis.gov
   1–800–553–6847 or, locally, 703–605–6000

A single copy of each NRC draft report for comment is available free, to the extent of supply, upon written request as follows:

Address: Office of the Chief Information Officer,
Reproduction and Distribution
Services Section
U.S. Nuclear Regulatory Commission
Washington, DC 20555–0001
E-mail: DISTRIBUTION@nrc.gov
Facsimile: 301–415–2289

Some publications in the NUREG series that are posted at NRC's Web site address http://www.nrc.gov/reading-rm/doc-collections/nuregs are updated periodically and may differ from the last printed version. Although references to material found on a Web site bear the date the material was accessed, the material available on the date cited may subsequently be removed from the site.

Non-NRC Reference Material

Documents available from public and special technical libraries include all open literature items, such as books, journal articles, and transactions, *Federal Register* notices, Federal and State legislation, and congressional reports. Such documents as theses, dissertations, foreign reports and translations, and non-NRC conference proceedings may be purchased from their sponsoring organization.

Copies of industry codes and standards used in a substantive manner in the NRC regulatory process are maintained at—

The NRC Technical Library
Two White Flint North
11545 Rockville Pike
Rockville, MD 20852–2738

These standards are available in the library for reference use by the public. Codes and standards are usually copyrighted and may be purchased from the originating organization or, if they are American National Standards, from—

American National Standards Institute
11 West 42nd Street
New York, NY 10036–8002
www.ansi.org
212–642–4900

Legally binding regulatory requirements are stated only in laws; NRC regulations; licenses, including technical specifications; or orders, not in NUREG-series publications. The views expressed in contractor-prepared publications in this series are not necessarily those of the NRC.

The NUREG series comprises (1) technical and administrative reports and books prepared by the staff (NUREG/XXXX) or agency contractors (NUREG/CR-XXXX), (2) proceedings of conferences (NUREG/CP-XXXX), (3) reports resulting from international agreements (NUREG/IA-XXXX), (4) brochures (NUREG/BR-XXXX), and (5) compilations of legal decisions and orders of the Commission and Atomic and Safety Licensing Boards and of Directors' decisions under Section 2.206 of NRC's regulations (NUREG-0750).

NUREG/CR–6801
ORNL/TM–2001/273

Recommendations for Addressing Axial Burnup in PWR Burnup Credit Analyses

Manuscript Completed: October 2002
Date Published: March 2003

Prepared by
J. C. Wagner, M. D. DeHart, and C. V. Parks

Oak Ridge National Laboratory
Managed by UT-Battelle, LLC
Oak Ridge, TN 37831–6370

R. Y. Lee, NRC Project Manager

Prepared for
Division of System Analysis and Regulatory Effectiveness
Office of Nuclear Regulatory Research
U.S. Nuclear Regulatory Commission
Washington, DC 20555–0001
NRC Job Code W6479

ABSTRACT

This report presents studies performed to support the development of a technically justifiable approach for addressing the axial-burnup distribution in pressurized-water reactor (PWR) burnup-credit criticality safety analyses. The effect of the axial-burnup distribution on reactivity and proposed approaches for addressing the axial-burnup distribution are briefly reviewed. A publicly available database of profiles is examined in detail to identify profiles that maximize the neutron multiplication factor, k_{eff}, assess its adequacy for PWR burnup credit analyses, and investigate the existence of trends with fuel type and/or reactor operations. A statistical evaluation of the k_{eff} values associated with the profiles in the axial-burnup-profile database was performed, and the most reactive (bounding) profiles were identified as statistical outliers. The impact of these bounding profiles on k_{eff} is quantified for a high-density burnup credit cask. Analyses are also presented to quantify the potential reactivity consequence of loading assemblies with axial-burnup profiles that are not bounded by the database. The report concludes with a discussion on the issues for consideration and recommendations for addressing axial burnup in criticality safety analyses using burnup credit for dry cask storage and transportation.

CONTENTS

Page

LIST OF FIGURES

LIST OF FIGURES (continued)

LIST OF FIGURES (continued)

LIST OF FIGURES (continued)

LIST OF FIGURES (continued)

LIST OF FIGURES (continued)

Figure **Page**

LIST OF TABLES

FOREWORD

In 1999 the United States Nuclear Regulatory Commission (U.S. NRC) issued initial recommended guidance for using reactivity credit due to fuel irradiation (i.e., burnup credit) in the criticality safety analysis of spent pressurized-water-reactor (PWR) fuel in storage and transportation packages. This guidance was issued by the NRC Spent Fuel Project Office (SFPO) as Revision 1 to Interim Staff Guidance 8 (ISG8R1) and published in the *Standard Review Plan for Transportation Packages for Spent Nuclear Fuel*, NUREG-1617 (March 2000). With this initial guidance as a basis, the NRC Office of Nuclear Regulatory Research initiated a program to provide the SFPO with technical information that would:

- enable realistic estimates of the subcritical margin for systems with spent nuclear fuel (SNF) and an increased understanding of the phenomena and parameters that impact the margin, and
- support the development of technical bases and recommendations for effective implementation of burnup credit and provide realistic SNF acceptance criteria while maintaining an adequate margin of safety.

ISG8R1 recommends that calculational models account for the axial variation of the burnup within a spent fuel assembly. However, guidance for an acceptable approach to account for the axial-burnup variation is not provided, and the lack of guidance has been identified as an impediment of effective implementation and utilization of burnup credit. Consequently, this report examines the effect of axial variations in burnup on SNF reactivity as a means to develop and propose a technically justifiable approach for addressing the axial-burnup distribution in PWR burnup-credit criticality safety analyses. The report reviews available data on the axial variation in burnup and the effect of axial-burnup profiles on reactivity in a high-capacity rail-type cask designed for burnup credit. A publicly available database of profiles is examined to identify profiles that maximize the neutron multiplication factor, k_{eff}, assess its adequacy for general PWR burnup-credit analyses, and investigate the existence of trends with fuel type and/or reactor operations. Based on this study and the related discussion, the report proposes recommendations for addressing the axial-burnup distribution in criticality safety analyses using burnup credit for cask storage and transportation. The use of burnup-credit results in fewer casks needing to be transported, thereby reducing regulatory burden on licensee while maintaining safety and enhance public confidence for transportation of SNF. Lastly, this effort will also contribute to NRC in making effective, efficient and realistic regulatory decisions.

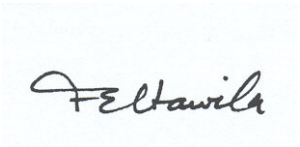

Farouk Eltawila, Director
Division of Systems Analysis and Regulatory Effectiveness

ACKNOWLEDGEMENTS

This work was performed under contract with the Office of Nuclear Regulatory Research, U.S. Nuclear Regulatory Commission (NRC). The authors gratefully acknowledge C. J. Withee of the NRC Spent Fuel Project Office for useful discussions, suggestions, and review of this document. The careful review of the draft manuscript by S. M. Bowman and R. M. Westfall is also very much appreciated. Finally, the authors are thankful to W. C. Carter for her preparation of the final report.

1 INTRODUCTION

The concept of taking credit for the reduction in reactivity due to fuel burnup is commonly referred to as burnup credit. The reduction in reactivity that occurs with fuel burnup is due to the change in concentration (net reduction) of fissile nuclides and the production of actinide and fission-product neutron absorbers. The change in the concentration of these nuclides with fuel burnup, and consequently the reduction in reactivity, is dependent upon the fuel design and depletion environment. Therefore, the utilization of credit for fuel burnup necessitates consideration of fuel operating conditions, including variations in spatial burnup.

Guidance[1,2] on burnup credit for pressurized-water-reactor (PWR) spent nuclear fuel (SNF), issued by the Nuclear Regulatory Commission's Spent Fuel Project Office, recommends the use of analyses that provide an "adequate representation of the physics" and notes particular concern with the axial and horizontal variation of burnup. The horizontal variation of burnup has been investigated elsewhere[3] and shown[4] to have a relatively minor impact on neutron multiplication in a typical rail-type burnup-credit cask. In contrast, the axial-burnup profile has a significant impact on reactivity,[5–7] and therefore is an important component of a burnup-credit safety analysis. However, the regulatory guidance[1,2] does not describe an acceptable means to account for axial burnup in a computational model. Guidance for an acceptable approach to address axial burnup should expedite the preparation and review of a burnup-credit application.

This report reviews axial-burnup data and evaluates the effect of axial burnup on SNF reactivity to support the development of a technically justifiable approach for addressing axial burnup, and subsequently the development of guidance for NRC staff to consider. The effect of the axial burnup on reactivity and proposed approaches for addressing axial burnup are briefly reviewed. A publicly available database of profiles[8] is examined in detail to identify profiles that maximize the neutron multiplication factor, k_{eff}. Further, the database is evaluated to assess its adequacy for burnup-credit analyses and to investigate the existence of trends with fuel type and/or reactor operations. For this assessment, a statistical evaluation of the k_{eff} values associated with the profiles in the axial-burnup profile database was performed. This statistical evaluation identifies the most reactive (bounding) profiles as statistical outliers that are not representative of typical discharged SNF assemblies. Additionally, analyses are presented to quantify the reactivity consequence of loading assemblies that have axial-burnup profiles that are not bounded by the database. The report concludes with a discussion on the issues for consideration and recommendations for addressing the axial-burnup distribution in criticality safety analyses using burnup credit for dry cask storage and transportation.

2 BACKGROUND

2.1 AXIAL-BURNUP DISTRIBUTIONS

At the beginning of life, a PWR fuel assembly will be exposed to a near-cosine axial-shaped flux, which will deplete fuel near the axial center at a greater rate than at the ends. As the reactor continues to operate, the cosine flux shape will flatten because of the fuel depletion and fission-product buildup that occurs near the center. Near the fuel assembly ends, burnup is suppressed due to leakage. Consequently, the majority of PWR SNF assemblies have similar axial-burnup profiles (or shapes) – relatively flat in the axial mid-section (with peak burnup of ~1.1 times the assembly-averaged burnup) and significantly under-burned fuel at the ends (with burnup of ~0.5 times the assembly-averaged burnup).[8] Figure 1 shows a representative PWR axial-burnup distribution, specified in terms of 18 equally-spaced axial regions. As is typical, the burnup is slightly higher at the bottom of the assembly than at the top. This variation is due to the difference in the moderator density (sometimes referred to as the "axial offset"). The cooler (higher density) water, at the assembly inlet, results in higher reactivity (which subsequently results in higher burnup) than the warmer moderator at the assembly outlet. Assemblies exposed to control rods or axial power shaping rods (APSRs) during their operating history deviate from this typical profile, but constitute only a small portion of discharged SNF. Since control rods and APSRs are typically employed early in an assembly's life, their effect tends to be burned-out by the time the assembly is discharged. Nevertheless, the axial-burnup profile is dependent on a number of reactor operating characteristics, and variations between individual assemblies exist. Because the burnup profile has a strong influence on reactivity, variations in axial burnup are important to criticality safety and must be addressed.

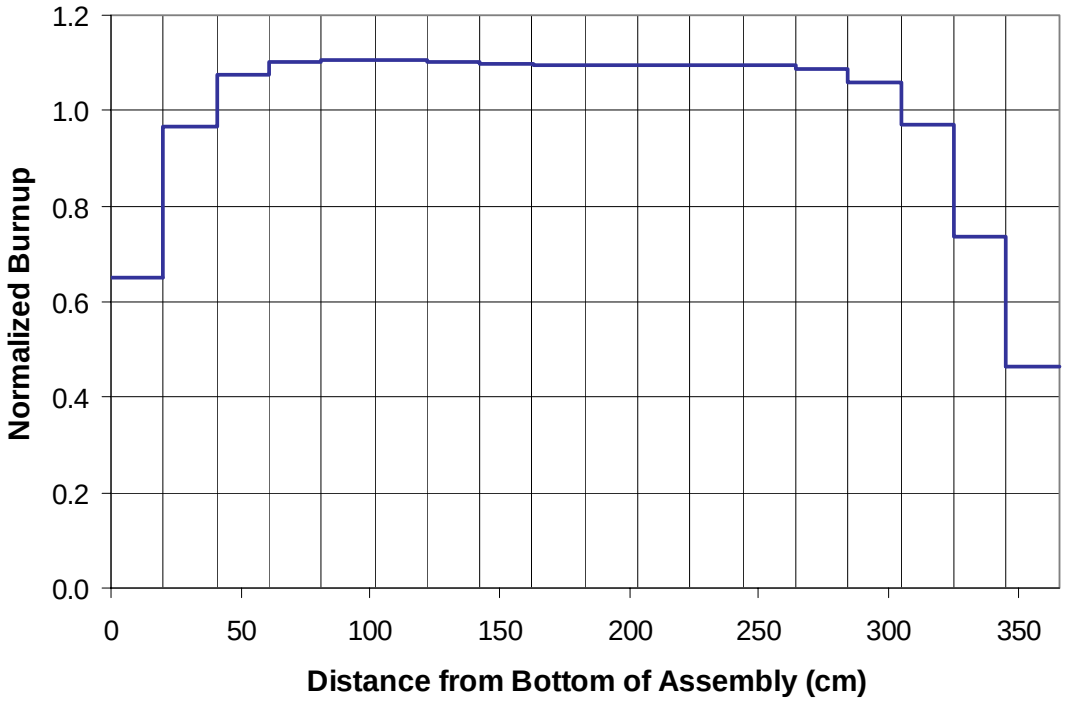

Figure 1 Representative normalized PWR axial-burnup distribution

2.2 DEFINITION OF "END EFFECT"

The accumulated burnup for a spent fuel assembly is typically readily available (from plant data) in terms of the assembly-averaged burnup. Although it is possible (and simpler) to calculate isotopic concentrations for the average burnup and assume that the material is uniformly distributed along the length of the assembly, this does not represent the actual burnup profile that exists in a spent fuel assembly. To accurately calculate the reactivity of spent fuel, the calculational model must include the axial variation in burnup. Inclusion of the axial variation is done by axially segmenting the calculational model to approximate the axially varying isotopic concentrations, which correspond to the burnup in each axial segment. Although this representation of axial burnup is more accurate, it requires significantly more effort: additional depletion calculations (one for each axial segment of differing burnup), more complex criticality models, and the transfer of a larger volume of data (spent fuel compositions) from the depletion calculations into the criticality model.

When assuming an axially uniform distribution of isotopics, the most reactive region of a fuel assembly is at the axial mid-plane, because leakage increases as one moves away from the center. In reality, the most reactive region of spent fuel is toward the assembly ends, where there exists a balance between reactivity due to lower burnup and increased leakage due to closer proximity to the fuel ends. The difference in the neutron multiplication factor (k_{eff}) between a calculation with explicit representation of the axial-burnup distribution and a calculation that assumes uniform axial burnup has become known as the *end effect;*

$$end\ effect\ (\Delta k)\ =\ k_{eff}^{with\ axial\ burnup}\ -\ k_{eff}^{uniform\ axial\ burnup}.$$

Although the assumption of uniform axial burnup has no physical validity for SNF, it has proven useful as a reference for comparison of the effect of axial-burnup distributions on k_{eff}.

2.3 REACTIVITY EFFECT OF AXIAL BURNUP

Numerous studies have been performed to quantify the reactivity effect associated with the axial variation in burnup. A review of those studies is available in Ref. 9. In general, the studies have shown that assuming uniform axial burnup is conservative for low burnups, but becomes increasingly nonconservative as burnup increases. The transition between conservative and nonconservative is dependent on numerous factors (including the initial enrichment of the fuel, the cooling time considered, and the nuclides that are included in the criticality model), but generally occurs in the burnup range of 15 to 25 GWd/MTU.

For a given axial-burnup profile, the end effect has been shown to be strongly dependent upon the cooling time and the presence of fission products in the criticality model.[10] An example of this dependence is given in Figure 2, which shows the end effect in a typical high capacity cask (GBC-32)[11] designed for burnup credit. The end effect is plotted as a function of burnup for two cooling times, with and without fission products present. The results in Figure 2 show that the end effect (1) increases with burnup, (2) becomes positive at a higher burnup if fission products are not included, (3) is reduced if fission products are neglected, and (4) increases with cooling time. These findings are consistent with those observed by the Organization for Economic Cooperation and Development's (OECD) Expert Group on Burnup Credit (EGBUC).[12,13]

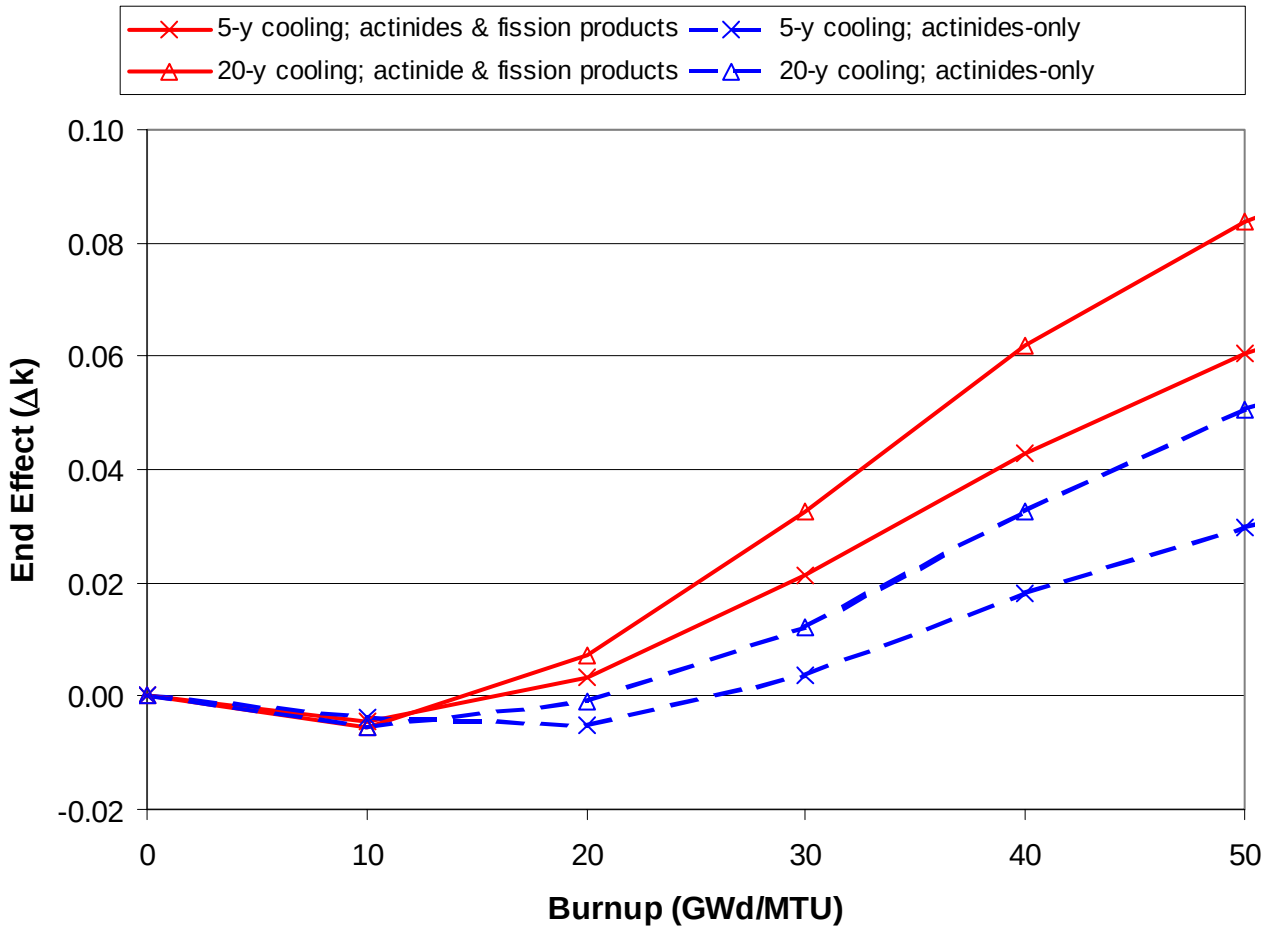

Figure 2 Example of end effect as a function of burnup for two cooling times with and without fission products present

Although the end effect is dependent upon many factors, it is primarily dependent on the slope of the burnup profile near the ends of the fuel, which is influenced by the fuel burnup, assembly design, and reactor operating environment. This point is illustrated in Figure 3, which shows the end effect as a function of burnup for three different axial-burnup profiles. Recognizing the importance of the axial-burnup profile, a database[8] of more than 3000 PWR axial-burnup profiles was generated. Using this database of profiles, studies[7] have identified the axial profiles that provide the largest (bounding) k_{eff} values over selected burnup ranges. This database is the most extensive set of available data and is examined in detail in the following sections.

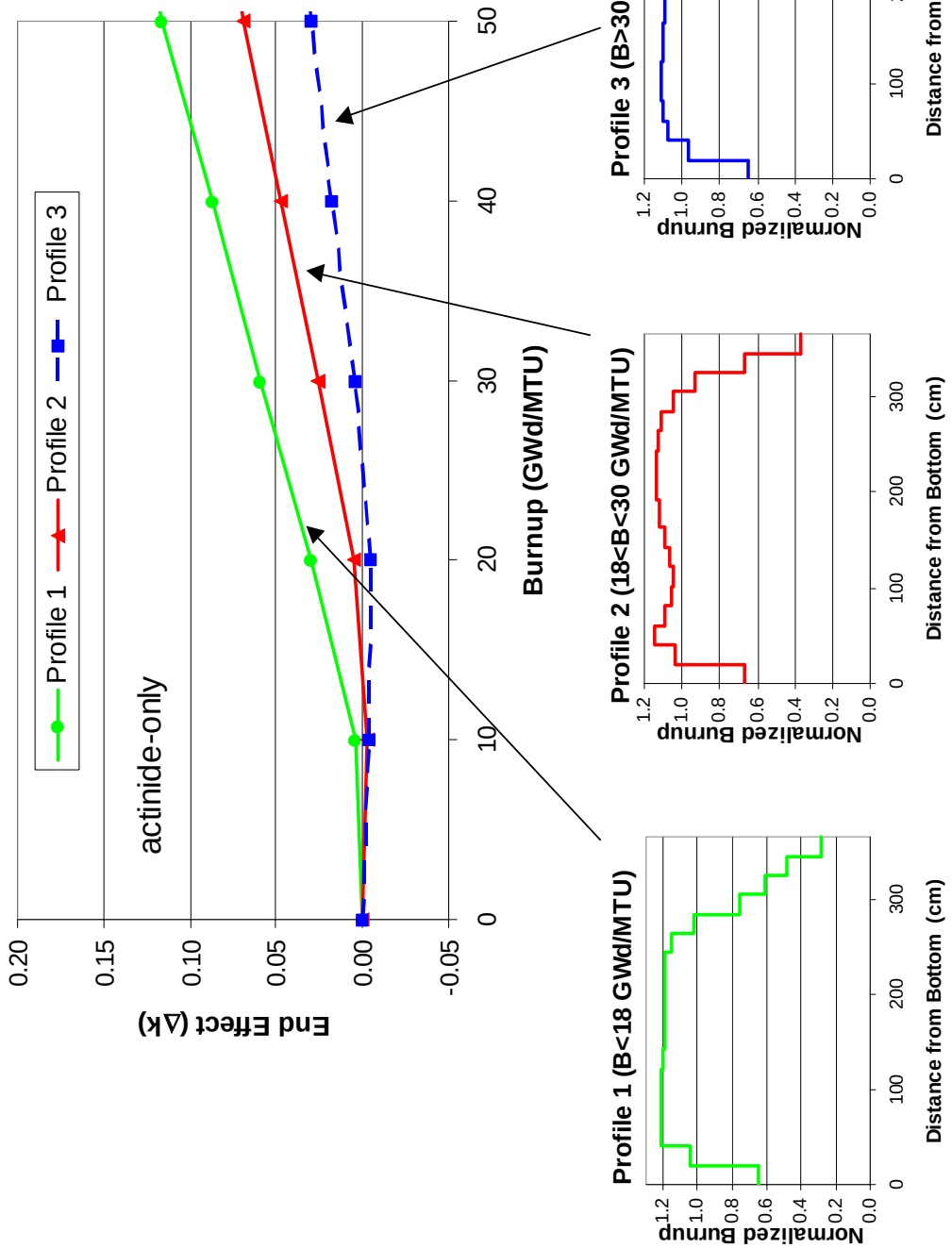

Figure 3 Examples of end effect as a function of burnup for three different axial-burnup profiles for fuel with 4.0 wt % ^{235}U enrichment and actinide-only nuclides. The profiles correspond to the suggested profiles from Ref. 3 for the specified burnup ranges.

3 AXIAL-BURNUP-PROFILE DATA

3.1 AXIAL-PROFILE DATABASE

The axial-burnup-profile database of Ref. 8 (YAEC-1937) contains 3169 PWR axial profiles from ~1700 different assemblies, which represent three fuel vendors, 20 different reactors, and 106 cycles of operation through the mid-1990s. The 106 cycles of operation include first cycles, out-in fuel management and low leakage fuel management.[8] The axial profiles in the database are specified in terms of 18 equally-spaced axial regions and were calculated with various three-dimensional (3-D) core physics codes that are the current methods used in fuel management, reload analysis, and core operational support. Although their accuracy is verified through safe reactor operation and industry history of operating within technical specifications, there has been a great deal of interest in quantifying the uncertainties in the calculated burnups, particularly as a function of axial height. Responding to this interest, a study[14] was performed to evaluate the uncertainties via in-core measurements and core neutronic calculations for a Westinghouse PWR. The uncertainty in burnup was determined by comparing calculated and measured reaction rates at the instrumented locations and using analytical methods and nearby measurements to infer "measurements" in the un-instrumented locations. The study[14] concluded that the uncertainty in burnup, evaluated over three cycles of operation, decreases with increasing burnup. For assemblies discharged after one cycle of burnup the uncertainty was estimated to be 1.90%; after two cycles of burnup the uncertainty was 0.98%; and after three cycles of burnup the uncertainty was 1.02%. The decrease in uncertainty after two-cycles of burnup is attributed[14] to the self-correcting nature of burnup. The part of the study that is particularly relevant to this discussion is the evaluation of the uncertainty in the axial distribution. Uncertainties of less than 7% are quoted[14] for the top and bottom ends of the assemblies.

The breakdown of the 3169 profiles, in terms of fuel vendor and design, are as follows: 1334 Babcock & Wilcox (B&W) 15×15 profiles from eight different reactors, 544 Combustion Engineering (CE) 14×14 profiles from one reactor, 228 CE 16×16 profiles from two reactors, 156 Westinghouse 15×15 profiles from two reactors, and 907 Westinghouse 17×17 profiles from eight different reactors. According to Ref. 15, 44,598 PWR assemblies have been discharged from commercial PWRs through 1994. Thus, the database, which contains profiles from ~1700 different assemblies, represents ~4% of the total number of PWR assemblies discharged through 1994. The data covers a range of burnup from 3.086 to 55.289 GWd/MTU and an enrichment range of 1.24 to 4.75 wt % ^{235}U. To illustrate the range and depth of the database, in terms of burnup and enrichment, the profiles have been divided into burnup and enrichment groups, where each group spans a burnup interval of 5 GWd/MTU and an enrichment interval of 0.5 wt % ^{235}U. The detailed breakdown of the number of profiles that fall within the burnup and enrichment groups is provided in Table 1. To aid the visualization of burnup and initial enrichment combinations represented in the database, Figure 4 plots the burnup and initial enrichment combination for each of the 3169 profiles in the database. Solid lines are included on Figure 4 to indicate the current limits of regulatory guidance[1,2] on maximum burnup and enrichment (i.e., 40 GWd/MTU and 4.0 wt % ^{235}U). For comparison purposes, Figure 5 plots the burnup and initial enrichment combinations from the latest available PWR SNF discharge data.[16] The burnup and enrichment regime covered by the regulatory guidance appears to be well covered by the database. Also, in comparison to the discharge data, the lower burnup and enrichment regime appears to be well covered; this is partially due to the fact that the database includes first and second cycle profiles for many of the assemblies. For extension beyond the current burnup and enrichment limits, expansion of the existing database to include more profiles with higher burnup and enrichments would be desirable.

Table 1 Number of axial-burnup-database[8] profiles that fall within various burnup and enrichment intervals

Upper bound of enrichment range (wt % ^{235}U)	Upper bound of burnup range (GWd/MTU)												Total
	5	10	15	20	25	30	35	40	45	50	55	60	
0.5	0	0	0	8	0	0	2	6	0	1	1	0	18[†]
1	0	0	0	0	0	0	0	0	0	0	0	0	0
1.5	0	0	3	2	3	0	0	0	0	0	0	0	8
2	1	10	29	31	16	1	0	0	0	0	0	0	88
2.5	0	3	37	49	16	12	1	0	0	0	0	0	118
3	8	88	79	165	109	127	110	28	5	0	1	0	720
3.5	0	45	103	171	124	114	209	163	69	20	0	0	1018
4	0	2	47	180	159	83	153	158	130	75	5	0	992
4.5	0	0	8	31	41	18	9	21	22	16	6	1	173
5	0	0	3	1	6	11	4	3	4	1	1	0	34
Total	9	148	309	638	474	366	488	379	230	113	14	1	3169

[†] These profiles had zero specified for their enrichment in the database (Ref. 8).

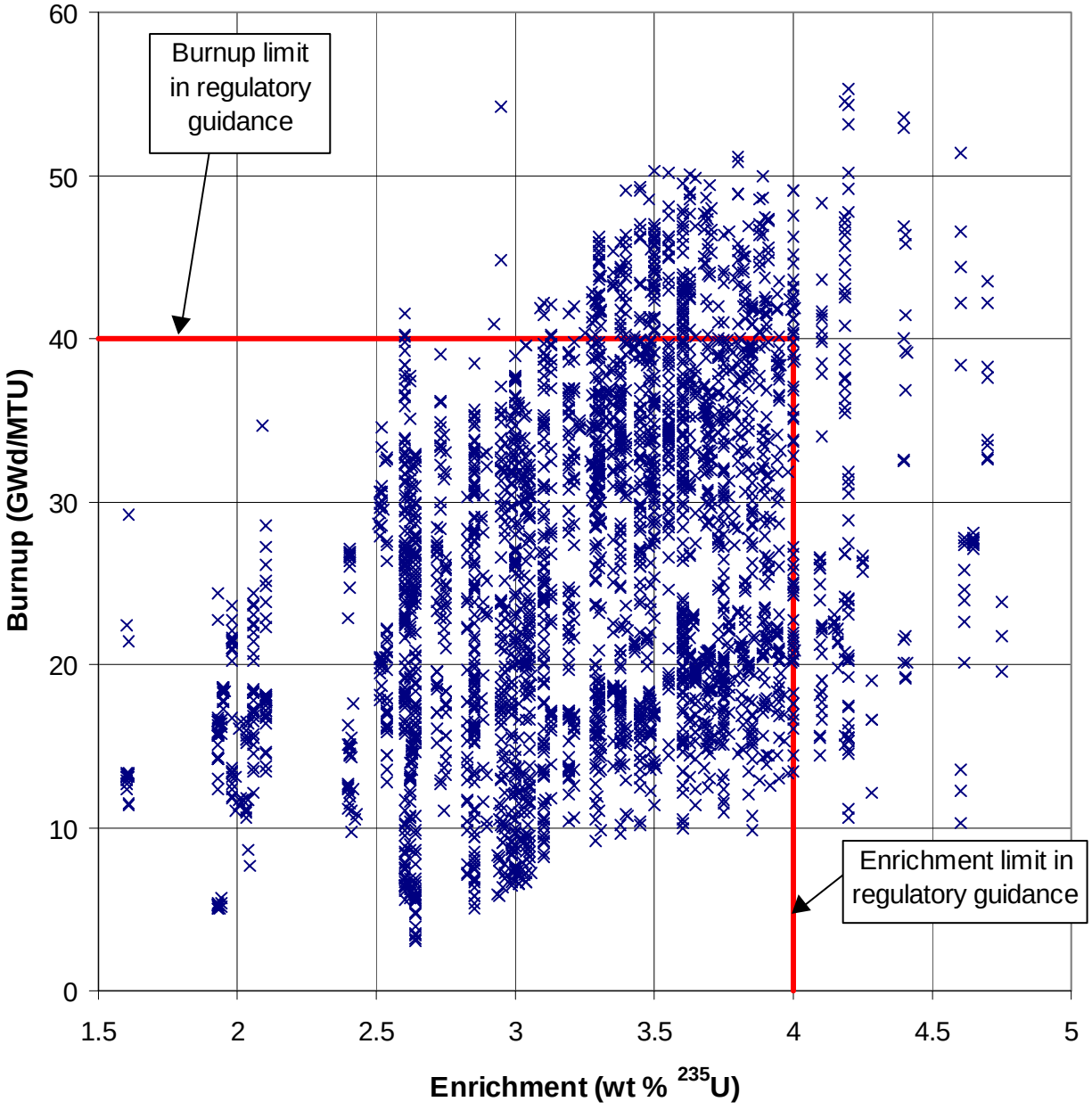

Figure 4 Burnup and initial enrichment combination for each of the axial-burnup-database[8] profiles

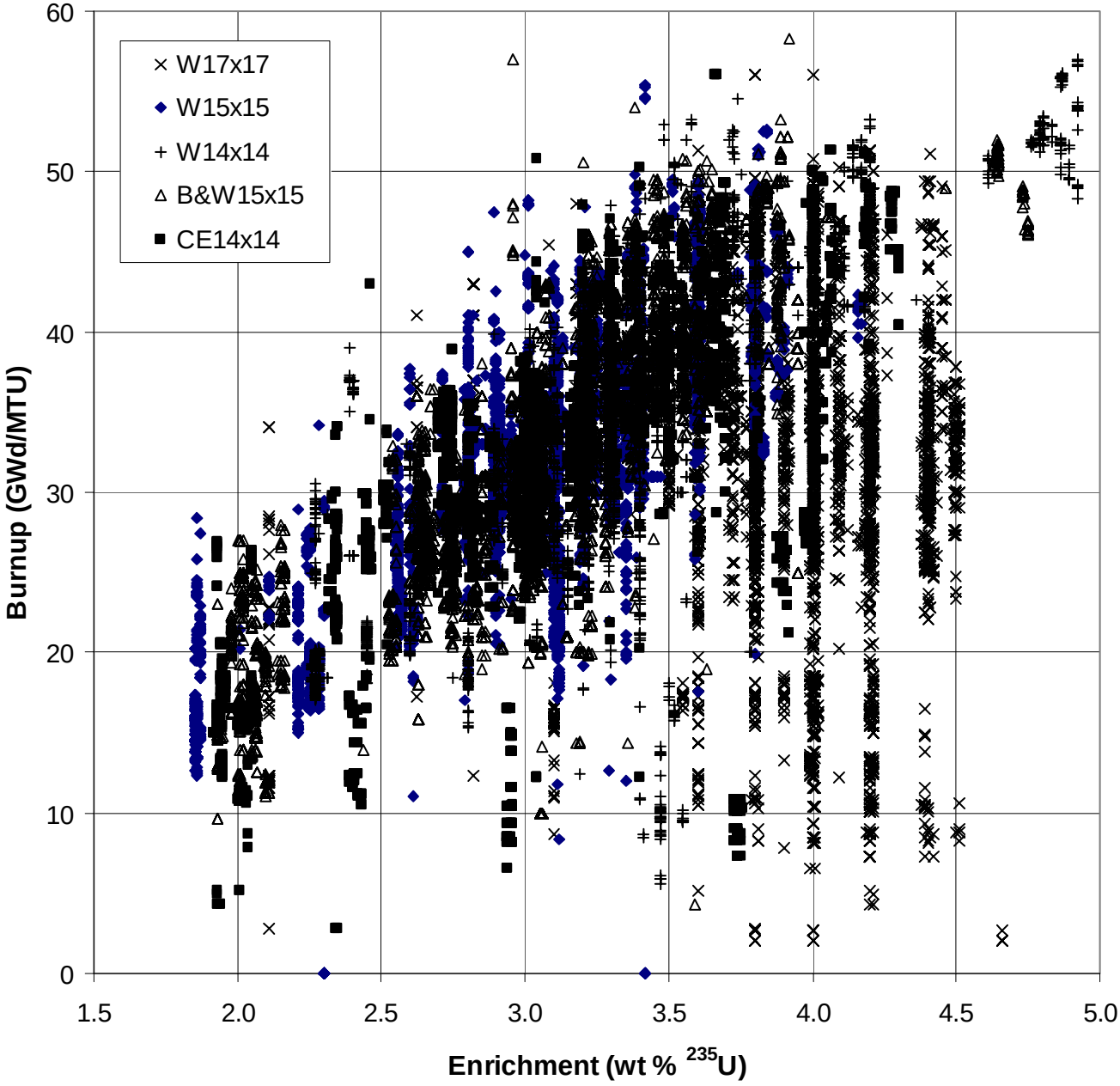

Figure 5 Burnup and enrichment combinations from discharged PWR SNF through 1998 (Ref. 16)

The profiles in the database[8] include fuel designs that used burnable absorbers with different poison absorber types such as: burnable poison rods (BPRs) of borosilicate glass and B_4C; and integral burnable absorbers (IBAs) of ZrB_2, B_4C, erbium and gadolinium. In addition, the profiles include assemblies exposed to control rods, including APSRs. Thus, in terms of categories, the database provides a very good representation of discharged PWR SNF assembly designs through the mid-1990s. An analysis of the database profiles, in terms of their impact on k_{eff}, is presented in Section 4.

It is worth noting that an early axial-profile database[17] for CE fuel of the 14×14 design was developed using data from a single plant. This database was a predecessor to the current database.

3.2 OTHER SOURCES OF DATA

In addition to the Ref. 8 database, other sources of data have either recently become available or may become available in the near future. For example, more than 1200 measured (derived from measured power densities) axial-burnup profiles from two German reactors have recently become available.[18] Although these profiles are limited to two reactors that may not be representative of U.S. PWR reactors, they provide significantly more detailed axial-burnup representation (e.g., the effect of the grid spacers is readily apparent) than is available in the Ref. 8 database. The axial-profile data in Ref. 18 is specified in terms of either 30 or 32 axial regions, depending on the plant from which the profiles originate, as compared to the axial-profile data in Ref. 8, which is specified in terms of 18 axial regions. Therefore, it is recommended that future work review these more-detailed, measured axial profiles for applicability to U.S. PWRs and evaluate their impact on SNF reactivity.

Additional data has also become available as a result of efforts performed under the Office of Civilian Radioactive Waste Management to analyze commercial reactor criticals (CRCs) for the Yucca Mountain Project[19] (YMP). Under this project, ~3400 axial-burnup profiles have been documented from Framatome-Cogema Fuels (formerly B&W) and Westinghouse PWR fuel assemblies. The profiles are tabulated within a series of CRC summary reports (see Ref. 20). A cursory comparison of these axial profiles to those contained in the Ref. 8 database suggests that the two sets of profiles are consistent, and thus provide some further confidence in the Ref. 8 database. However, future work should consider a more detailed evaluation of these data.

4 ANALYSES

4.1 DETERMINATION OF BOUNDING PROFILES

To account for axial burnup in a burnup-credit criticality safety evaluation, one must develop an approach to address the impact of the axial-burnup distribution in a generic manner. One such approach is to identify and use axial-burnup profiles that are bounding in terms of the value of k_{eff}, and yet sufficiently realistic as to not provide excess conservatism. The approach to date in the U.S. has been to determine bounding axial profiles from actual burnup profiles; either identifying specific profiles that are bounding or developing "artificial" bounding profiles based on the characteristics of actual bounding profiles. The following subsections briefly describe efforts related to identifying bounding axial profiles.

4.1.1 Previous Work

Previous work[6,7,21] in determining bounding axial-burnup profiles has employed a relatively straightforward approach – perform criticality calculations for each available burnup profile to determine the profile that produces the largest end effect (i.e., the difference in k_{eff} between a calculation with the axial-burnup distribution and a calculation that assumes uniform axial burnup). The first systematic evaluation[6] of profiles considered the Ref. 17 profile database and established characteristics that define bounding profiles for criticality considerations. Additionally, this work investigated the influence of calculational assumptions on the end effect and developed an approach for defining artificial bounding profiles based on the actual profiles.

Following the development of the Ref. 8 profile database, analyses were performed to determine the bounding axial-burnup profiles based on that database. After excluding a number of burnup profiles for various reasons (e.g., non-uniform axial enrichment and incomplete data), the remaining 2988 burnup profiles were arranged into 12 burnup groups, each corresponding to a burnup range of ~4 GWd/MTU. One-dimensional (1-D) diffusion calculations, assuming 35-cm-thick pure-water regions on each end of the fuel, were performed for each profile. Axially varying burnup was included by linear interpolation of 2-group assembly-averaged cross sections, which were generated by CASMO-3. Thus, all analyses of Ref. 7 include the actinide and fission-product nuclides available in CASMO-3. The results of the criticality calculations were used to rank the axial-burnup profiles in terms of their corresponding reactivity effect. Based on the calculated results, the axial-burnup profile within each burnup group that yielded the largest positive reactivity effect was identified. These bounding profiles are listed in Table 2, along with the specification of the burnup ranges for the 12 burnup-groups. Based on the calculated results and physical arguments, "artificial" bounding axial profiles were also developed for each of the twelve burnup-groups. Although the purpose for developing these artificial profiles is not discussed, it is assumed they were developed to introduce additional conservatism in recognition of the fact that the database is not exhaustive.

Table 2 Bounding profiles by burnup group (*Source*: Ref. 7)

Burnup groups	*1*	*2*	*3*	*4*	*5*	*6*	*7*	*8*	*9*	*10*	*11*	*12*
Axial height (%)	Burnup ranges (GWd/MTU)											
	>46	42–46	38–42	34–38	30–34	26–30	22–26	18–22	14–18	10–14	6–10	<6
2.78	0.573	0.674	0.660	0.585	0.652	0.619	0.630	0.668	0.649	0.633	0.662	0.574
8.33	0.917	0.949	0.936	0.957	0.967	0.924	0.936	1.034	1.044	0.989	0.931	0.947
13.89	1.066	1.053	1.045	1.091	1.074	1.056	1.066	1.150	1.208	1.019	1.049	1.091
19.44	1.106	1.085	1.080	1.121	1.103	1.097	1.103	1.094	1.215	0.857	1.059	1.105
25.00	1.114	1.095	1.091	1.126	1.108	1.103	1.108	1.053	1.214	0.776	1.108	1.094
30.56	1.111	1.095	1.093	1.111	1.106	1.101	1.109	1.048	1.208	0.754	1.144	1.087
36.11	1.106	1.093	1.092	1.094	1.102	1.103	1.112	1.064	1.197	0.785	1.168	1.086
41.69	1.101	1.091	1.090	1.093	1.097	1.112	1.119	1.095	1.189	1.013	1.183	1.087
47.22	1.097	1.089	1.089	1.092	1.094	1.125	1.126	1.121	1.188	1.185	1.189	1.091
57.80	1.093	1.088	1.088	1.091	1.094	1.136	1.132	1.135	1.192	1.253	1.190	1.096
58.33	1.089	1.086	1.088	1.092	1.095	1.143	1.135	1.140	1.195	1.278	1.183	1.102
63.89	1.086	1.084	1.086	1.099	1.096	1.143	1.135	1.138	1.190	1.283	1.167	1.105
69.44	1.081	1.081	1.084	1.096	1.095	1.136	1.129	1.130	1.156	1.276	1.135	1.105
75.00	1.073	1.073	1.077	1.087	1.086	1.115	1.109	1.106	1.022	1.251	1.079	1.096
80.56	1.051	1.053	1.057	1.073	1.059	1.047	1.041	1.049	0.756	1.193	0.976	1.066
86.11	0.993	0.987	0.996	1.003	0.971	0.882	0.871	0.933	0.614	1.075	0.806	0.986
91.67	0.832	0.800	0.823	0.796	0.738	0.701	0.689	0.669	0.481	0.863	0.596	0.806
97.22	0.512	0.524	0.525	0.393	0.462	0.456	0.448	0.373	0.284	0.515	0.375	0.474

As mentioned, the burnup profile changes with burnup – tending to flatten with increasing burnup. Consequently, if an axial-burnup profile from a low burnup assembly is used in a calculation involving high burnup, the end effect is typically over-estimated. Hence, for determination of bounding profiles, it is common to sort the profiles into burnup ranges (e.g., the 12 burnup groups used in Ref. 7).

For each profile, a calculation was performed with the burnup profile, initial enrichment and assembly-averaged discharge burnup. Therefore, the bounding profile evaluation[7] does not completely isolate the effect of the profile from the effects of variations in initial enrichment and discharge burnup. Even though the end effect is not strongly dependent on minor variations in the initial enrichment and the discharge burnup cannot vary significantly within a burnup group (see Table 2), a bounding profile analysis should be performed consistently (i.e., at the same initial enrichment and burnup).

Based on the results of Ref. 7, analyses[21] have been performed to address bounding axial-burnup distributions for actinide-only applications and for broader burnup ranges. The evaluation concluded that the bounding axial-burnup profiles identified in Ref. 7, which included actinides and fission products, were also valid for the actinide-only condition. However, this actinide-only ranking analysis was based on a comparison of relatively few axial-burnup profiles. Additionally, bounding axial profiles for only three burnup ranges were determined (based on the 12 actual bounding profiles from Ref. 7, see Table 2) and suggested for use with a proposed actinide-only burnup-credit methodology.[3] For ease of comparison, these three profiles are provided in Table 3 and plotted in Figure 6.

4.1.2 Independent Bounding Profile Analysis

In support of a more detailed assessment of the Ref. 8 database and to evaluate the dependency of bounding profiles on characteristics such as cooling time and the presence of fission products, an independent bounding profile analysis has been performed as part of this work. A 1-D discrete ordinates criticality calculation was performed for each of the 2988 profiles considered in Ref. 7. However, unlike the work of Ref. 7, in this analysis the profiles in each burnup group were evaluated consistently (i.e., at the same initial enrichment and burnup) and the profiles were ranked in terms of their corresponding k_{eff} (as opposed to being ranked in terms of their end effect, which is dependent on calculations that assume uniform axial burnup). Since the end effect has been found to be relatively insensitive to initial enrichment, the bounding profile analysis assumed 4.0 wt % ^{235}U initial enrichment for all calculations. For a few of the lower burnup groups, the calculations were repeated at lower initial enrichments to verify that the determination of bounding profiles was insensitive to the choice of initial enrichment. The calculations in each burnup group, except for the highest and lowest burnup group, assumed the median burnup. For the lowest burnup group (i.e., burnup < 6 GWd/MTU) a burnup of 4 GWd/MTU was assumed. For the highest burnup group (i.e., burnup > 46 GWd/MTU), a burnup of 50 GWd/MTU was assumed.

Table 3 Proposed bounding axial profiles from Ref. 3

Burnup groups	*1*	*2*	*3*
Axial	Burnup ranges (GWd/MTU)		
height (%)	<18	18–30	>30
2.78	0.649	0.668	0.652
8.33	1.044	1.034	0.967
13.89	1.208	1.150	1.074
19.44	1.215	1.094	1.103
25.00	1.214	1.053	1.108
30.56	1.208	1.048	1.106
36.11	1.197	1.064	1.102
41.69	1.189	1.095	1.097
47.22	1.188	1.121	1.094
57.80	1.192	1.135	1.094
58.33	1.195	1.14	1.095
63.89	1.190	1.138	1.096
69.44	1.156	1.130	1.095
75.00	1.022	1.106	1.086
80.56	0.756	1.049	1.059
86.11	0.614	0.933	0.971
91.67	0.481	0.669	0.738
97.22	0.284	0.373	0.462

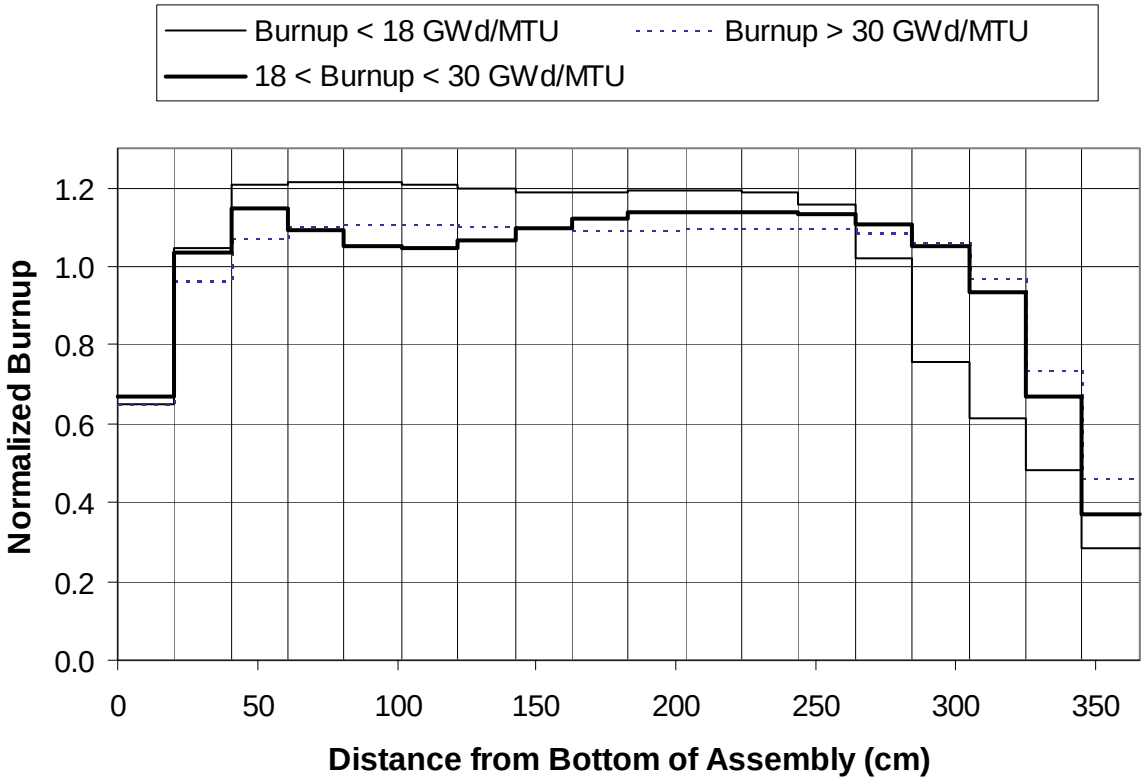

Figure 6 Proposed bounding axial profiles from Ref. 3

The criticality calculations for this independent bounding profile evaluation corresponded to an infinite radial array of fuel pins from a Westinghouse 17×17 OFA assembly design. The calculations were performed for out-of-reactor conditions (i.e., unborated water at 20° C) and 5-year cooling, and included the actinide and fission-product nuclides (Set 2) listed in Table 4. The actual calculational model is a water-reflected slab to represent the finite-length infinite arrays of pins. The slab is composed of homogenized mixtures, to model the different burnup regions, with cross sections prepared using an infinite, 1-D pin cell model. The criticality calculations were performed with the XSDRNPM 1-D discrete ordinates code,[22] using the SCALE 44-group cross-section library. Cell-weighted cross sections were generated by CSASIX.[22] The depleted fuel compositions were calculated with the SAS2H sequence[22] and the ORIGEN-S code[22] of SCALE. All SAS2H calculations utilized the SCALE 44-group library and were performed using constant (as a function of burnup) operational parameters for fuel temperature (1000.0 K), moderator temperature (600.0 K), soluble boron concentration (650 ppm) and specific power (continuous operation at 60 MW/MTU). Isotopic compositions for each burnup of interest were extracted from SAS2H output for use in XSDRNPM. Similar to the previous bounding analysis[7] and consistent with the specification of the axial profiles in Ref. 8 database, the burnup profile was represented via 18 equally-spaced axial regions. Previous work[6] has shown that specifying the axial burnup profile with greater resolution (i.e., smaller axial regions) has no significant impact on the calculated end effect. However, additional studies have been performed as part of this work to investigate the effect of profile resolution and reflector materials. These studies are provided in Appendix A.

Despite the differences in approach, the independent calculations performed for this work generally confirmed the bounding profiles determined in Ref. 7. Where differences in bounding profiles were observed (5 out of 12), the differences were due to more than one profile resulting in essentially the same k_{eff} value. In those particular cases, the difference between calculations with the bounding profile determined in this analysis and the bounding profile determined by Ref. 7 is less than 0.2% Δk. Consequently, this analysis has generally confirmed the previously determined bounding profiles. The bounding profiles, as determined in this analysis, are given in Table 5 for reference. To illustrate how the bounding profiles vary with burnup and the variation in profiles within the Ref. 8 database, the 12 bounding profiles, as determined in this analysis, are plotted in Figures 7–18. The end effect associated with each of the profiles in the lowest burnup group (i.e., group 12) is negative.

To address questions regarding the applicability of 1-D ranking analyses to 3-D burnup-credit casks, analyses were also performed with each of the profiles using the GBC-32 cask.[11] The criticality calculations were performed with the CSAS25 sequence of SCALE, which executes the KENO V.a Monte Carlo code. The calculations utilized the SCALE 238-group cross-section library, and included the actinide and fission-product nuclides (Set 2) listed in Table 4. The 3-D calculations confirmed the results of the 1-D ranking analysis.

Finally, a study was performed to address questions about the applicability of the bounding profiles, which were determined based on calculations that include the major fission products and assume 5-year cooling time, to evaluations that assume actinides-only and/or longer cooling times. This study essentially consisted of repeating the 1-D bounding profile analysis described above, which corresponded to 5-year cooling time and included the major fission products, for the following additional conditions: (1) actinide-only nuclides (set 1 nuclides shown in Table 4) and 5-year cooling time, (2) actinide-only nuclides (set 1 nuclides shown in Table 4) and 20-year cooling time, and (3) actinide and fission-product nuclides (set 2 nuclides shown in Table 4) and 20-year cooling time, and comparing the results. The determination of the bounding profiles was found to be relatively insensitive to these changes in the basic assumptions, due primarily to the fact that, for most of the burnup groups, the bounding profile is notably more reactive than the other profiles in the group. Hence, for the axial-burnup profiles considered, the results suggest that the bounding profiles determined with fission products present and 5-year cooling are

valid for actinide-only calculations within the timeframe of interest to burnup-credit analyses for dry storage and transportation (. 40 years).

In summary, the independent bounding profile analyses (both 1-D and 3-D) have confirmed the bounding profiles determined by Ref. 7. Where differences in bounding profiles were observed, the differences were due to more than one profile resulting in essentially the same k_{eff} value (i.e., within 0.2% Δk).

Table 4 Nuclide classifications used for the analyses

Set 1: Actinide-only nuclides (10 total)									
U-234	U-235	U-238	Pu-238	Pu-239	Pu-240	Pu-241	Pu-242	Am-241	O[†]
Set 2: Actinide and fission-product nuclides (29 total)									
U-234	U-235	U-236	U-238	Pu-238	Pu-239	Pu-240	Pu-241	Pu-242	Am-241
Am-243	Np-237	Mo-95	Tc-99	Ru-101	Rh-103	Ag-109	Cs-133	Sm-147	Sm-149
Sm-150	Sm-151	Sm-152	Nd-143	Nd-145	Eu-151	Eu-153	Gd-155	O[†]	

[†]Oxygen is neither an actinide nor a fission product, but is included in this list because it is an integral part of fuel, and hence included in the calculations.

Table 5 Bounding axial profiles by burnup group as determined independently with 1-D XSDRNPM calculations

Burnup group	1†	2†	3	4†	5	6	7	8	9	10	11†	12†
Axial height (%)	Burnup ranges (GWd/MTU)											
	> 46	42–46	38–42	34–38	30–34	26–30	22–26	18–22	14–18	10–14	6–10	< 6
2.78	0.582	0.666	0.660	0.648	0.652	0.619	0.630	0.668	0.649	0.633	0.658	0.631
8.33	0.920	0.944	0.936	0.955	0.967	0.924	0.936	1.034	1.044	0.989	1.007	1.007
13.89	1.065	1.048	1.045	1.070	1.074	1.056	1.066	1.150	1.208	1.019	1.091	1.135
19.44	1.105	1.081	1.080	1.104	1.103	1.097	1.103	1.094	1.215	0.857	1.070	1.133
25.00	1.113	1.089	1.091	1.112	1.108	1.103	1.108	1.053	1.214	0.776	1.022	1.098
30.56	1.110	1.090	1.093	1.112	1.106	1.101	1.109	1.048	1.208	0.754	0.989	1.069
36.11	1.105	1.086	1.092	1.108	1.102	1.103	1.112	1.064	1.197	0.785	0.978	1.053
41.69	1.100	1.085	1.090	1.105	1.097	1.112	1.119	1.095	1.189	1.013	0.989	1.047
47.22	1.095	1.084	1.089	1.102	1.094	1.125	1.126	1.121	1.188	1.185	1.031	1.050
57.80	1.091	1.084	1.088	1.099	1.094	1.136	1.132	1.135	1.192	1.253	1.082	1.060
58.33	1.088	1.085	1.088	1.097	1.095	1.143	1.135	1.140	1.195	1.278	1.110	1.070
63.89	1.084	1.086	1.086	1.095	1.096	1.143	1.135	1.138	1.190	1.283	1.121	1.077
69.44	1.080	1.086	1.084	1.091	1.095	1.136	1.129	1.130	1.156	1.276	1.124	1.079
75.00	1.072	1.083	1.077	1.081	1.086	1.115	1.109	1.106	1.022	1.251	1.120	1.073
80.56	1.050	1.069	1.057	1.056	1.059	1.047	1.041	1.049	0.756	1.193	1.101	1.052
86.11	0.992	1.010	0.996	0.974	0.971	0.882	0.871	0.933	0.614	1.075	1.045	0.996
91.67	0.833	0.811	0.823	0.743	0.738	0.701	0.689	0.669	0.481	0.863	0.894	0.845
97.22	0.515	0.512	0.525	0.447	0.462	0.456	0.448	0.373	0.284	0.515	0.569	0.525

† Differs from bounding profile determined in Ref. 7, but is essentially equivalent in terms of k_{eff} (difference between calculations with this profile and the bounding profile determined in Ref. 7 is less than 0.2% Δk).

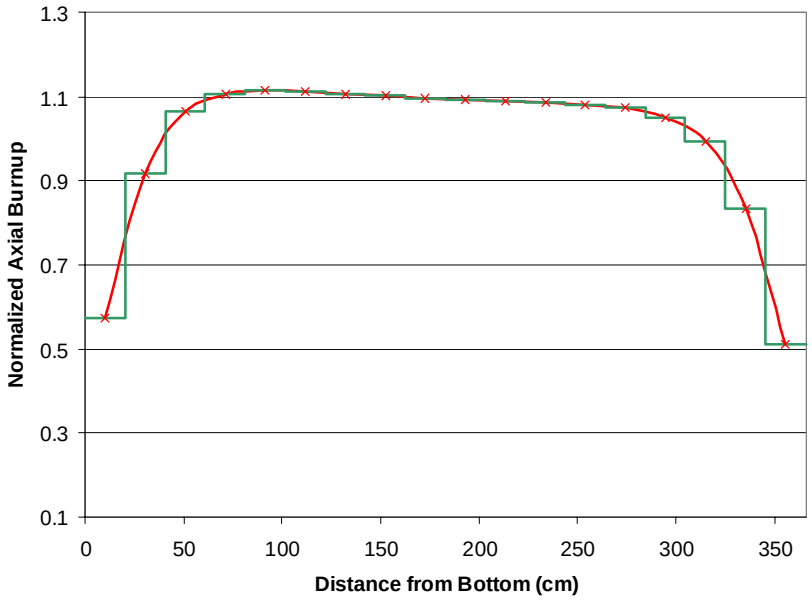

Figure 7 Bounding profile for burnup group 1 (burnup > 46 GWd/MTU)

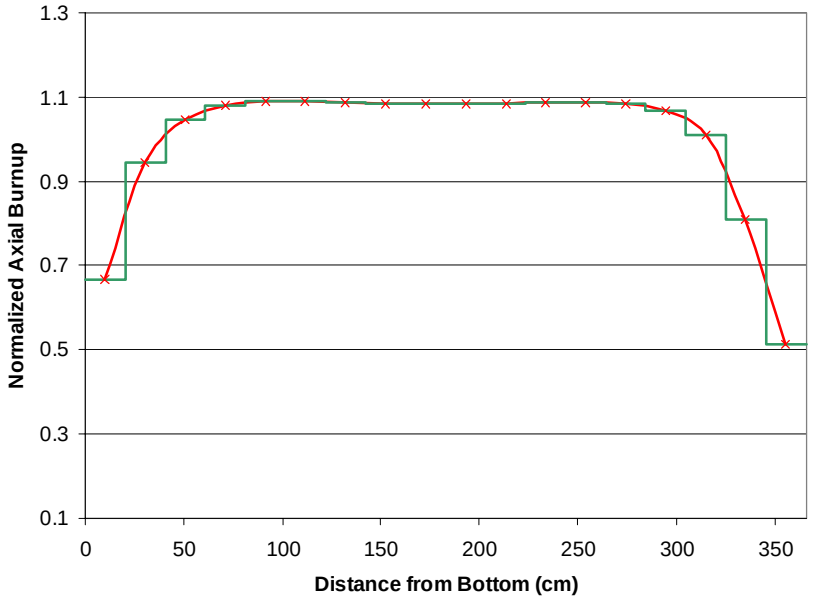

Figure 8 Bounding profile for burnup group 2 (42 < burnup < 46 GWd/MTU)

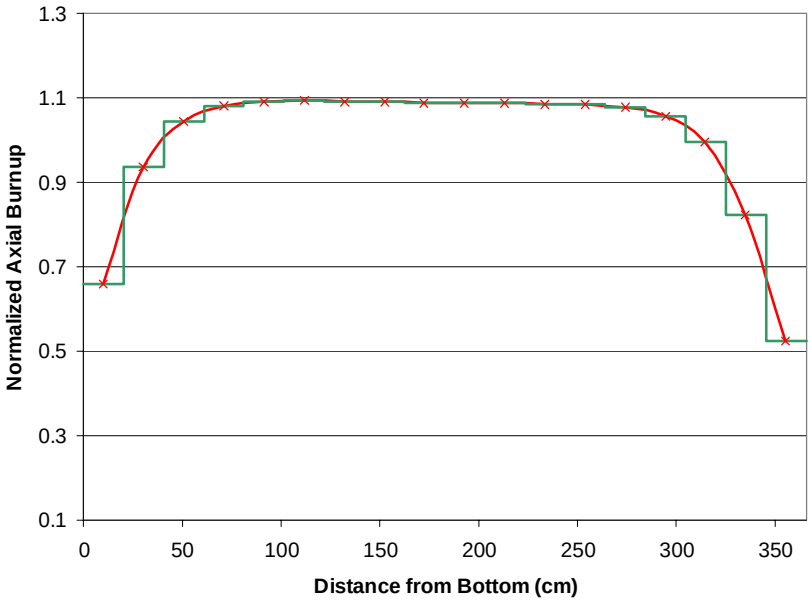

Figure 9 Bounding profile for burnup group 3 (38 < burnup < 42 GWd/MTU)

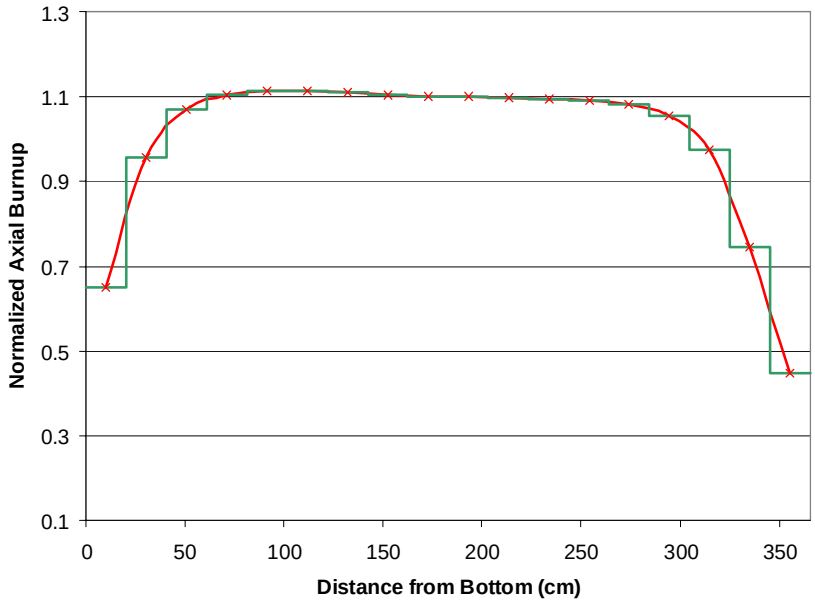

Figure 10 Bounding profile for burnup group 4 (34 < burnup < 38 GWd/MTU)

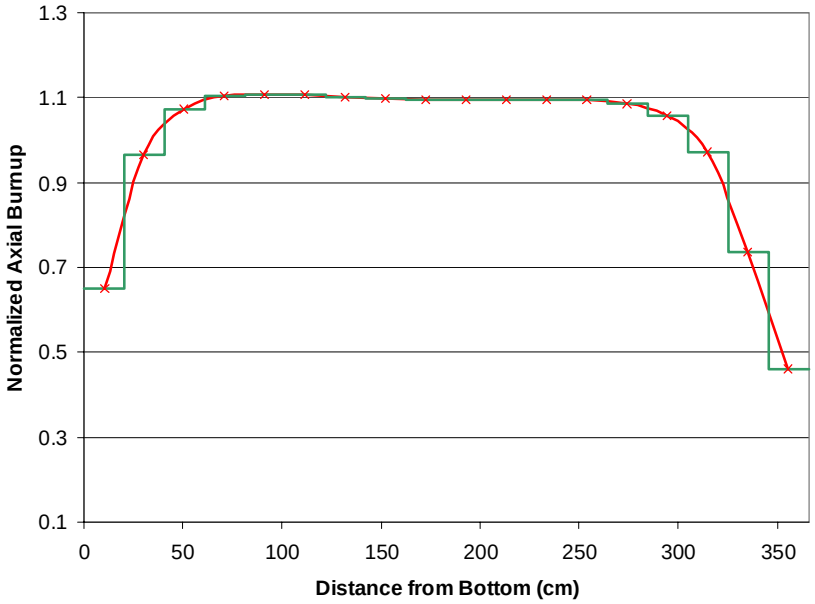

Figure 11 Bounding profile for burnup group 5 (30 < burnup < 36 GWd/MTU)

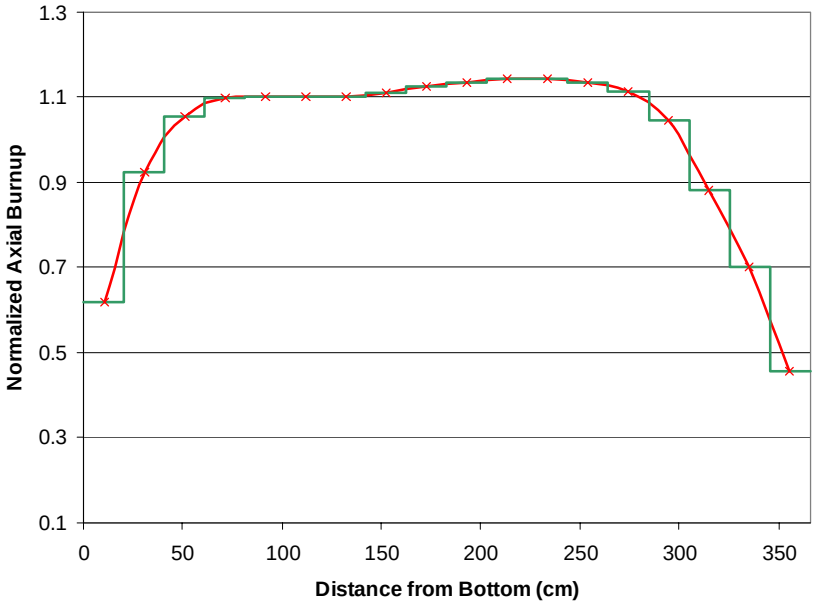

Figure 12 Bounding profile for burnup group 6 (26< burnup < 30 GWd/MTU)

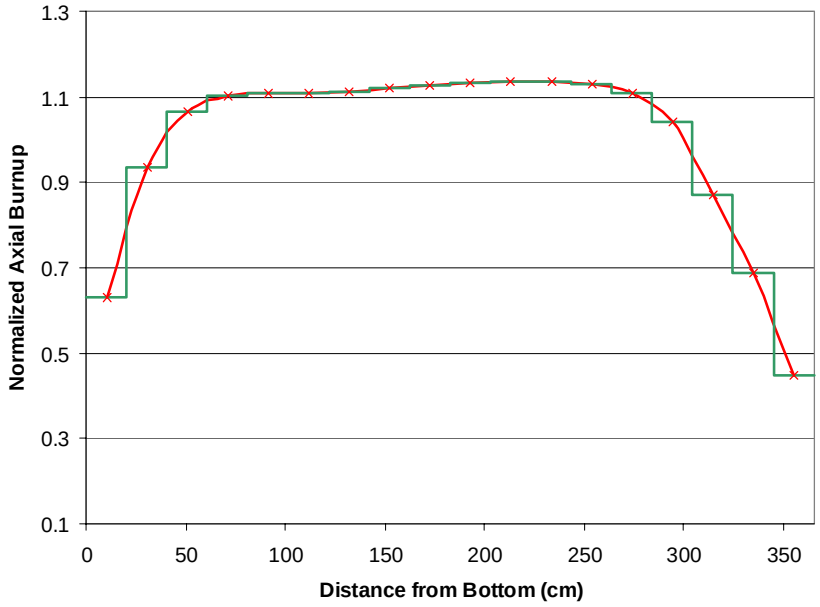

Figure 13 Bounding profile for burnup group 7 (22 < burnup < 26 GWd/MTU)

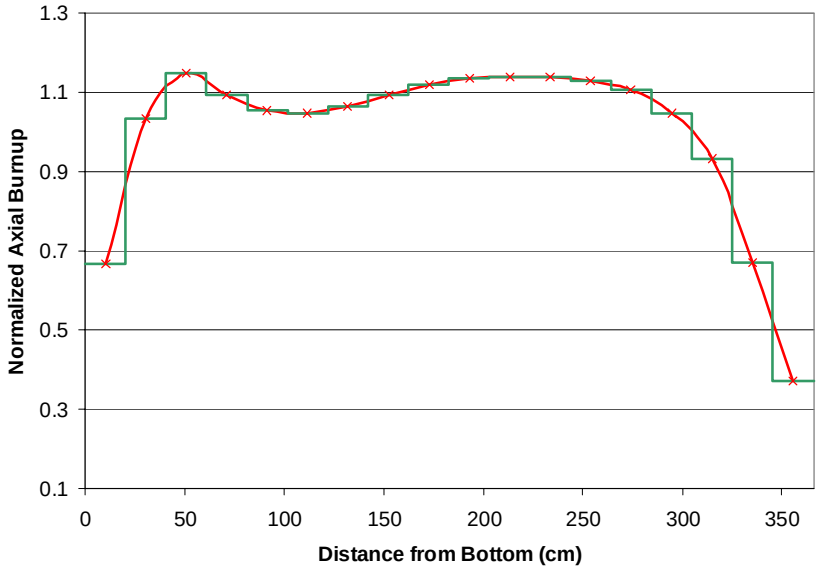

Figure 14 Bounding profile for burnup group 8 (18 < burnup < 22 GWd/MTU)

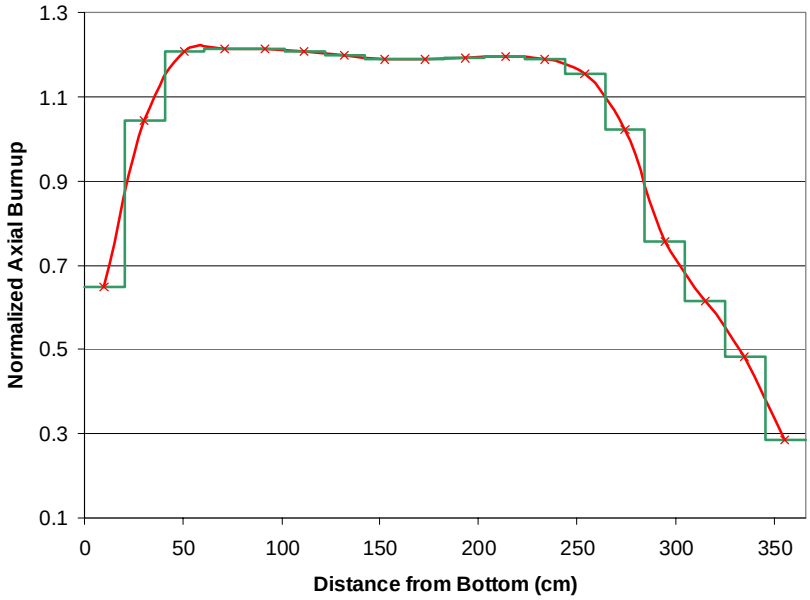

Figure 15 Bounding profile for burnup group 9 (14 < burnup < 18 GWd/MTU)

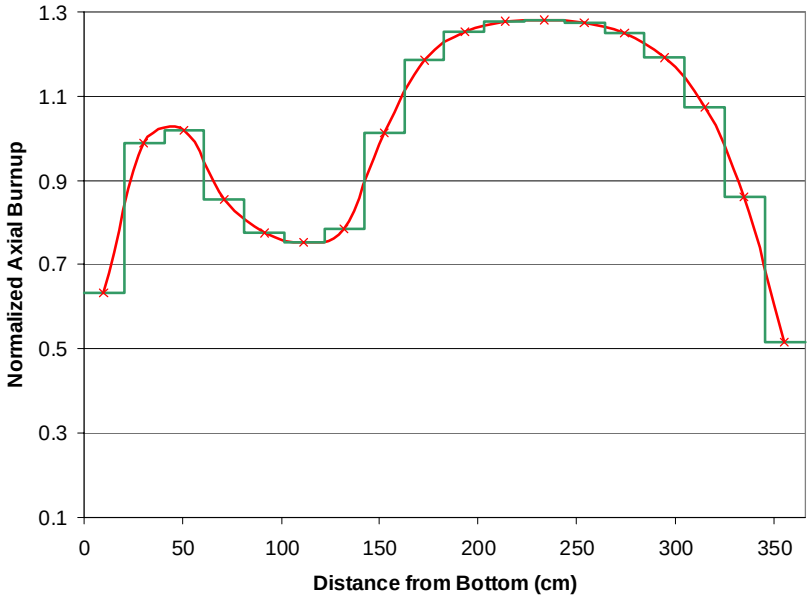

Figure 16 Bounding profile for burnup group 10 (10 < burnup< 14 GWd/MTU)

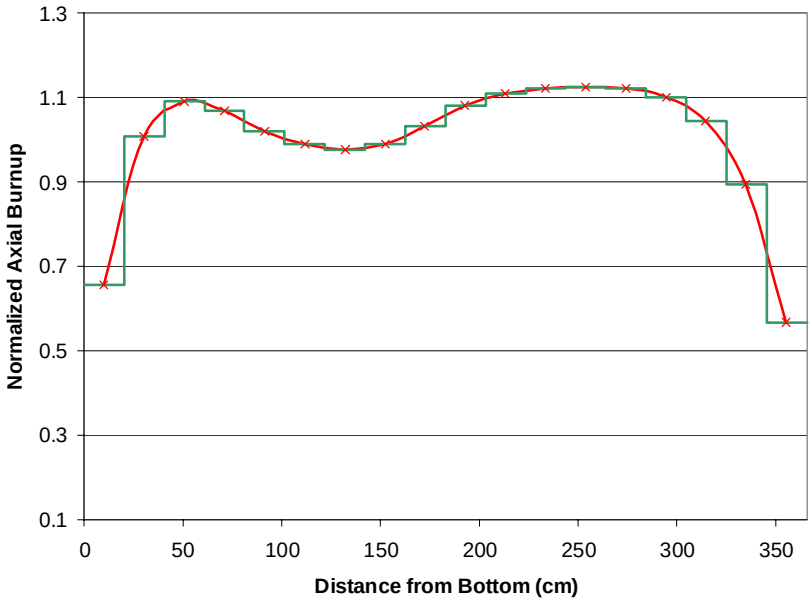

Figure 17 Bounding profile for burnup group 11 (6 < burnup < 10 GWd/MTU)

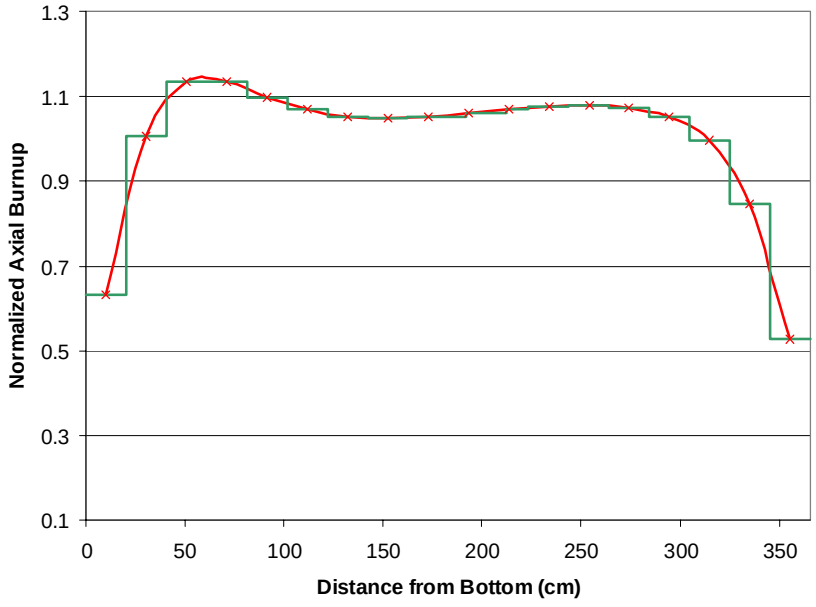

Figure 18 Bounding profile for burnup group 12 (burnup < 6 GWd/MTU)

4.2 EXAMINATION OF AXIAL-PROFILE DATABASE

4.2.1 Statistical Comparison of Profiles

Although the Ref. 8 database is comprehensive, it is not exhaustive. An obvious issue has been the adequacy of this (or any) finite database to completely represent the nearly-infinite variety of possible profiles resulting from irradiation in U.S. PWRs. To address this issue, a statistical evaluation was performed on the neutron multiplication factors resulting from the profiles contained in the database to assess the likelihood of the existence of axial profiles that have significantly higher reactivity. Based on the Ref. 8 database, the k_{eff} value associated with each of the axial-burnup profiles was calculated, as described in Subsection 4.1.2 (i.e., 1-D, actinides and fission products, and 5-year cooling time). Then, the mean and standard deviation for each of 12 burnup groups (see Table 2) were determined. The results are used to (1) assess how representative the bounding profiles are of the rest of the profiles and (2) provide an indication of the probability that other axial profiles might exist that are more reactive than the bounding profiles.

Comparison of the individual k_{eff} values to the mean and standard deviation for each burnup group reveals that the bounding profiles provide a significant increase in reactivity compared with the average. Figures 19–30 show the spread of k_{eff} values that result from the set of profiles in each of the 12 burnup groups considered. Note that the figures display the discrete k_{eff} values associated with each of the profiles in a given burnup group and are in arbitrary order. In addition to the individual calculated k_{eff} values, the figures show the mean k_{eff} value and indicators for 1, 2, and 3 standard deviations. An examination of the calculated k_{eff} values reveals that, for all but one of the 12 burnup groups, the k_{eff} value associated with the bounding axial profile, is more than 3 standard deviations above the mean and, in most cases, is more than 4 standard deviations above the mean. The only exception is burnup group 12 (burnup < 6 GWd/MTU), which has relatively few profiles (33 profiles) and is of little interest to burnup credit, particularly since the burnup profiles in group 12 yield a negative end effect. Nevertheless, the k_{eff} value associated with the bounding axial profile in group 12 is 2.2 standard deviations above the mean. The results are summarized in Table 6, which lists the mean, standard deviation, maximum, minimum, number of standard deviations that the maximum k_{eff} value is above the mean, and the maximum and average end effect for each burnup group. Additionally, the statistical distribution (in terms of percent) of k_{eff} values within each group is shown in Table 7. The results in these tables demonstrate that the bounding profiles from the Ref. 8 database can be considered statistical outliers, as opposed to representative of typical SNF profiles. For confirmatory purposes, a statistical comparison was also performed on the k_{eff} values from 3-D calculations with the GBC-32 cask, which were described in the previous section. The results, which are provided in Appendix B, are completely consistent with those described above. Consequently, for the fuel characteristics and reactor operations included in the database, one can infer that the probability that other axial profiles exist that are notably more reactive than the bounding profiles (determined from the Ref. 8 database) is very small. Trends with fuel characteristics and reactor operations are explored in the following section.

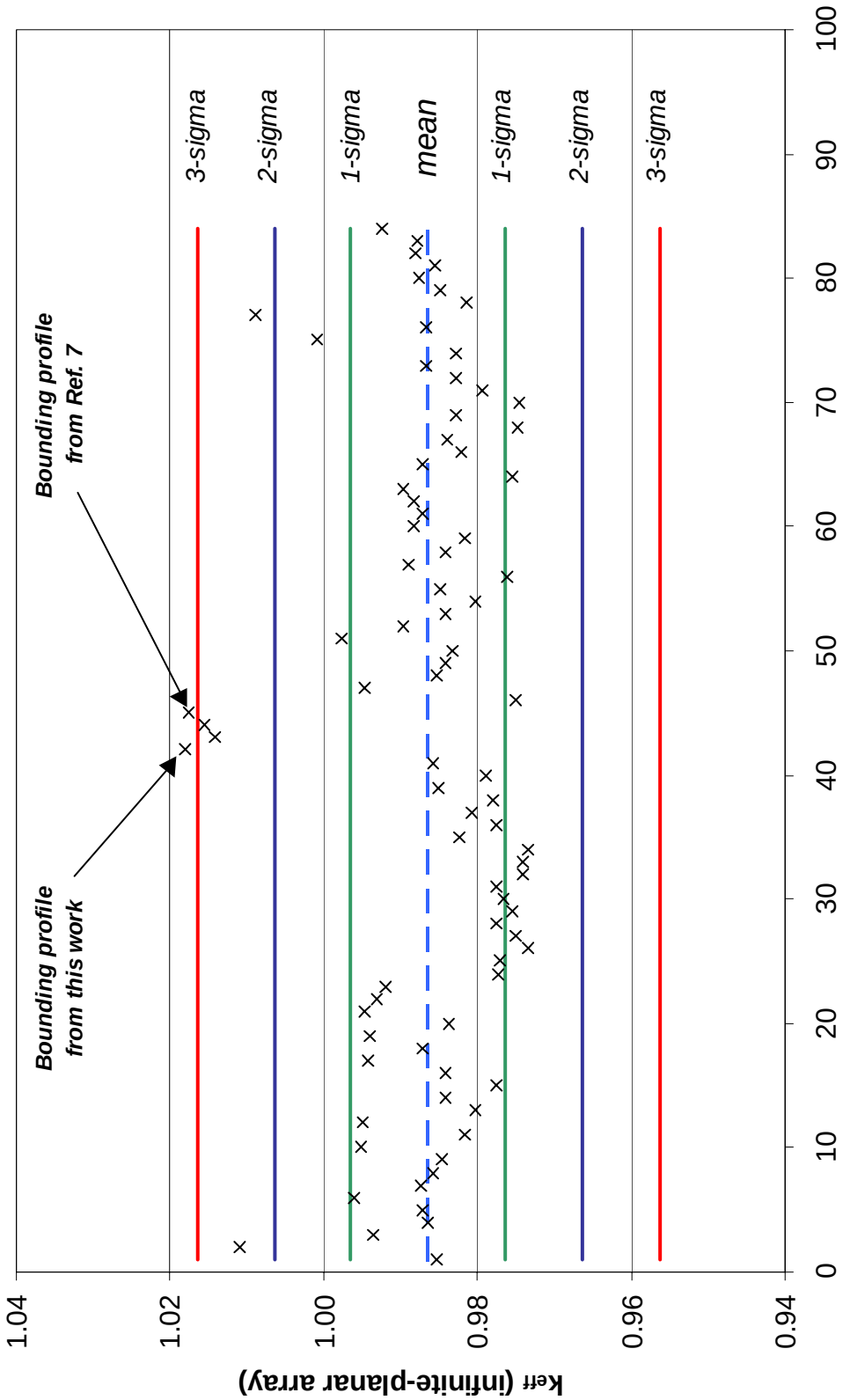

Figure 19 Plot of k_{eff} values for axial-burnup profiles in burnup group 1 (burnup > 46 GWd/MTU). Total number of profiles in this burnup group is 84.

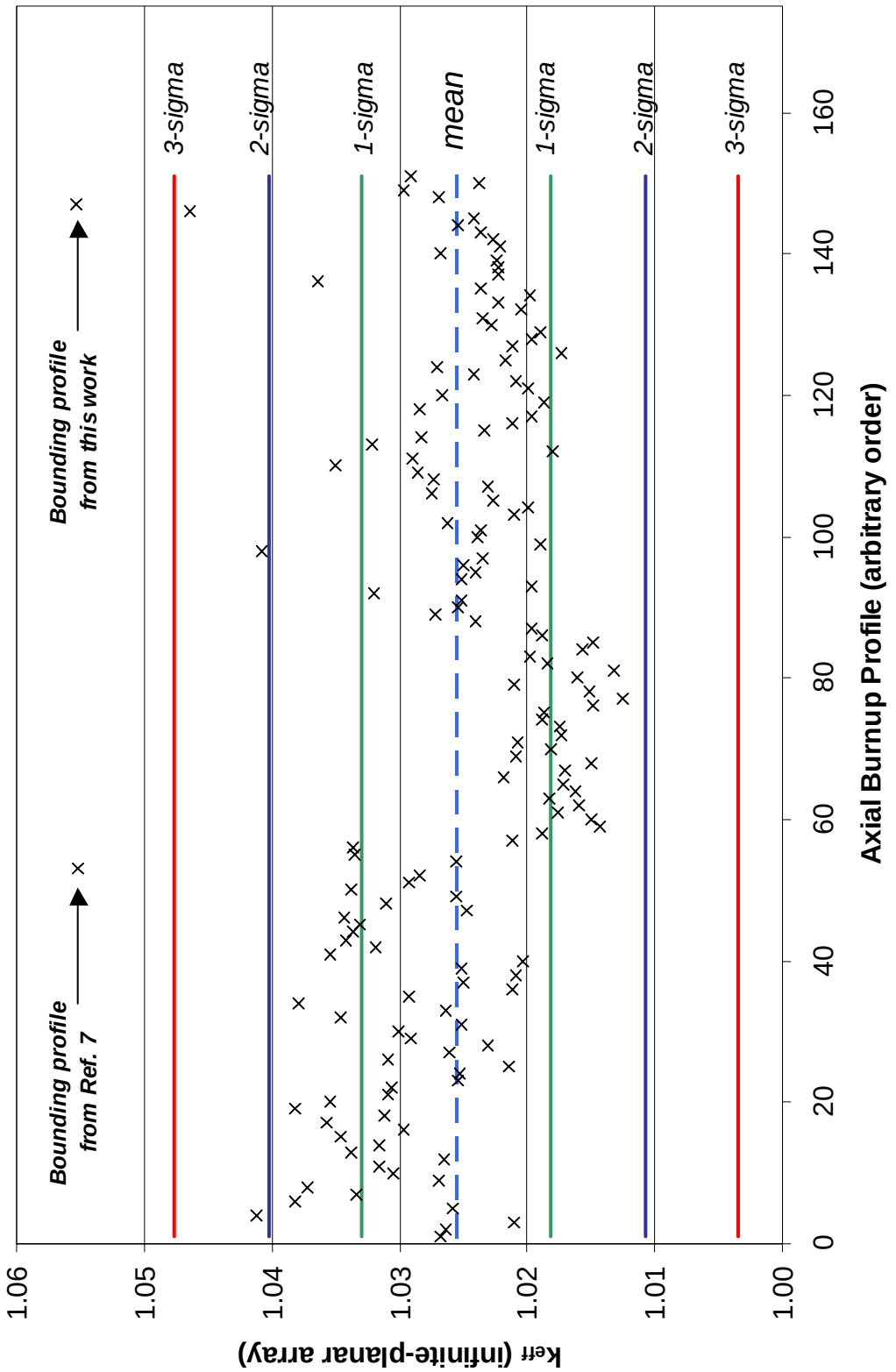

Figure 20 Plot of k_{eff} values for axial-burnup profiles in burnup group 2 (42 < burnup < 46 GWd/MTU). Total number of profiles in this burnup group is 151.

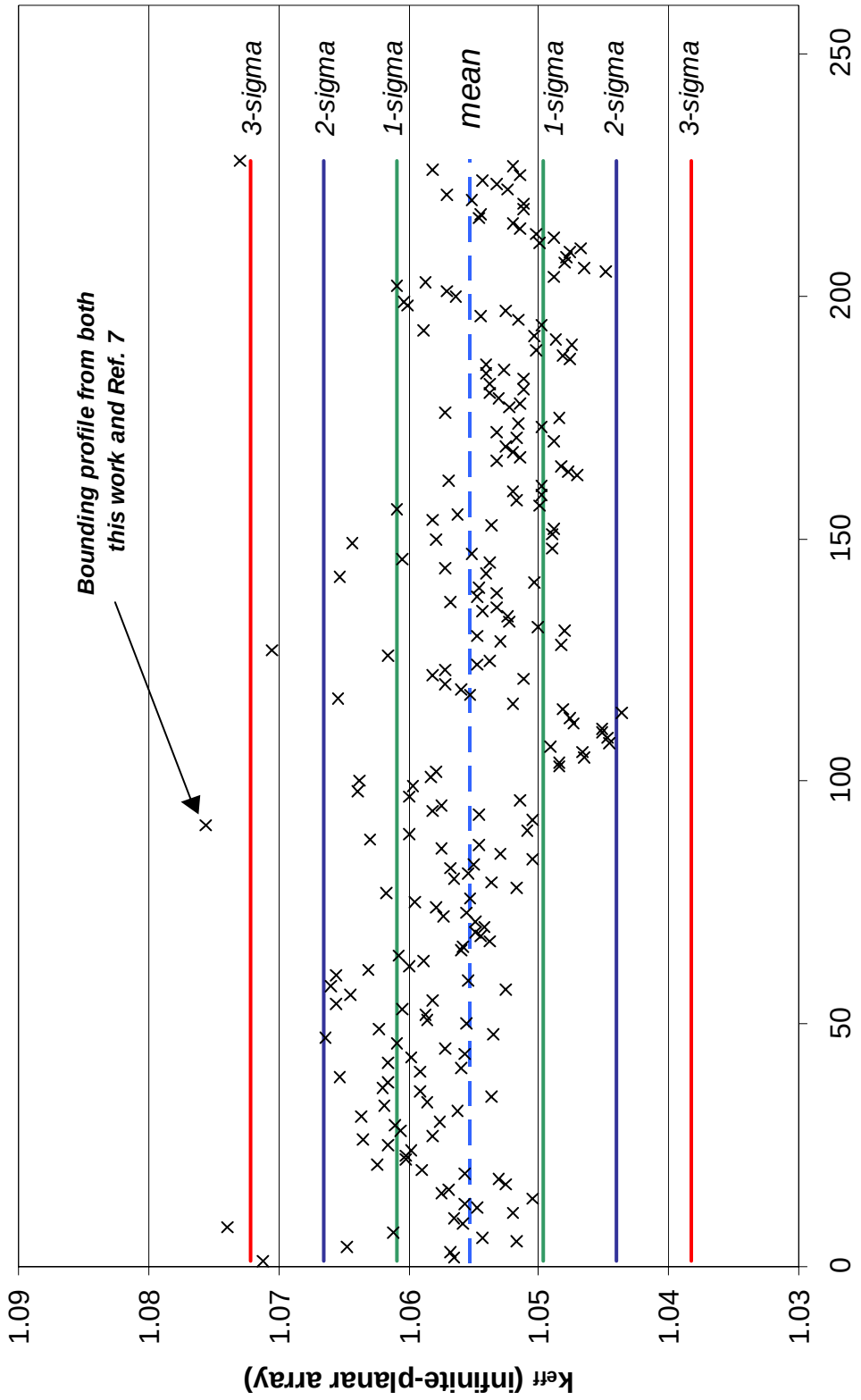

Figure 21 Plot of k_{eff} values for axial-burnup profiles in burnup group 3 (38 < burnup < 42 GWd/MTU). Total number of profiles in this burnup group is 228.

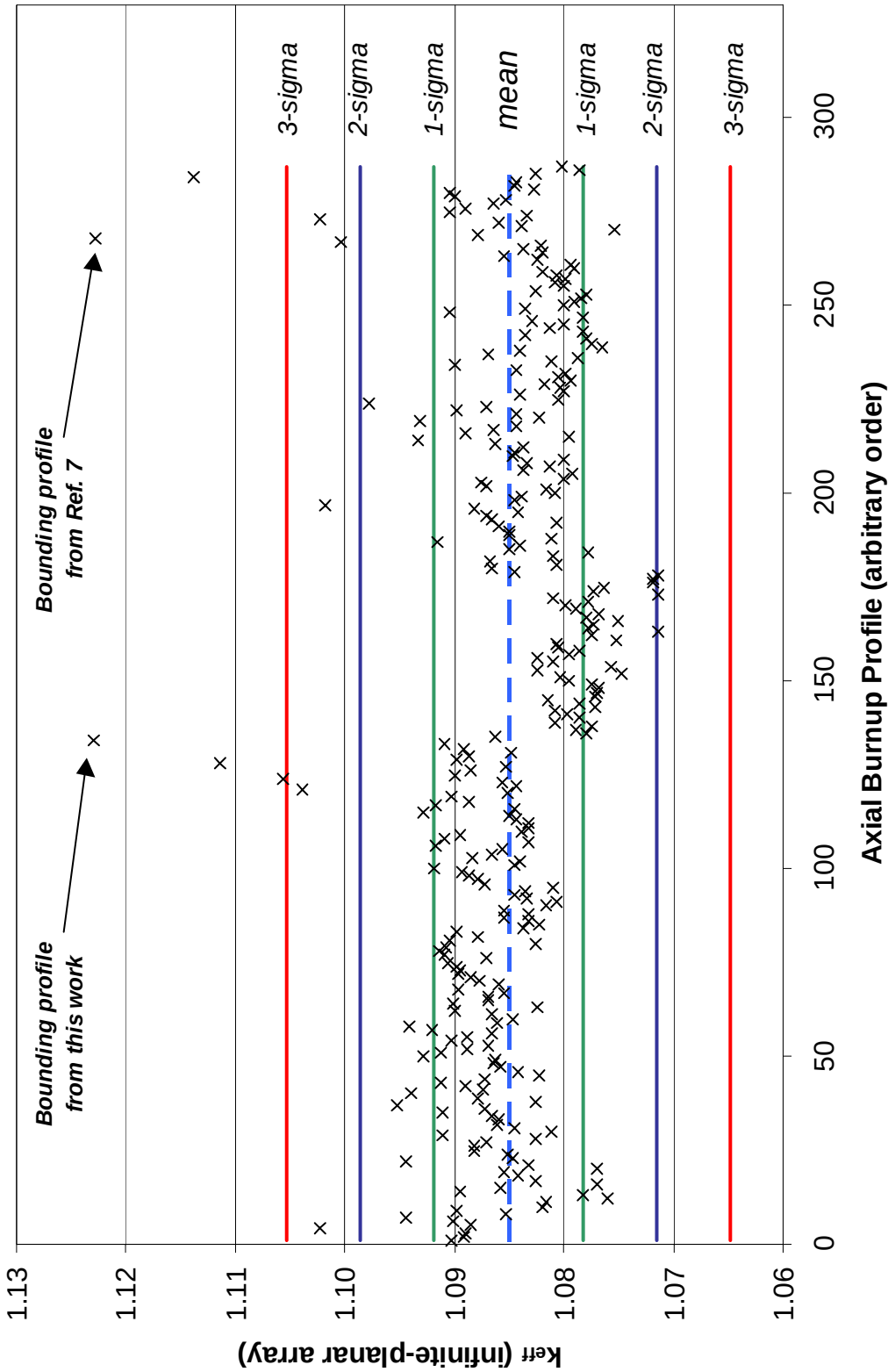

Figure 22 Plot of k_{eff} values for axial-burnup profiles in burnup group 4 (34 < burnup < 38 GWd/MTU). Total number of profiles in this burnup group is 287.

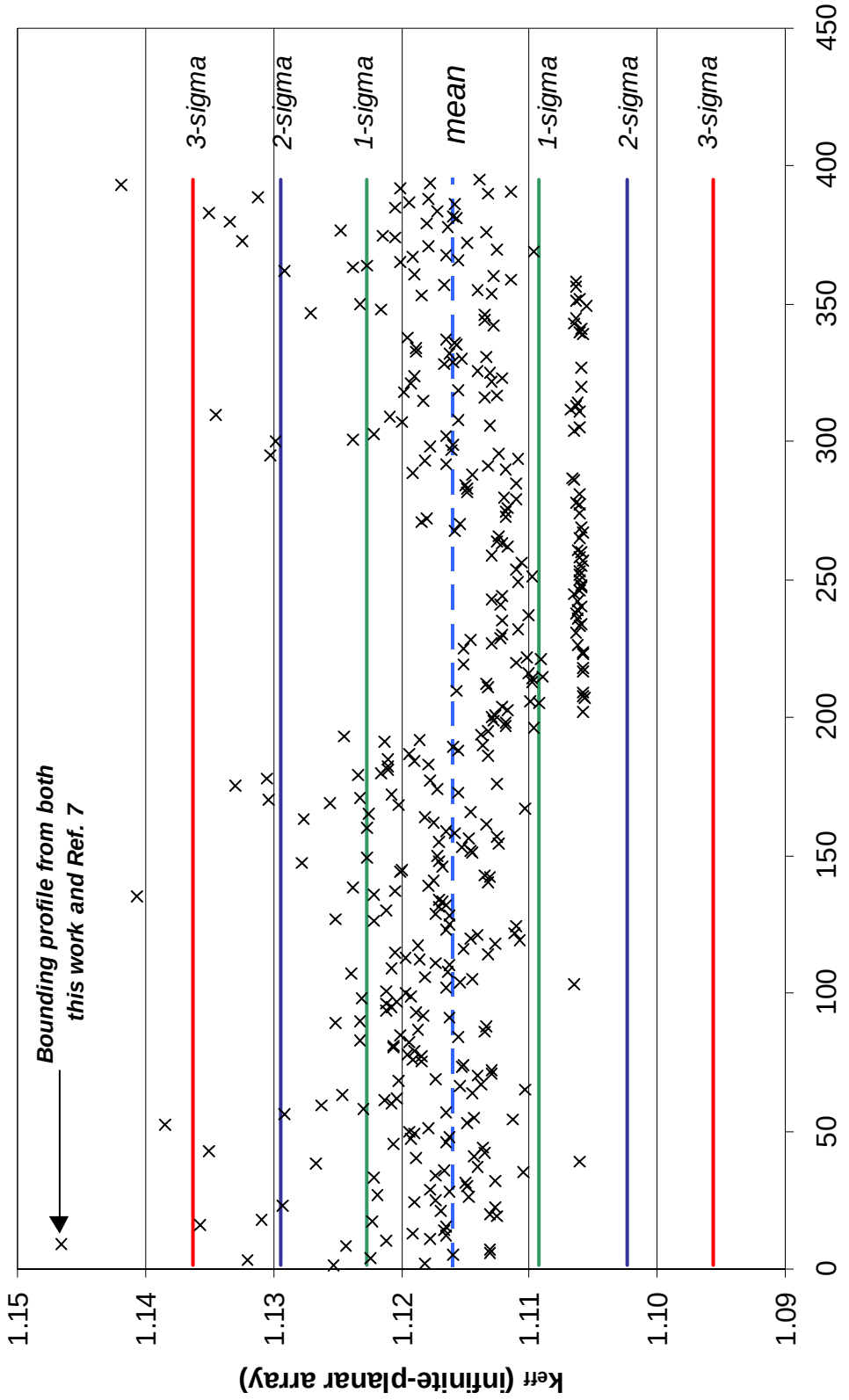

Figure 23 Plot of k_{eff} values for axial-burnup profiles in burnup group 5 (30 < burnup < 34 GWd/MTU). Total number of profiles in this burnup group is 395.

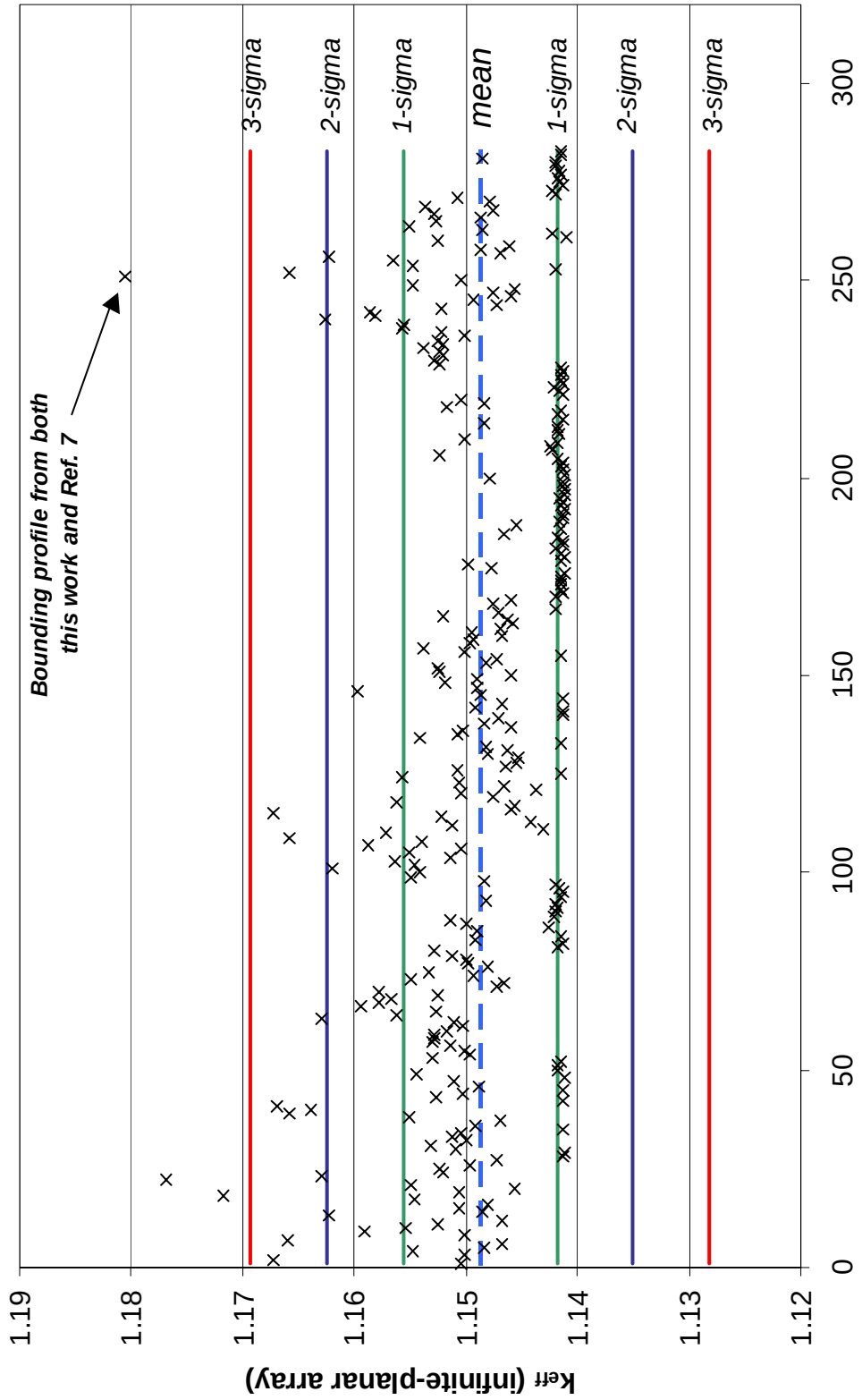

Figure 24 Plot of k_{eff} values for axial-burnup profiles in burnup group 6 (26 < burnup < 30 GWd/MTU). Total number of profiles in this burnup group is 283.

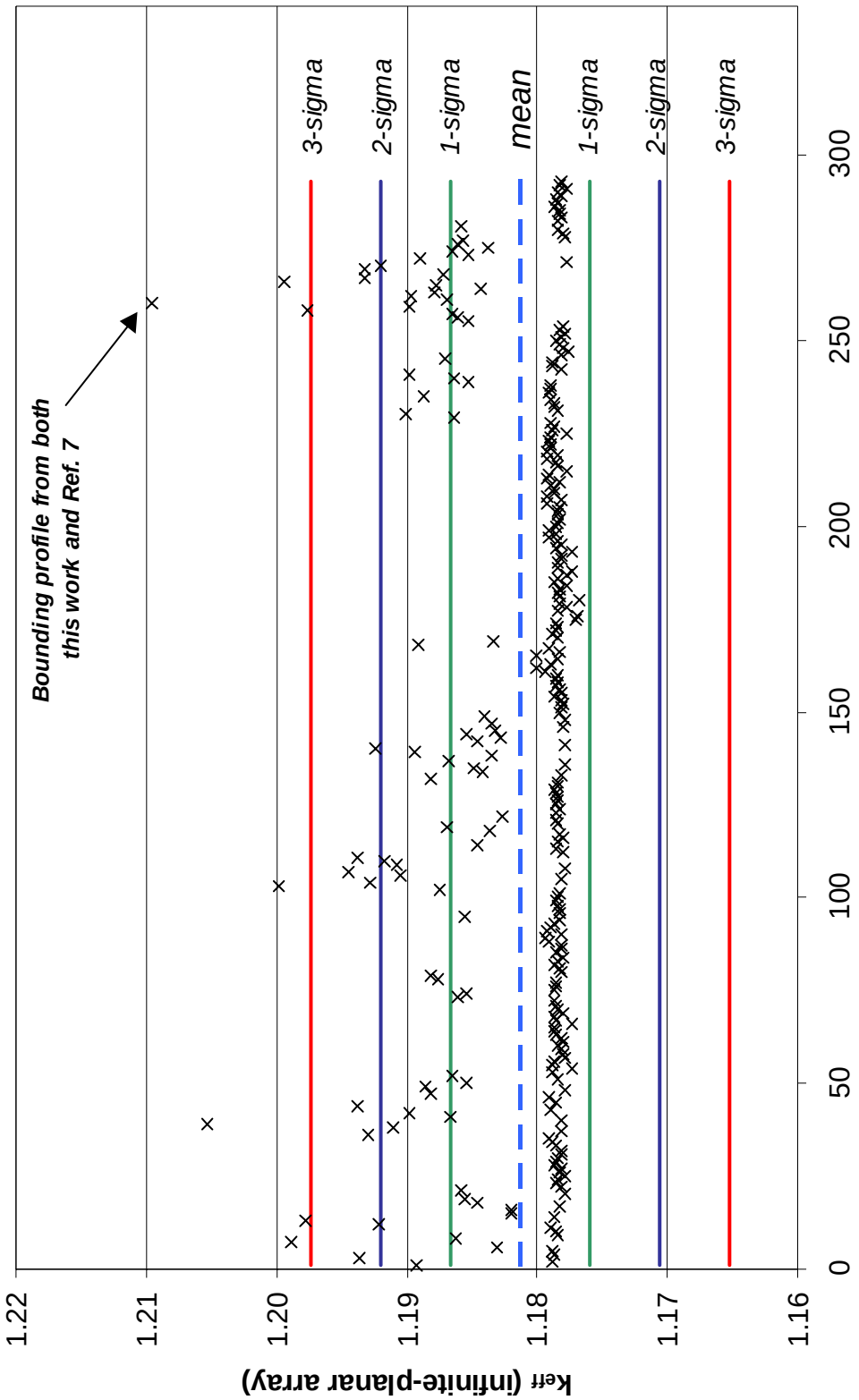

Figure 25 Plot of k_{eff} values for axial-burnup profiles in burnup group 7 (22 < burnup < 26 GWd/MTU). Total number of profiles in this burnup group is 293.

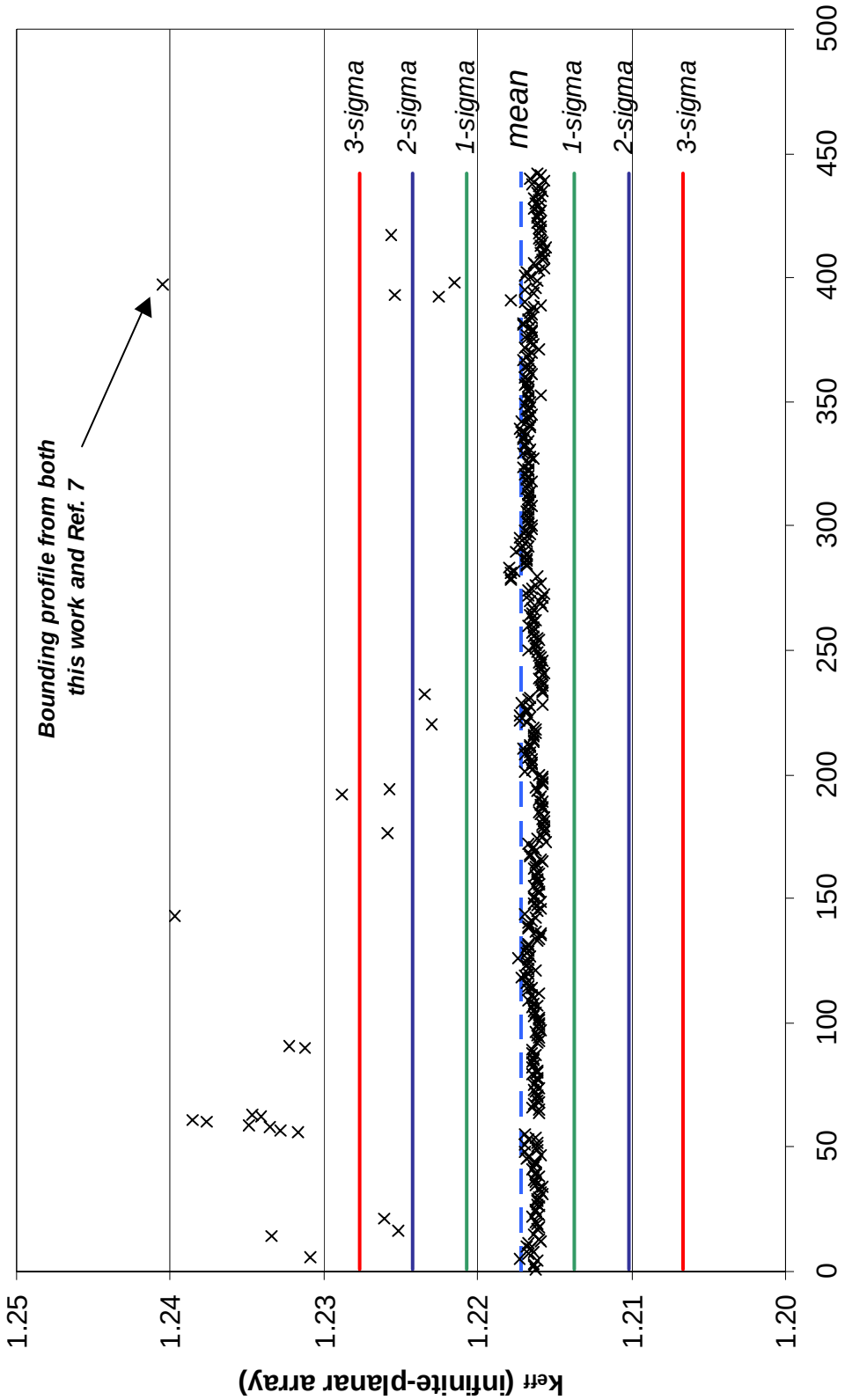

Figure 26 Plot of k_{eff} values for axial-burnup profiles in burnup group 8 (18 < burnup < 22 GWd/MTU). Total number of profiles in this burnup group is 442.

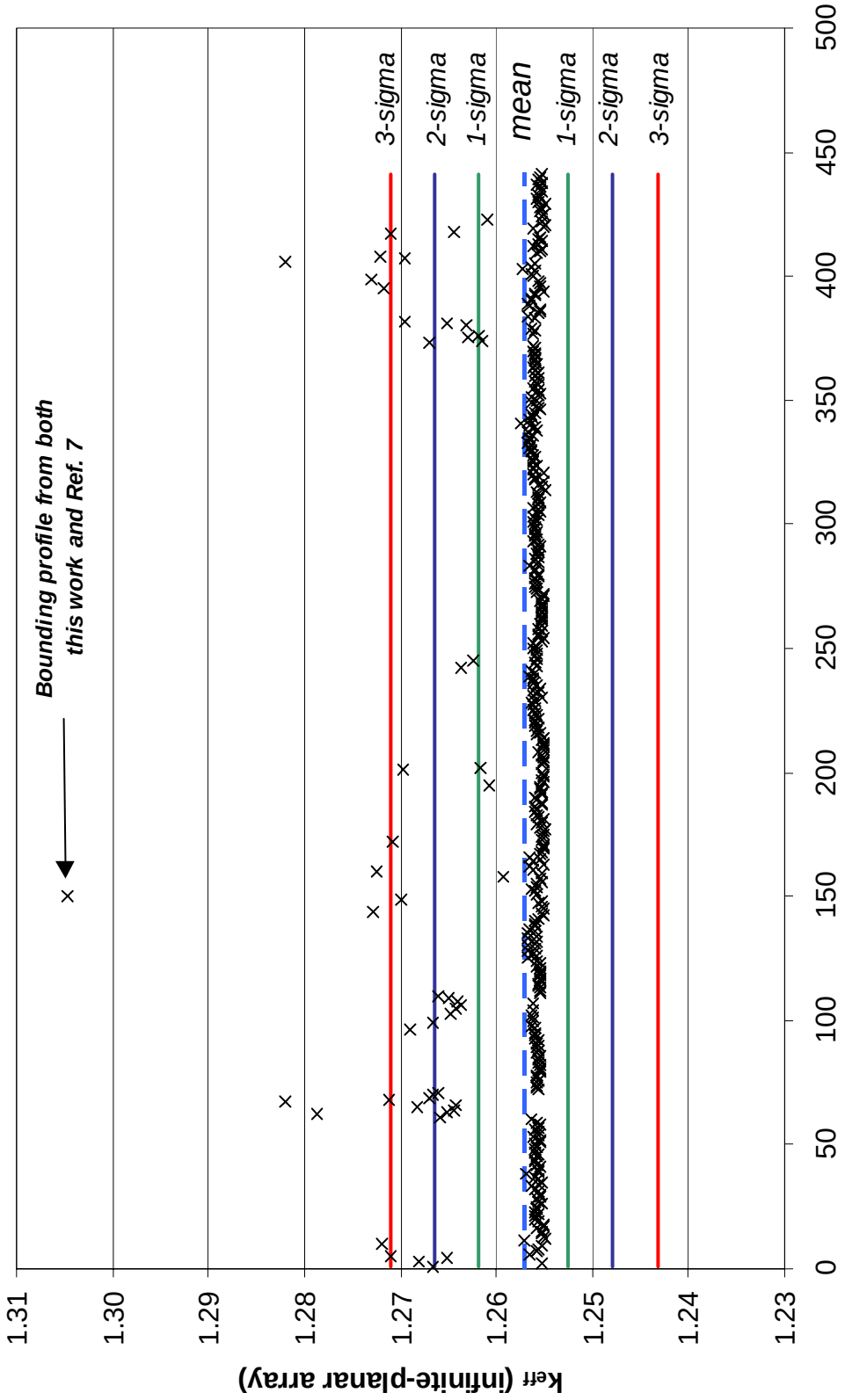

Figure 27 Plot of k_{eff} values for axial-burnup profiles in burnup group 9 (14 < burnup < 18 GWd/MTU). Total number of profiles in this burnup group is 441.

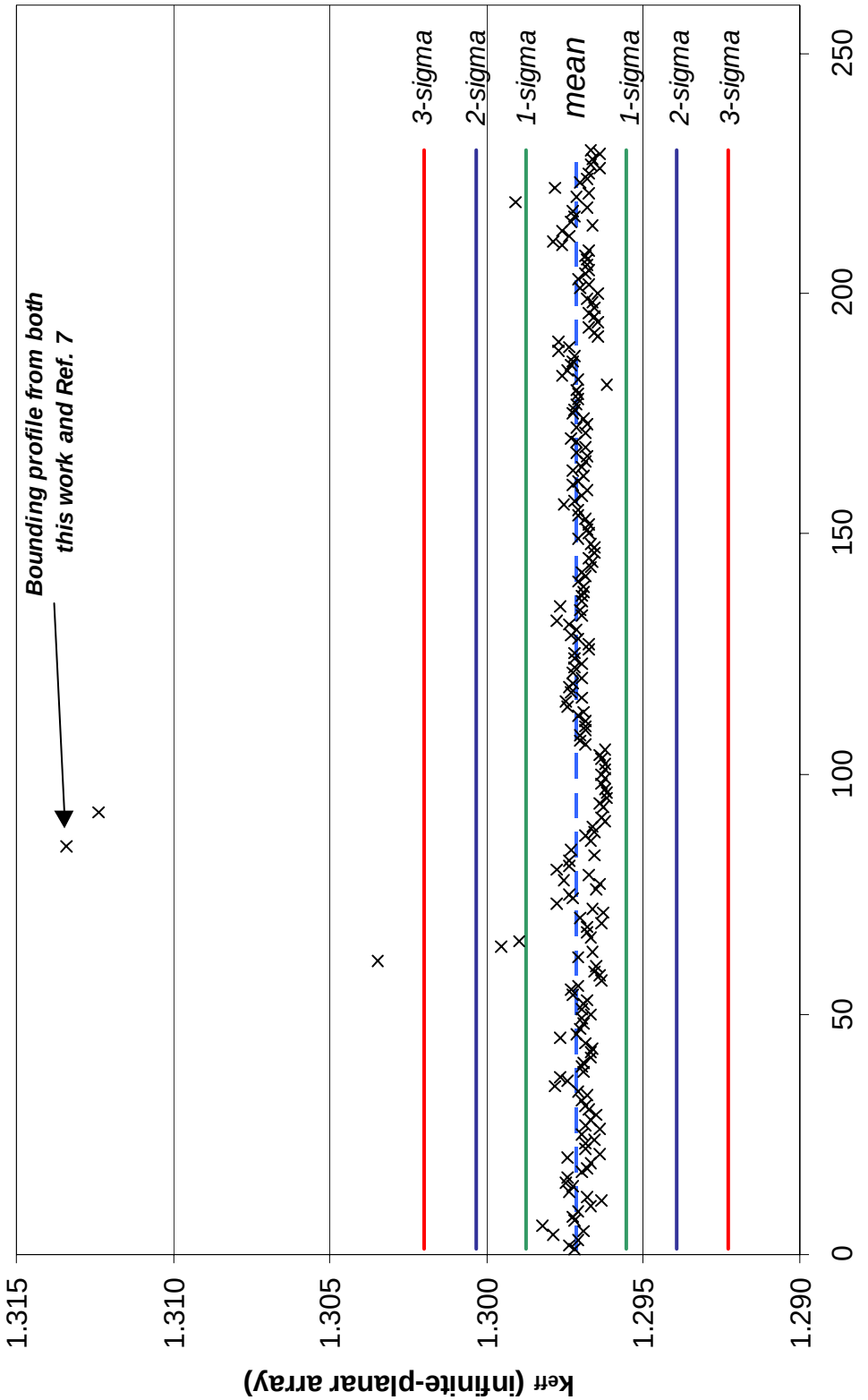

Figure 28 Plot of k_{eff} values for axial-burnup profiles in burnup group 10 (10 < burnup < 14 GWd/MTU). Total number of profiles in this burnup group is 230.

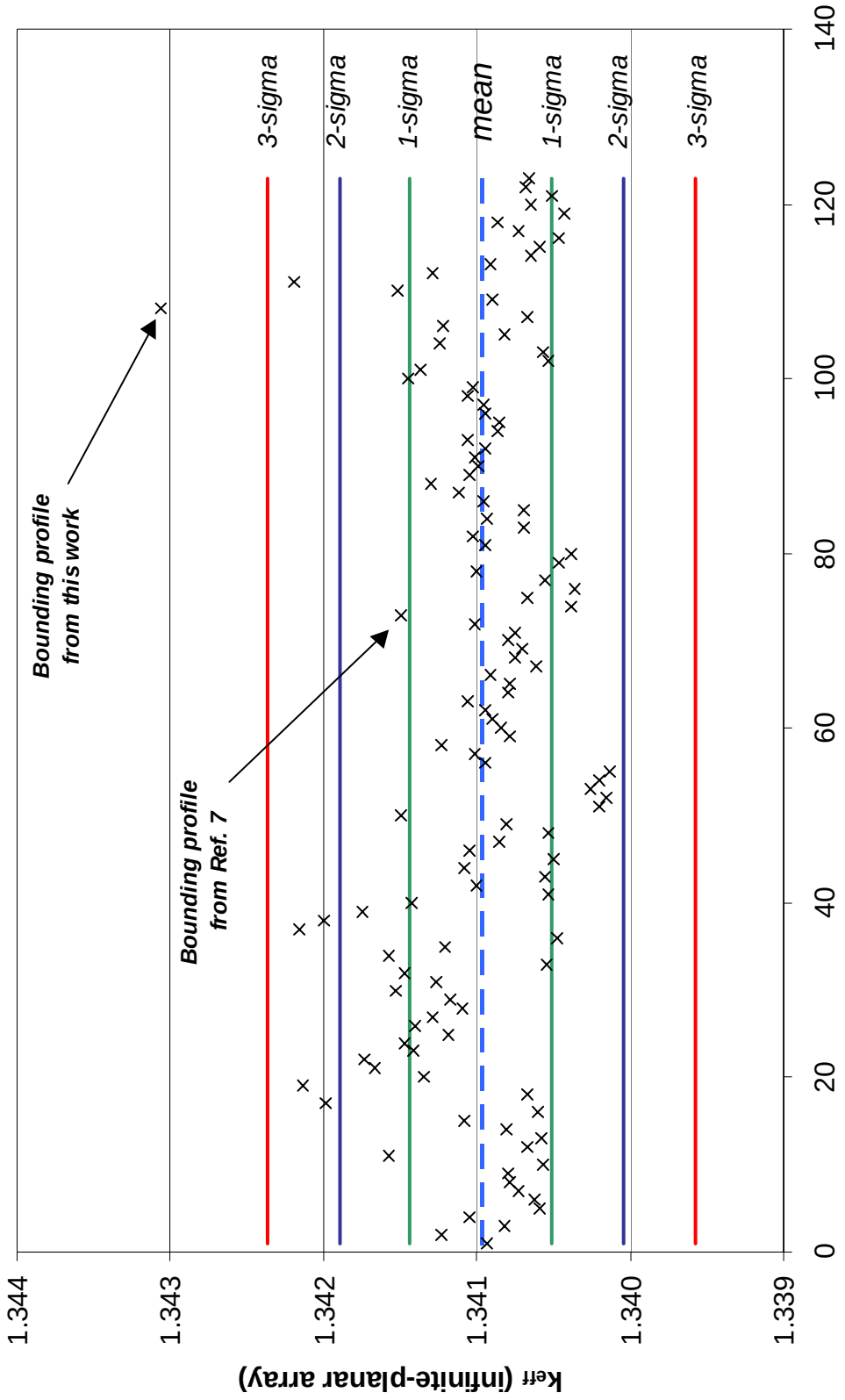

Figure 29 Plot of k_{eff} values for axial-burnup profiles in burnup group 11 (6 < burnup < 10 GWd/MTU). Total number of profiles in this burnup group is 123.

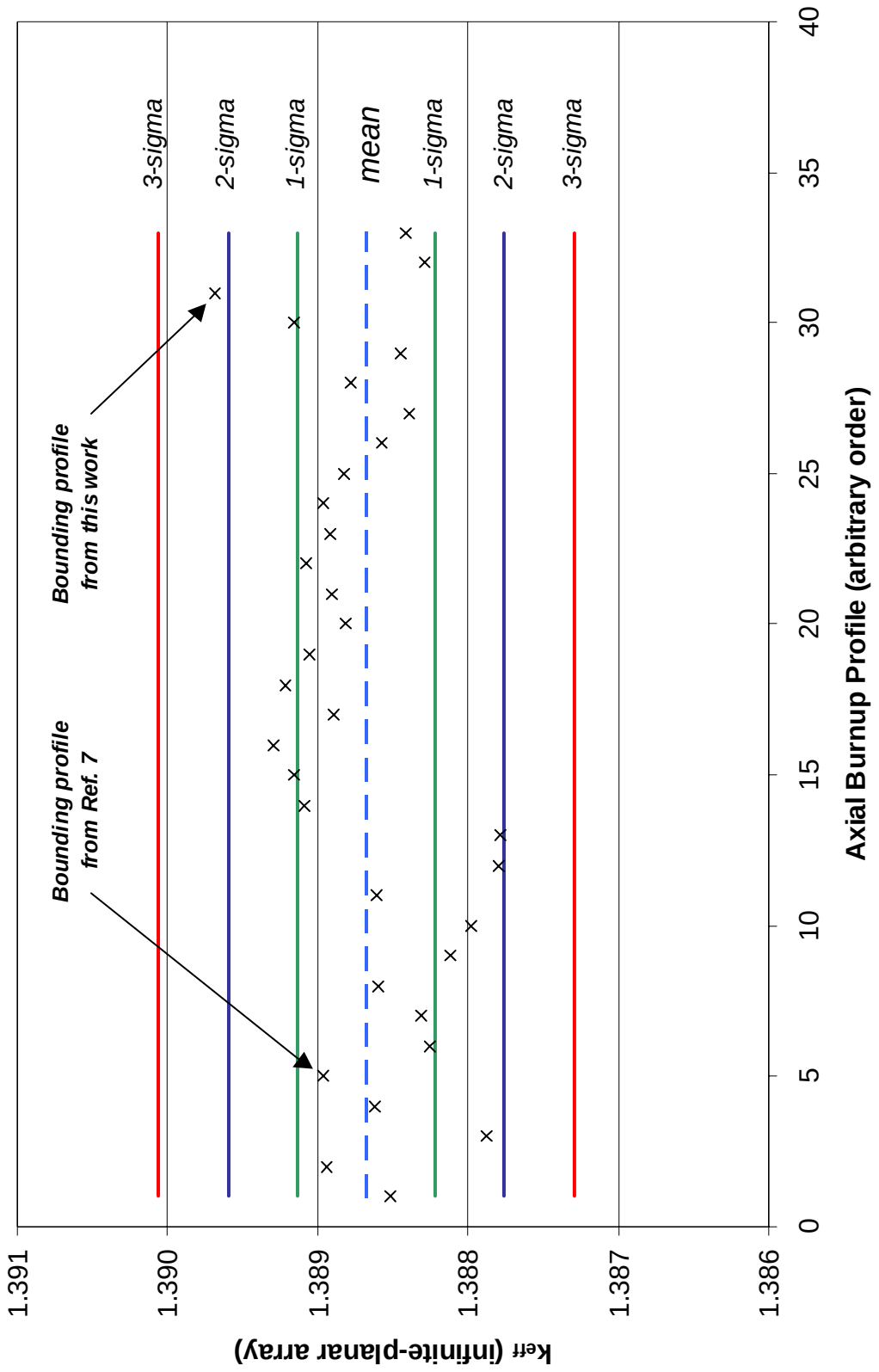

Figure 30 Plot of k_{eff} values for axial-burnup profiles in burnup group 12 (burnup < 6 GWd/MTU). Total number of profiles in this burnup group is 33.

Table 6 Summary of k_{eff} values (infinite radial array) with the Ref. 8 database

Burnup group	Analysis burnup (GWd/MTU)	k_{eff} values				Number of standard deviations that the maximum k_{eff} value is above the mean	End effect	
		Mean	Standard deviation	Minimum	Maximum		Maximum	Minimum
1	50	0.98642	0.01003	0.97335	1.01800	3.1	0.04754	0.01596
2	44	1.02552	0.00738	1.01252	1.05540	4.1	0.04098	0.01110
3	40	1.05524	0.00564	1.04364	1.07555	3.6	0.02932	0.00901
4	36	1.08505	0.00677	1.07133	1.12293	5.6	0.04532	0.00744
5	32	1.11594	0.00676	1.10556	1.14655	4.5	0.03258	0.00197
6	28	1.14874	0.00688	1.14102	1.18054	4.6	0.03090	!0.00090
7	24	1.18131	0.00535	1.17679	1.20963	5.3	0.02322	!0.00510
8	20	1.21719	0.00352	1.21551	1.24055	6.6	0.01634	!0.00702
9	16	1.25716	0.00464	1.25485	1.30460	10.2	0.04133	!0.00611
10	12	1.29713	0.00161	1.29617	1.31339	10.1	0.00940	!0.00686
11	8	1.34097	0.00046	1.34013	1.34306	4.5	!0.00394	!0.00603
12	4	1.38868	0.00046	1.38779	1.38968	2.2	!0.00260	!0.00360

Table 7 Statistical distribution (in terms of percent) of k_{eff} values in each burnup group

Burnup group	Standard deviations from the mean									
	1	2	3	4	5	6	7	8	9	10
1	77.4[†]	92.9	97.6	100.0						
2	70.2	96.7	98.7	98.7	100.0					
3	69.3	97.4	98.7	100.0						
4	80.1	95.5	98.3	99.0	99.3	100.0				
5	72.9	95.4	99.0	99.7	100.0					
6	62.5	95.1	98.9	99.3	100.0					
7	84.6	93.9	97.6	99.3	99.7	100.0				
8	94.3	95.2	96.6	97.3	98.9	99.3	100.0			
9	89.8	94.1	97.5	99.1	99.3	99.8	99.8	99.8	99.8	99.8
10	97.4	98.7	98.7	99.1	99.1	99.1	99.1	99.6	99.6	100.0
11	74.8	95.1	99.2	99.2	100.0					
12	69.7	97.0	100.0							

[†] Interpret as 77.4 percent of the profiles in burnup group 1 yield k_{eff} values that are within 1 standard deviation of the mean.

4.2.2 Comparison of Profiles from Different Fuel Designs and Reactors

A concern with any data set (such as the axial-profile database) is the possibility that the data set is biased by one or more data subsets. In the case of the Ref. 8 database, the concern is whether the conclusions reached by analysis of the database are dictated by data from a single reactor or fuel type. Although the spread in the results shown in the previous section and the fact that the 12 bounding profiles include profiles from 7 different plants suggest that this is not the case, trends with fuel type and reactor are investigated in this section. The calculated results associated with each of the axial-burnup profiles have been plotted in terms of fuel type and reactor to assess the existence of trends with fuel type and/or reactor operations.

Figures 31–42 plot the Δk values (k_{eff} value associated with a given profile minus average k_{eff} value for the burnup group) in terms of fuel type (e.g., B&W 15 × 15) for each of the burnup groups. The bounding profiles are evident in these figures. Although these figures demonstrate that the bounding profile is often associated with the B&W 15 × 15 assembly, one should note that the B&W 15 × 15 fuel type is by far the most prevalent fuel type in the database (1334 of the 3169 profiles; 42% of the total, representing eight different reactors). The Δk values for each of the fuel types exhibit similar variability, which suggests an absence of any clear trends with fuel type. However, it appears that the CE fuel types may exhibit a smaller end effect on average.

Figures 43–54 show the Δk values (k_{eff} value associated with a given profile minus average k_{eff} value for the burnup group) in terms of reactor (e.g., Davis Besse) for each of the burnup groups. The Δk values for each of the reactors exhibit similar variability, which suggests an absence of any clear trends with reactor-specific operations. However, the results of these and previous figures suggest greater variability in the Δk values from reactors utilizing B&W 15 × 15 assemblies. This observation has been confirmed by comparison of the standard deviations in k_{eff} values from the various fuel types. It is difficult to decipher whether the greater observed variability for the B&W 15 × 15 assemblies is real, or can be attributed to the greater representation within the database relative to the other fuel types. Based on visual examination of the profiles and a review of past B&W plant operations, it is suspected that the variability is real and associated with the use of control rods and axial power shaping rods.

4.2.3 Observations

Some specific comments on the examination of the axial-profile database[8] are offered below.

1. Some of the B&W plants, such as Davis Besse and Crystal River, have used control rods for routine reactor control, which suppresses the burnup near the top (see for example Figure 15) and leads to more reactive axial profiles. Also, B&W plants are the only ones that use axial power shaping rods, which can suppress the burnup near the center (see Figures 14 and 16). Of the 12 bounding profiles plotted in Figures 7–18, eleven are from B&W 15 × 15 plants.

2. Regarding the four most reactive profiles in burnup group 1 (see Figure 19), these profiles are from Millstone Unit 3. Fifty-six of the 62 profiles in the Ref. 8 database from Millstone Unit 3 are "zoned" profiles, which means they have axial blanket (or end) regions with reduced enrichment. Axial blankets are low enrichment (between ~0.71 and 2.6 wt % ^{235}U) regions, generally six inches in length, at the top and bottom of some assemblies; the majority of currently discharged SNF do not have axial blankets. Reduced fuel enrichment at the top and bottom, where power and fuel utilization are low, reduces neutron leakage from the top and bottom of the core and improves fuel cycle economics through greater fuel utilization. Hence, the trend in fuel design is towards greater use of

axial blankets. Because the axial blankets have significantly lower enrichment than the central region, the end effect for assemblies with axial blankets is typically very small or negative. Furthermore, the lower the initial enrichment of the axial blankets is with respect to the higher enrichment central region, the lower is the end effect. Consequently, profiles from assemblies with axial blankets were not considered in this or previous (Ref. 7) bounding profile analyses.

The six Millstone Unit 3 profiles that do not have axial blankets, and particularly the four profiles in burnup group 1, exhibit an end effect that is much greater than the average. To understand the reason for this, the contributor of those profiles was contacted and it was confirmed that these particular profiles were used in transition cores from non-axial blanketed fuel to axial blanketed fuel. In other words, these six assemblies (without axial blankets) experienced burnup in proximity to assemblies with axial blankets. Hence, the burnup near the ends of these assemblies was suppressed by neighboring assemblies with axial blankets.

3. In communicating with one contributor of axial profiles, it was discovered that the axial profiles in the Ref. 8 database might not be truly representative of *typical* SNF. Because this particular contributor was aware of the intended purpose of the axial-profile database (establish bounding axial profiles for burnup-credit analyses based on actual profiles), he elected to contribute profiles that exhibited the most significant burnup gradient near the ends. Thus, this contributor effectively biased his contributed profiles toward higher end effects. Upon learning this, the principal author of the Ref. 8 database was contacted to inquire about the nature of the instructions that were given to potential axial-burnup profile contributors. The Ref. 8 author supplied the actual solicitation for axial-burnup profiles and confirmed that potential contributors were simply asked to supply axial-burnup profiles; they were not asked to selectively submit profiles. However, because the intended purpose was described in the solicitation, it is possible that other contributors (in addition to the one noted above) may have selectively submitted their most-reactive profiles. Although it is doubtful that others took the time to selectively submit profiles, this possibility could actually bias the database toward higher reactivity axial profiles. Note, however, that if this is the case, it would introduce a conservative bias into the database.

4. It is apparent from this examination that a wide variety of assemblies and profiles are represented. For example, inspection of the bounding profiles for burnup groups 8–10 (see Figures 14–16) suggests that these profiles have experienced significant exposure to control rods and/or APSRs. It is worth noting that these particular profiles are from assemblies with very low enrichment (~2 wt % ^{235}U); indicating they correspond to early operations in which control rods were used to a greater extent than they currently are used. As trends in fuel design and reactor operations change, the database should be expanded to include the potential effects on axial profiles.

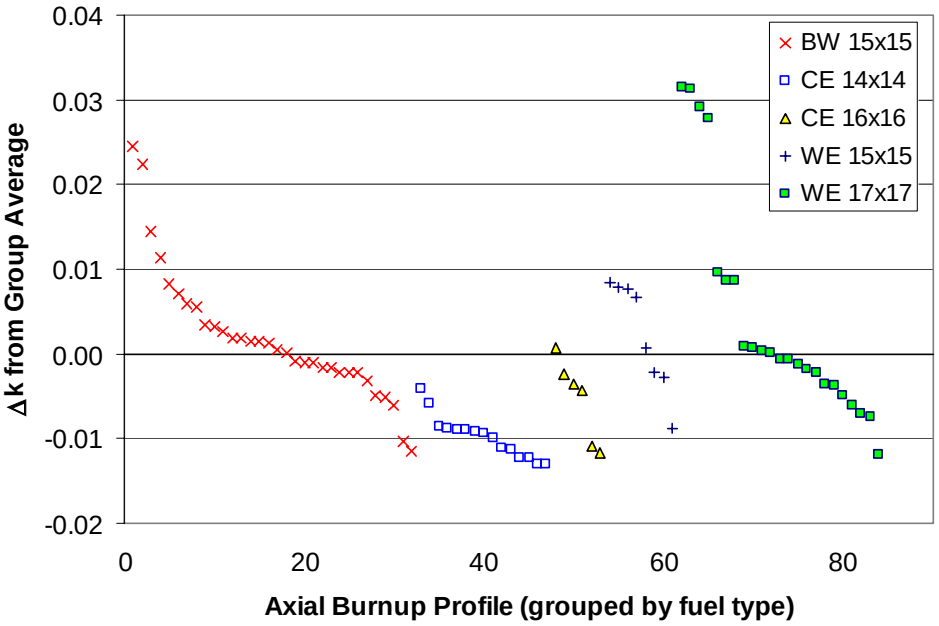

Figure 31 Δ*k* values plotted in terms of fuel type for axial-burnup profiles in burnup group 1 (burnup > 46 GWd/MTU)

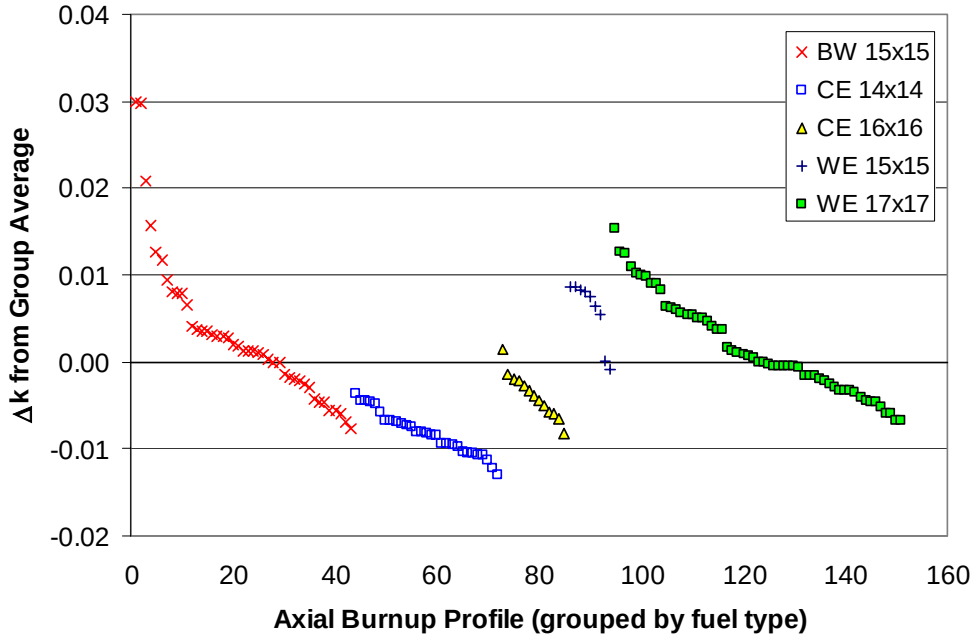

Figure 32 Δ*k* values plotted in terms of fuel type for axial-burnup profiles in burnup group 2 (42 < burnup < 46 GWd/MTU)

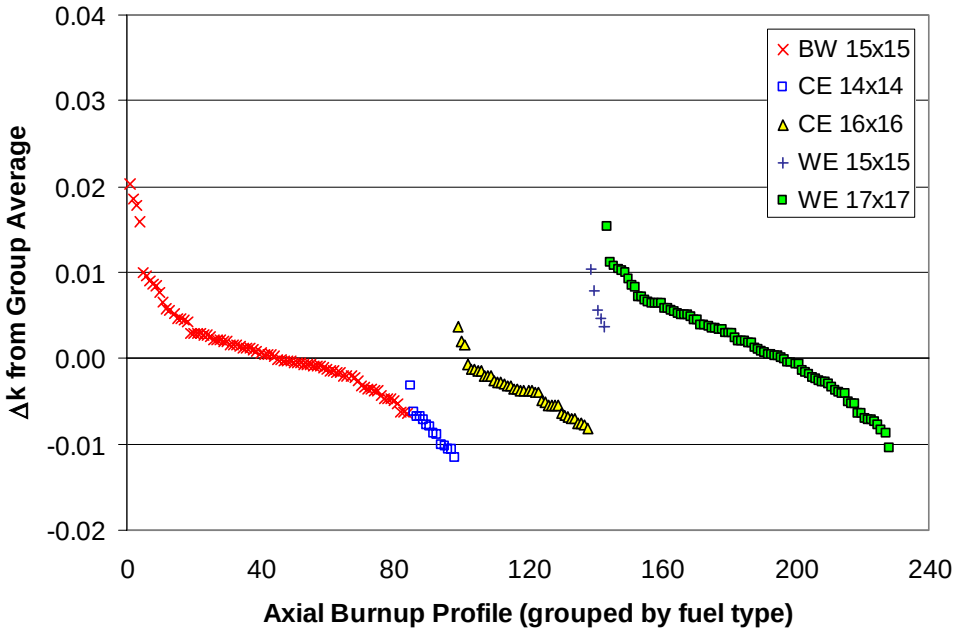

Figure 33 Δ*k* values plotted in terms of fuel type for axial-burnup profiles in burnup group 3 (38 < burnup < 42 GWd/MTU)

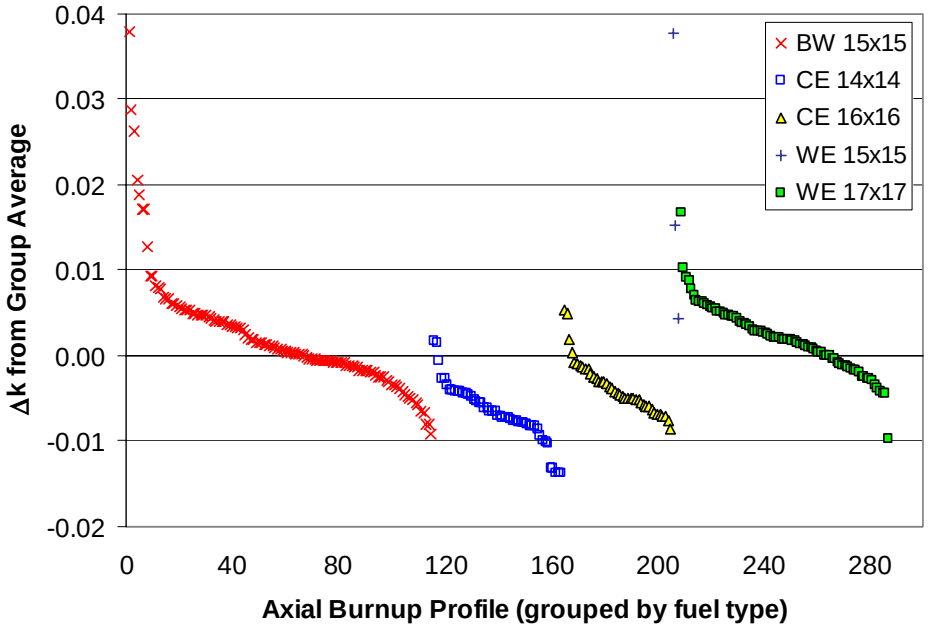

Figure 34 Δ*k* values plotted in terms of fuel type for axial-burnup profiles in burnup group 4 (34 < burnup < 38 GWd/MTU)

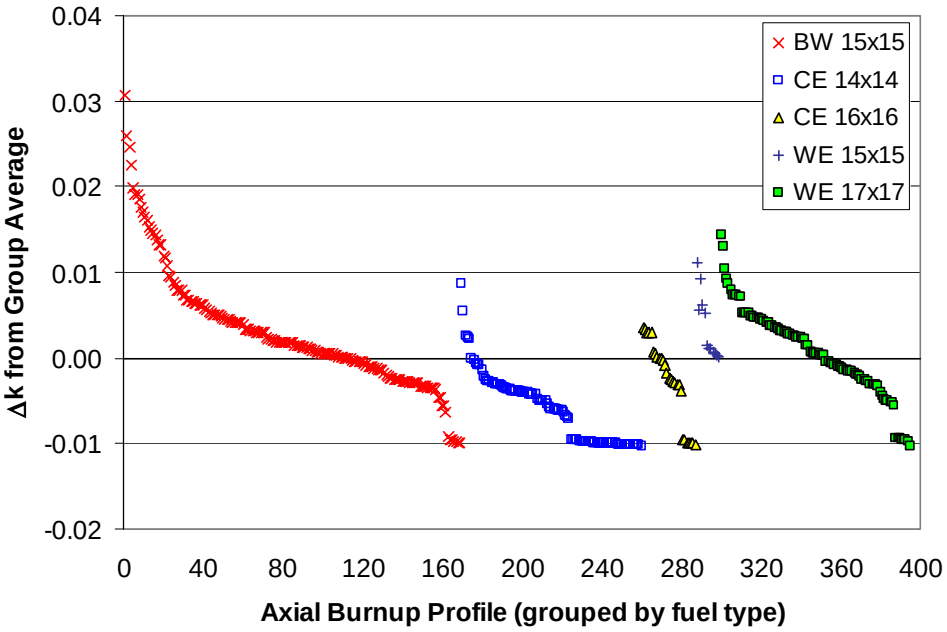

Figure 35 Δ*k* values plotted in terms of fuel type for axial-burnup profiles in burnup group 5 (30 < burnup < 34 GWd/MTU)

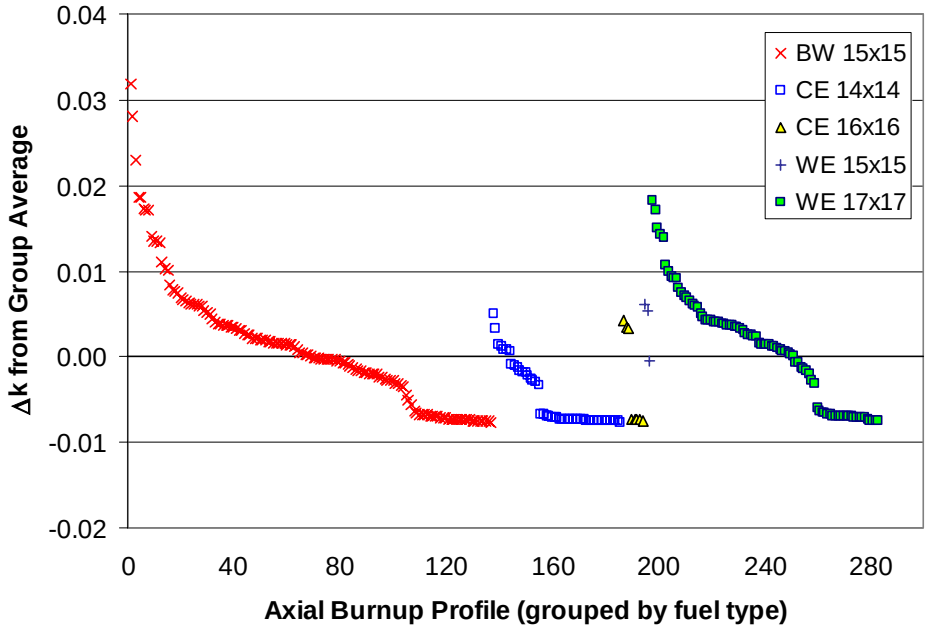

Figure 36 Δ*k* values plotted in terms of fuel type for axial-burnup profiles in burnup group 6 (26 < burnup < 30 GWd/MTU)

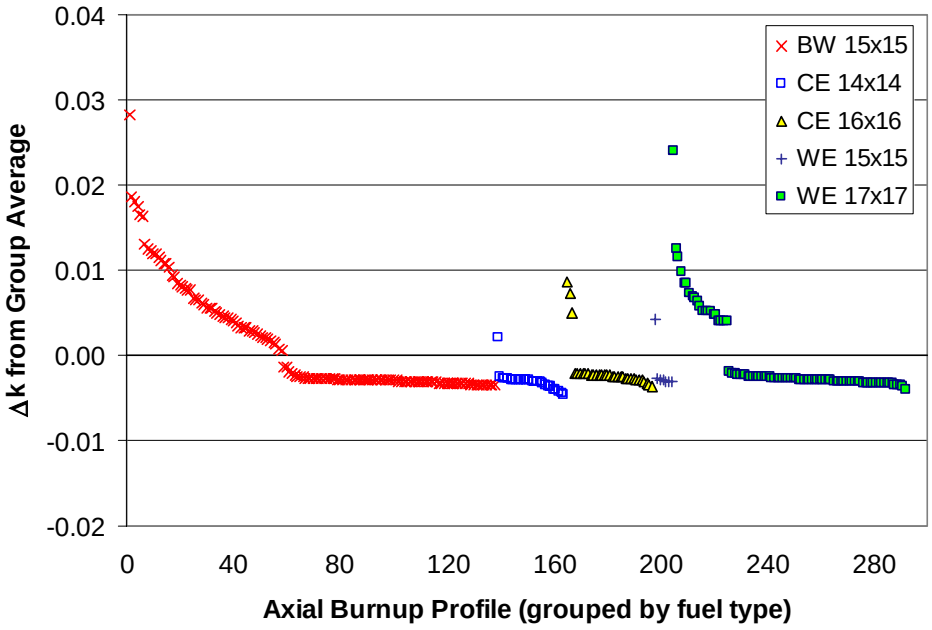

Figure 37 Δ*k* values plotted in terms of fuel type for axial-burnup profiles in burnup group 7 (22 < burnup < 26 GWd/MTU)

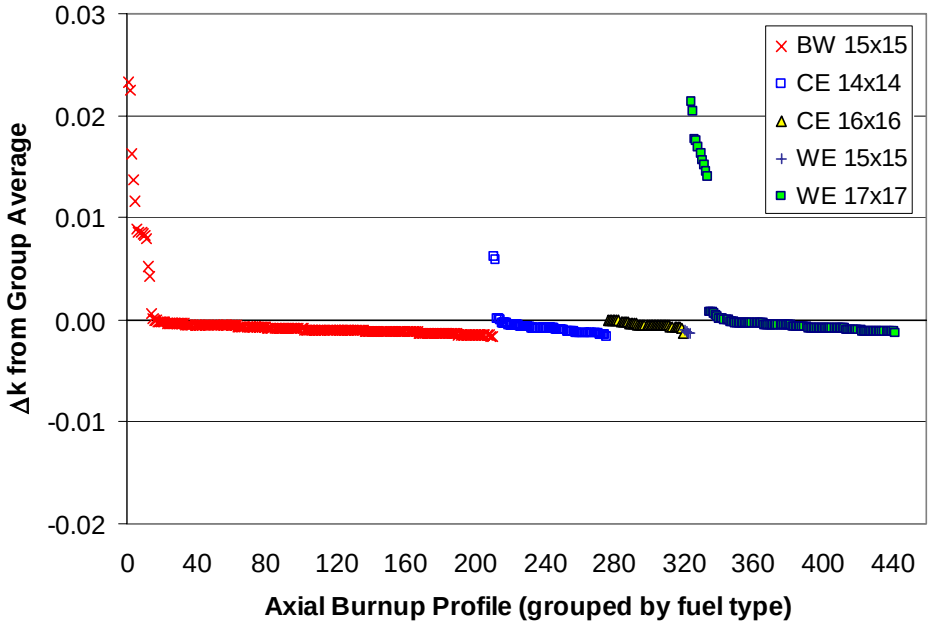

Figure 38 Δ*k* values plotted in terms of fuel type for axial-burnup profiles in burnup group 8 (18 < burnup < 22 GWd/MTU)

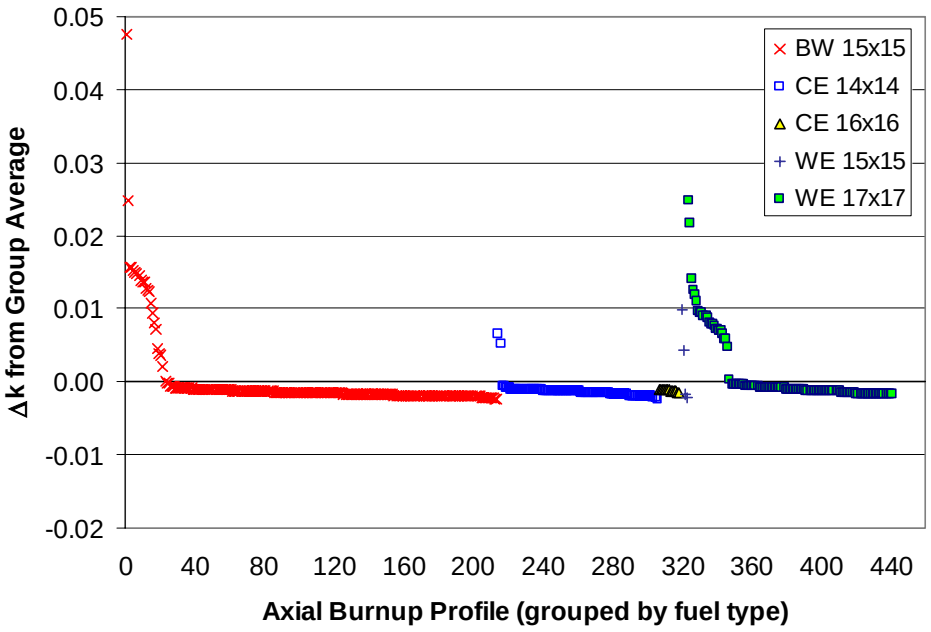

Figure 39 Δ*k* values plotted in terms of fuel type for axial-burnup profiles in burnup group 9 (14 < burnup < 18 GWd/MTU)

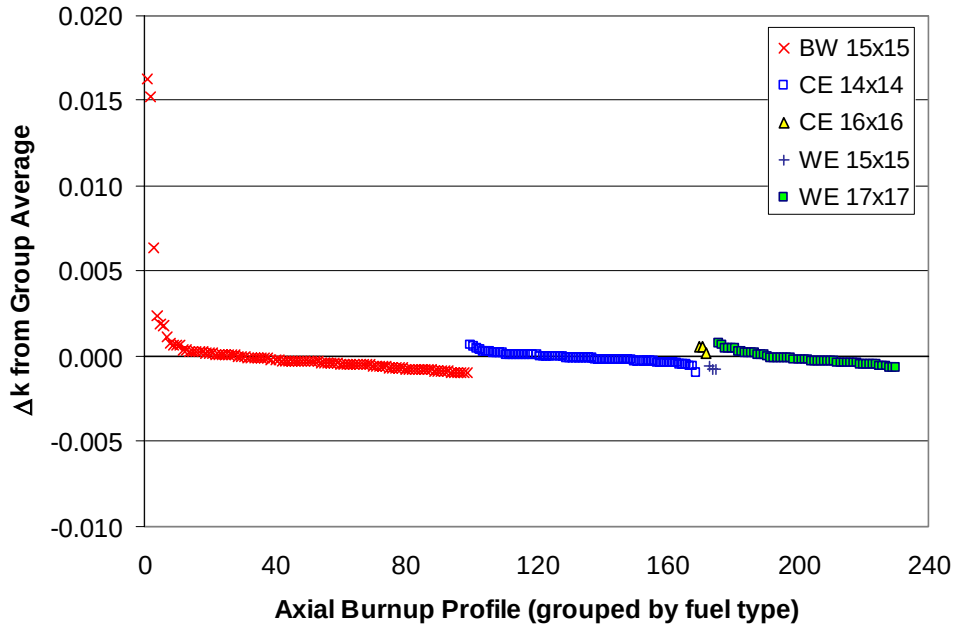

Figure 40 Δ*k* values plotted in terms of fuel type for axial-burnup profiles in burnup group 10 (10 < burnup < 14 GWd/MTU)

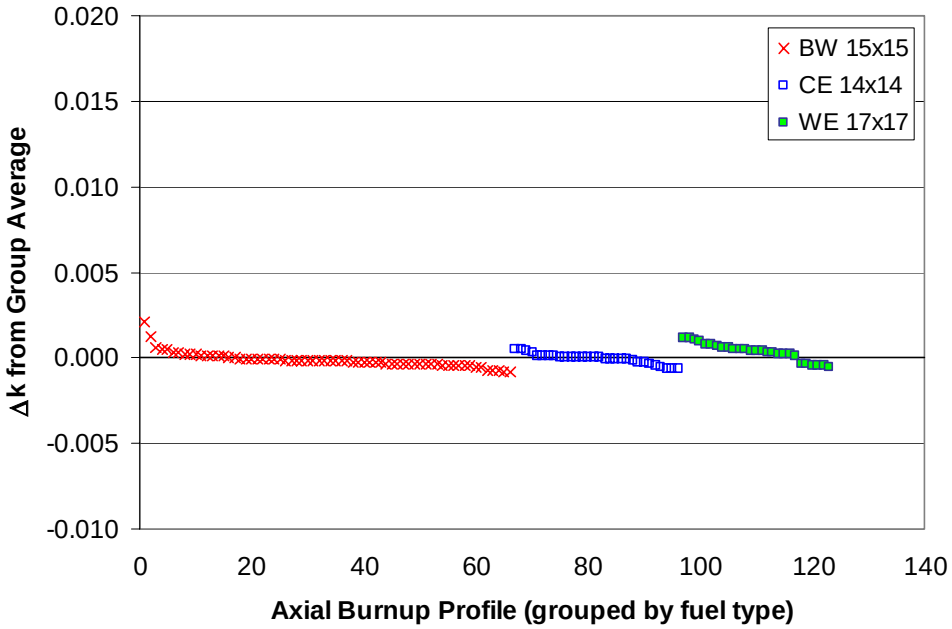

Figure 41 Δ*k* values plotted in terms of fuel type for axial-burnup profiles in burnup group 11 (6 < burnup < 10 GWd/MTU)

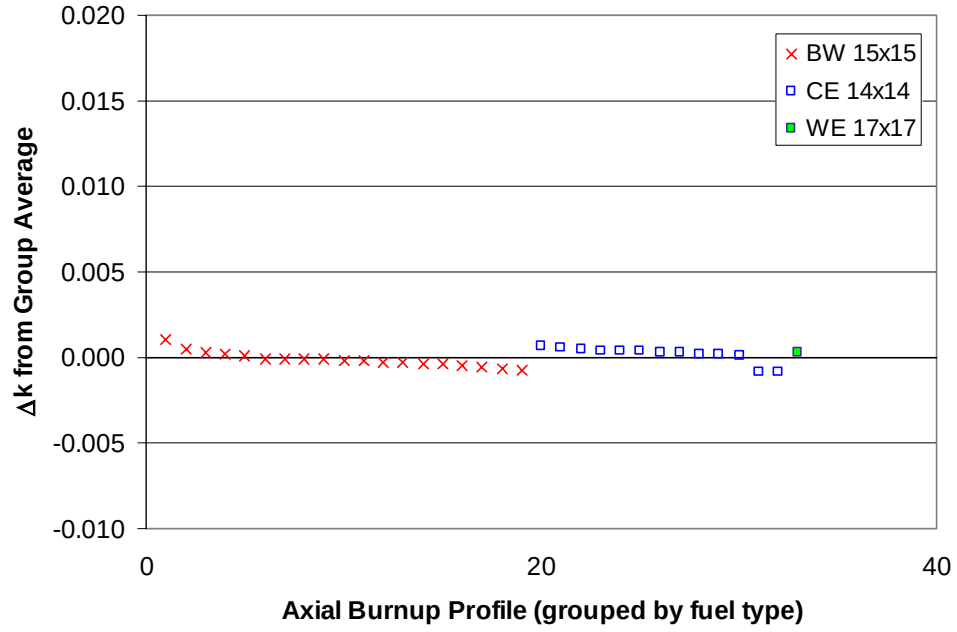

Figure 42 Δ*k* values plotted in terms of fuel type for axial-burnup profiles in burnup group 12 (burnup <6 GWd/MTU)

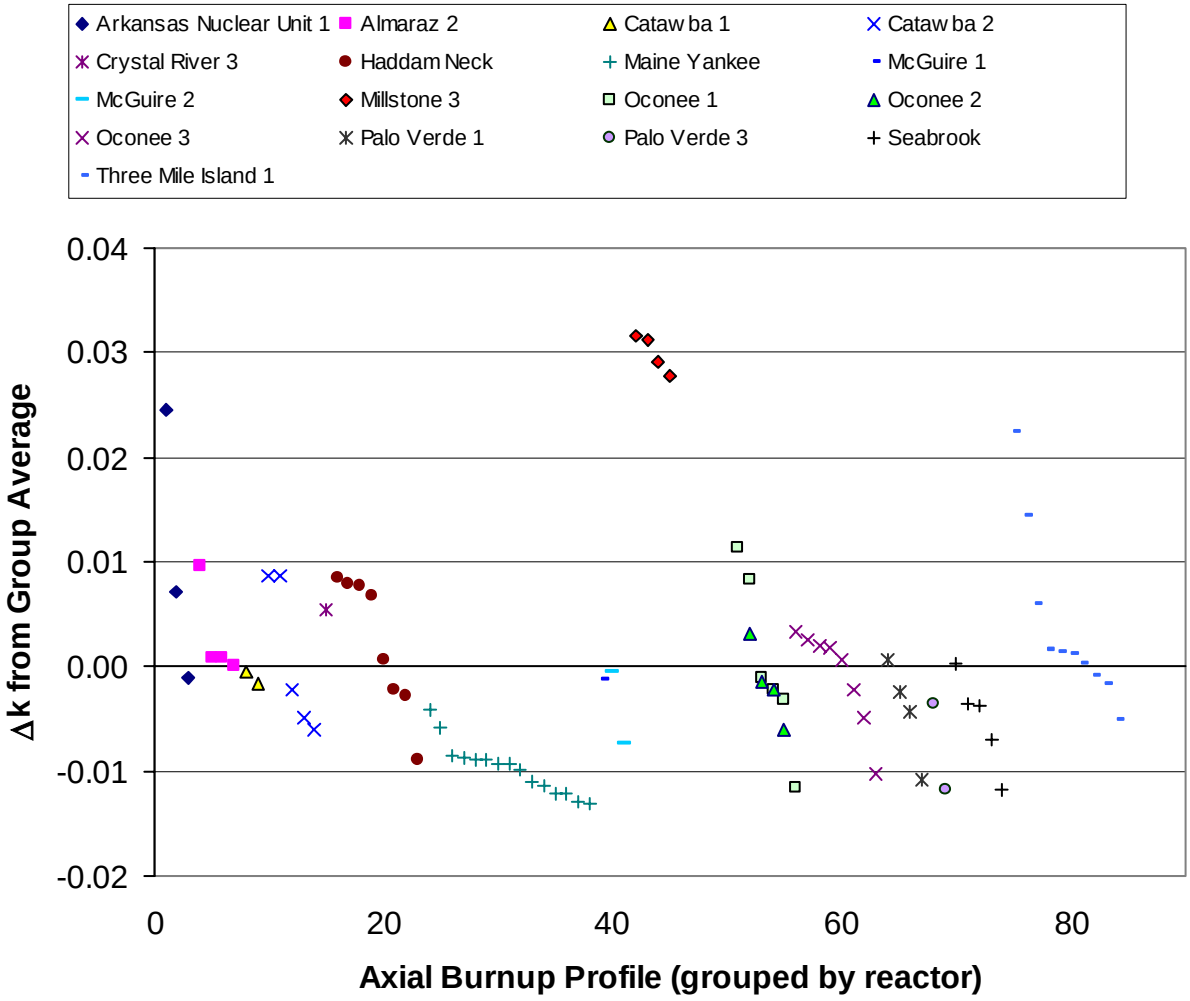

Figure 43 Δ*k* values plotted in terms of reactor for axial-burnup profiles in burnup group 1 (burnup > 46 GWd/MTU)

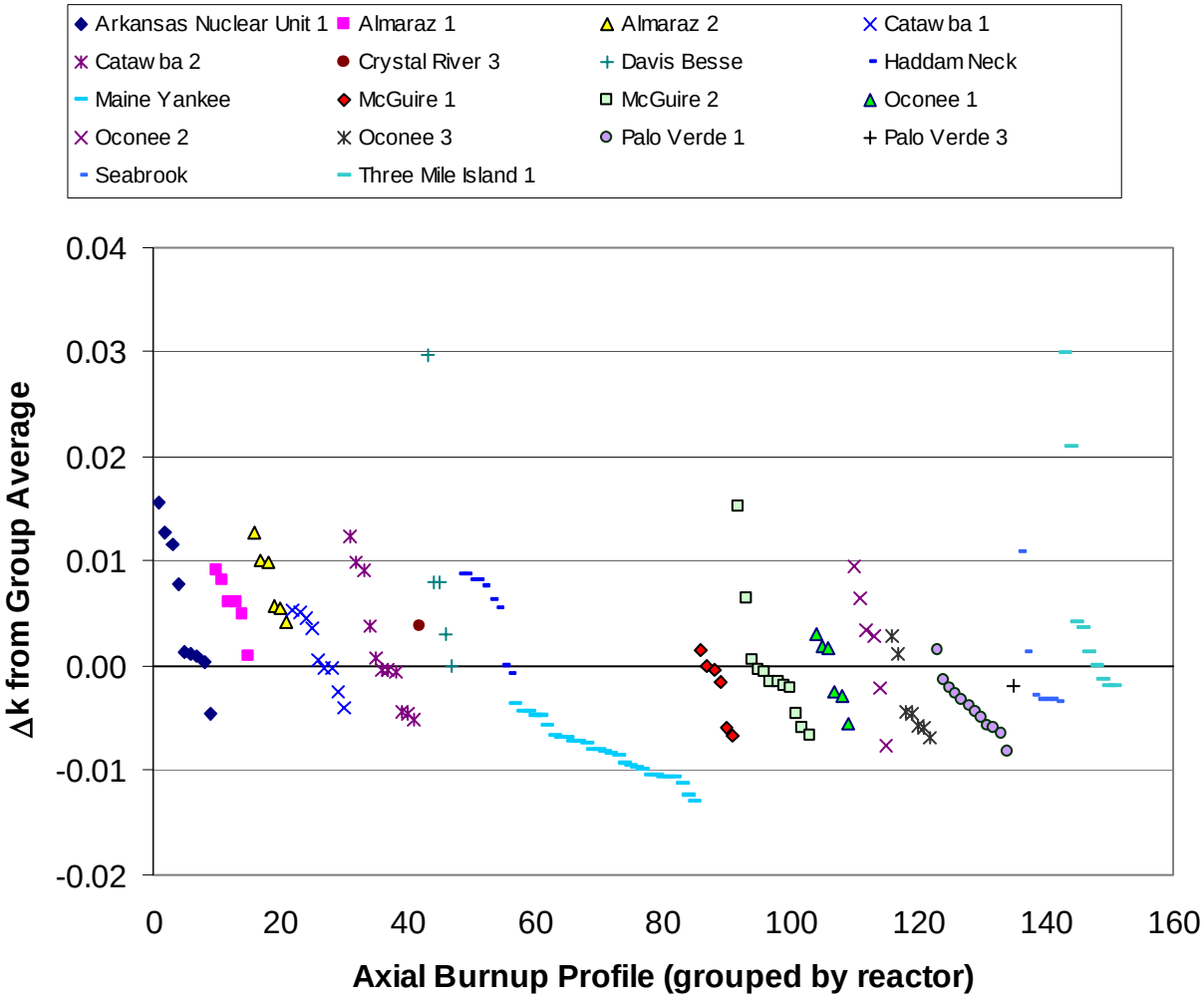

Figure 44 Δ*k* values plotted in terms of reactor for axial-burnup profiles in burnup group 2 (42 < burnup < 46 GWd/MTU)

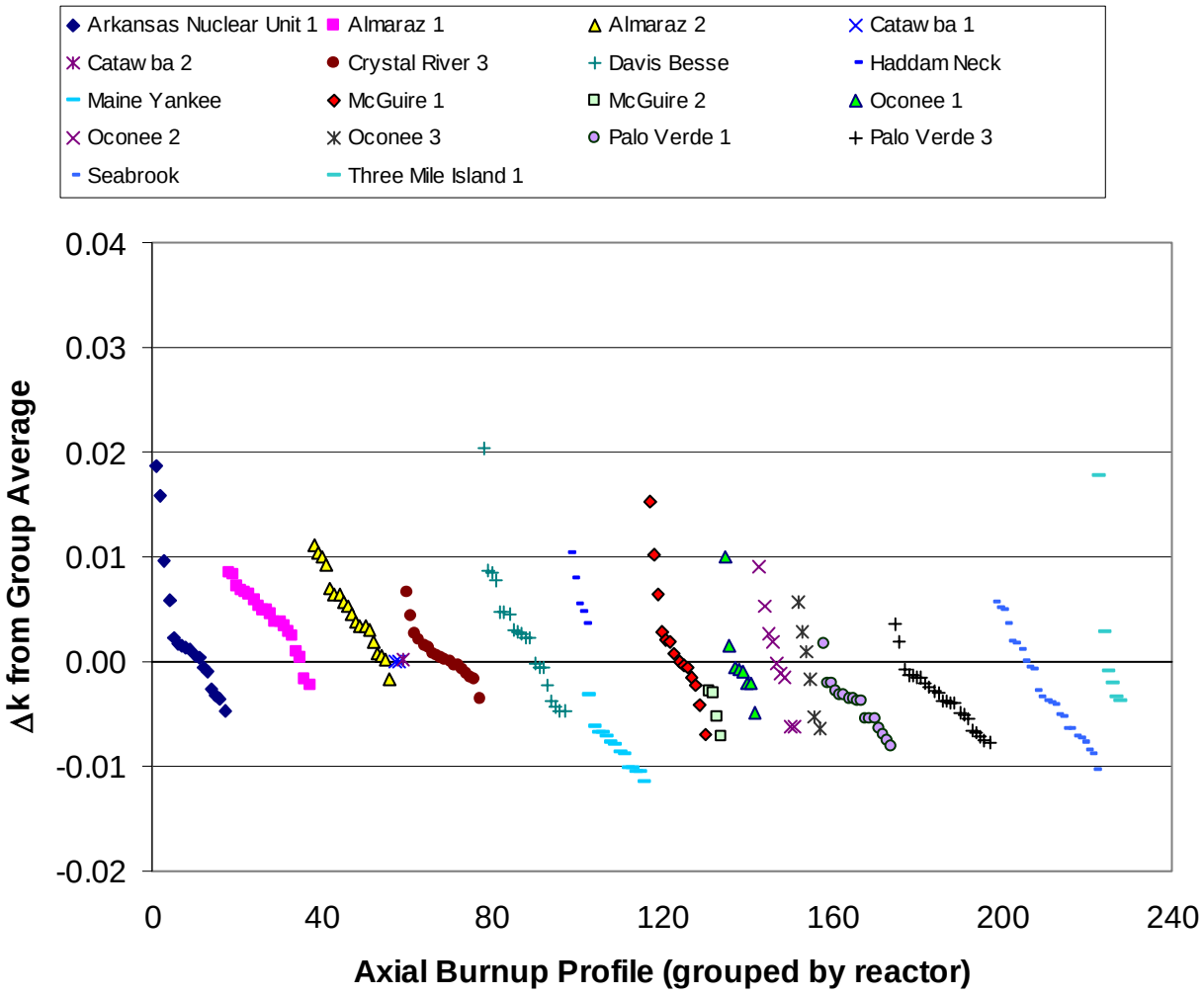

Figure 45 Δ*k* values plotted in terms of reactor for axial-burnup profiles in burnup group 3 (38 < burnup < 42 GWd/MTU)

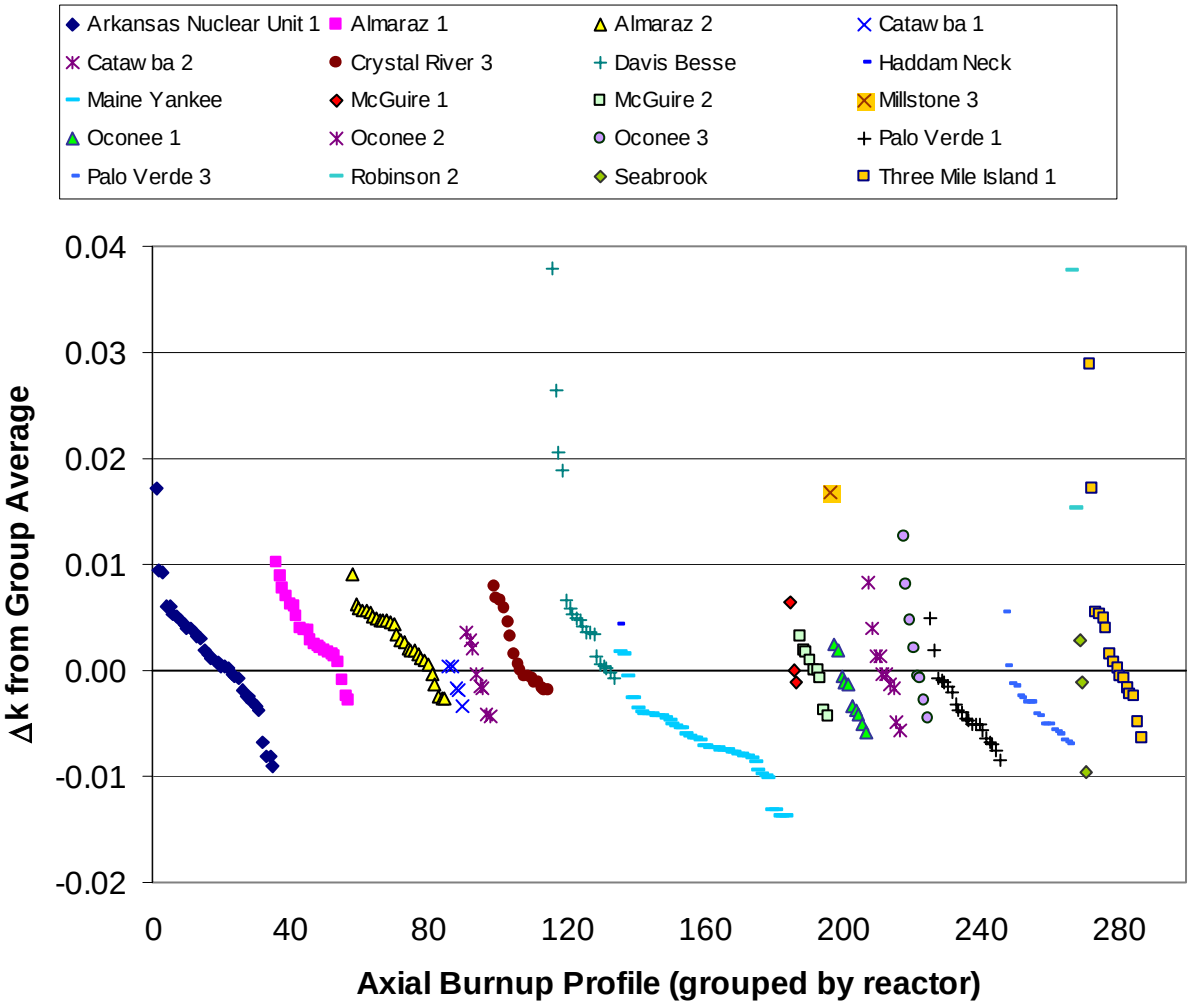

Figure 46 Δ*k* values plotted in terms of reactor for axial-burnup profiles in burnup group 4 (34 < burnup < 38 GWd/MTU)

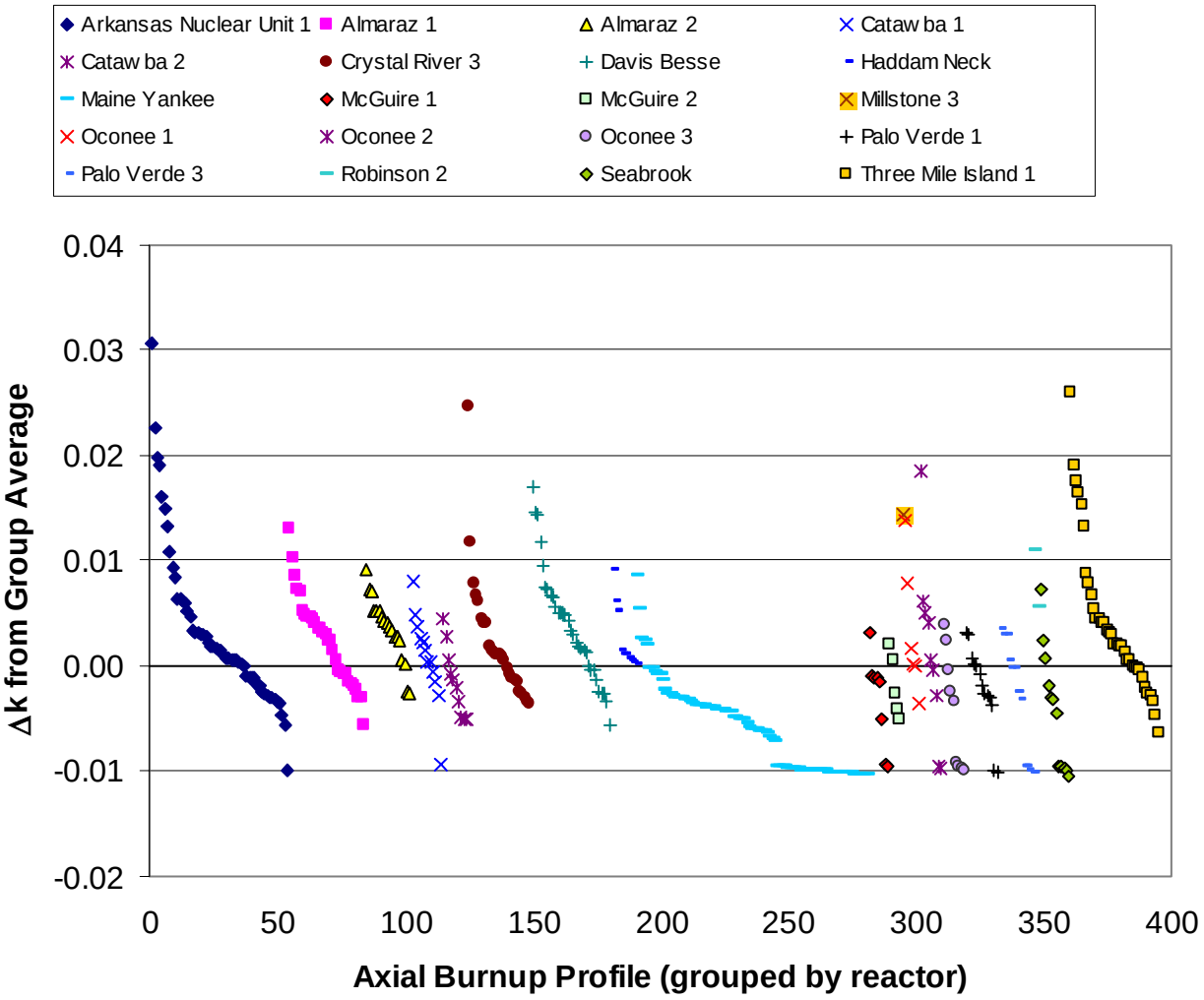

Figure 47 Δ*k* values plotted in terms of reactor for axial-burnup profiles in burnup group 5 (30 < burnup < 34 GWd/MTU)

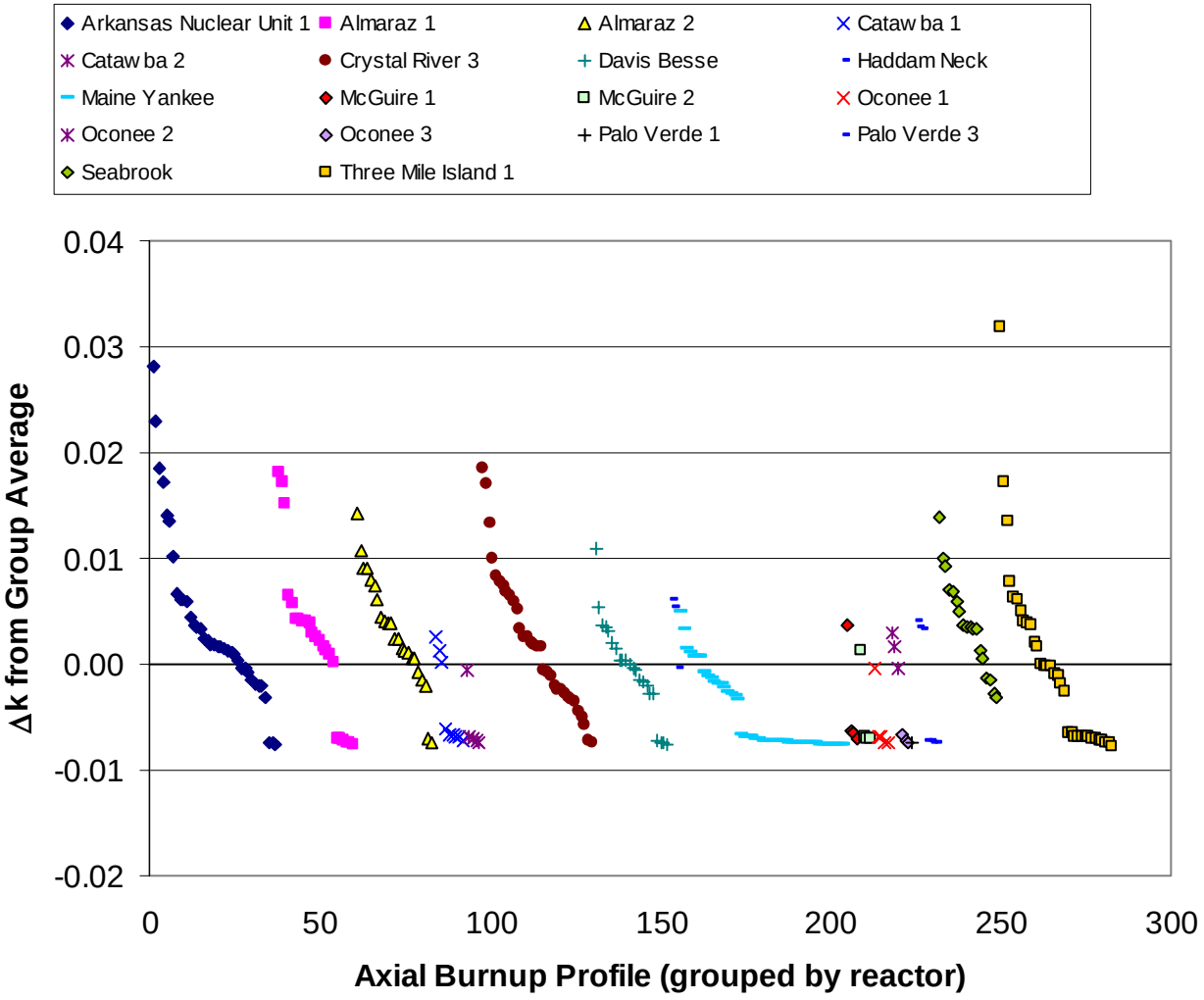

Figure 48 Δ*k* values plotted in terms of reactor for axial-burnup profiles in burnup group 6 (26 < burnup < 30 GWd/MTU)

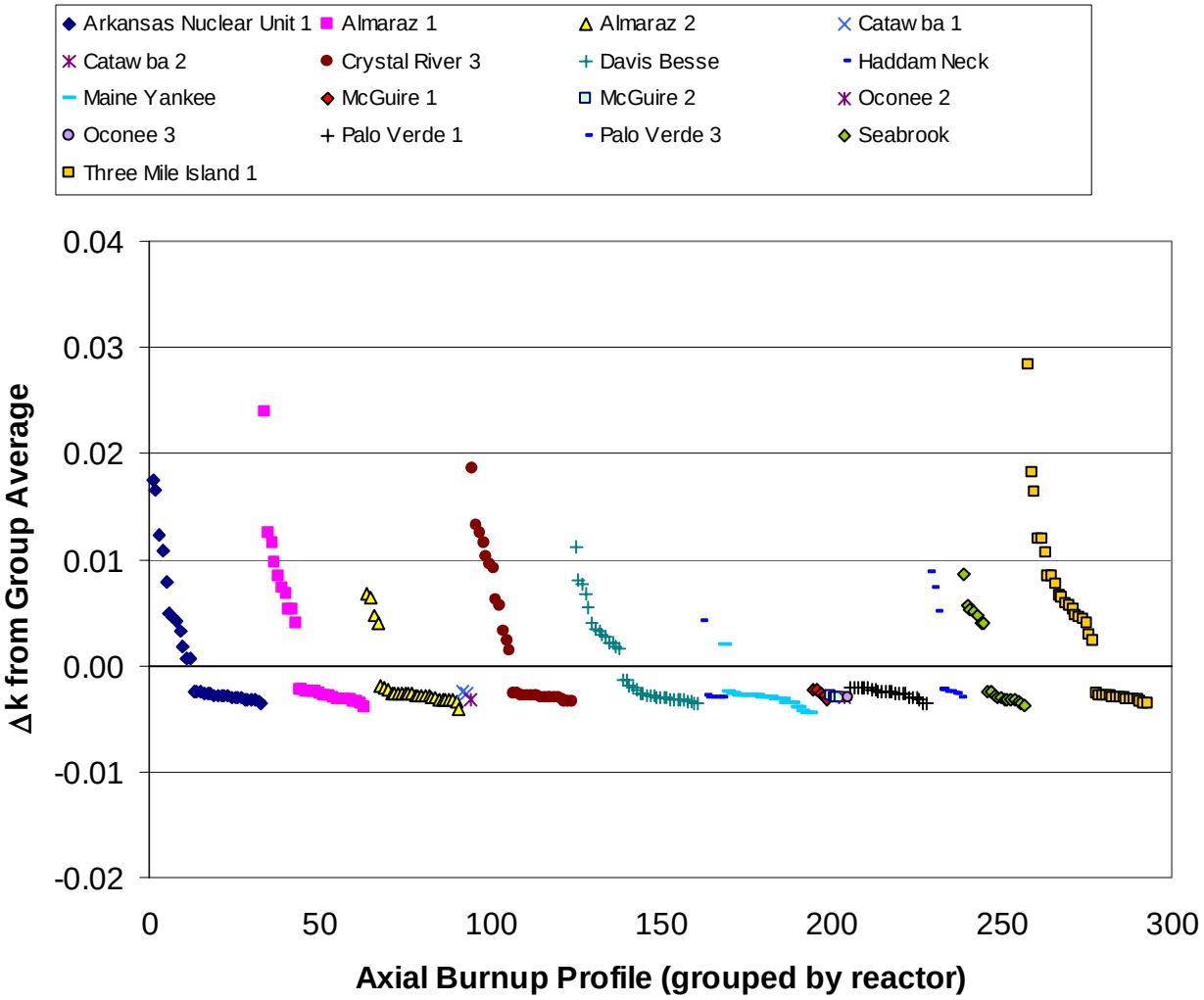

Figure 49 Δ*k* values plotted in terms of reactor for axial-burnup profiles in burnup group 7 (22 < burnup < 26 GWd/MTU)

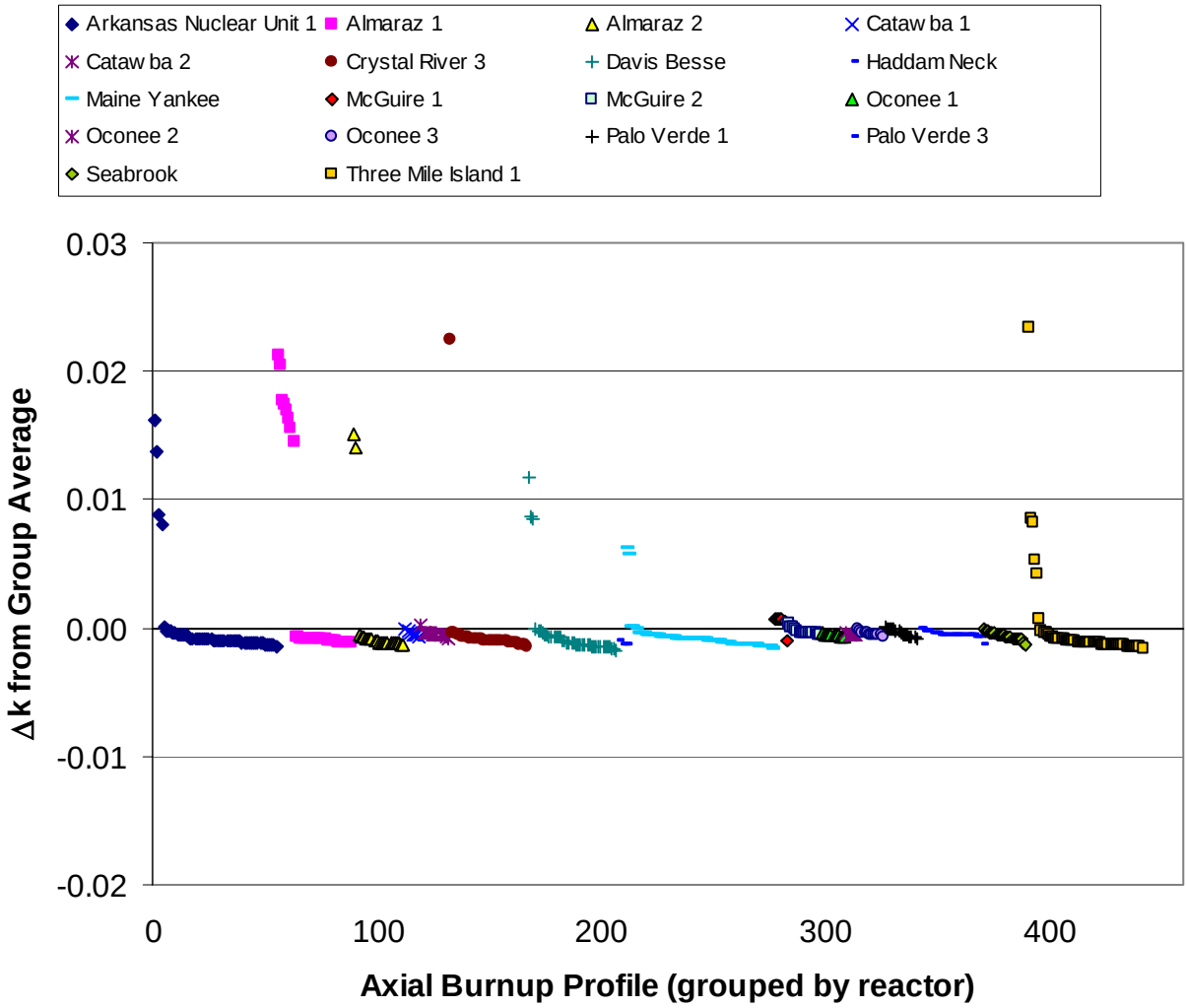

Figure 50 Δ*k* values plotted in terms of reactor for axial-burnup profiles in burnup group 8 (18 < burnup < 22 GWd/MTU)

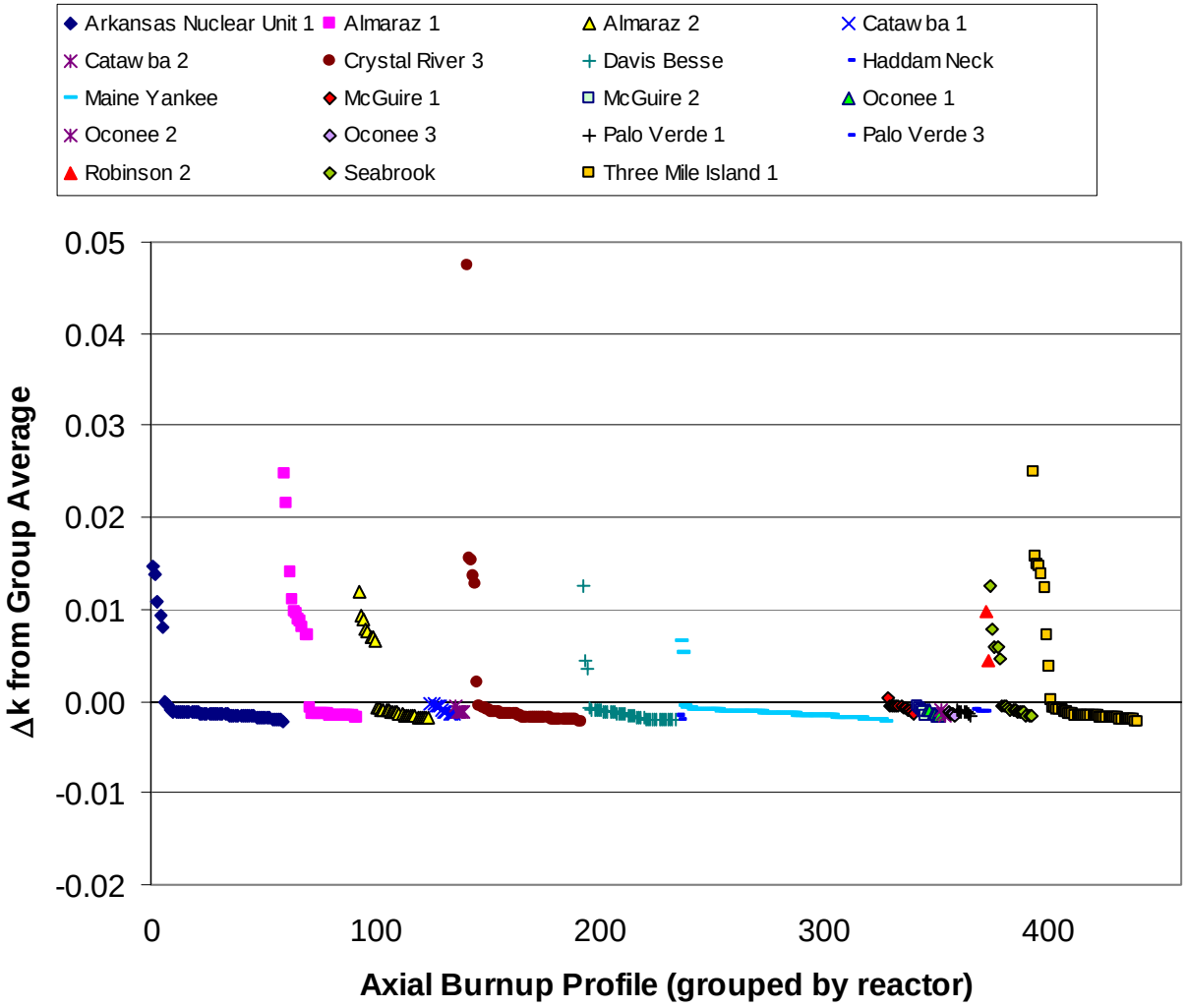

Figure 51 Δ*k* values plotted in terms of reactor for axial-burnup profiles in burnup group 9 (14 < burnup < 18 GWd/MTU)

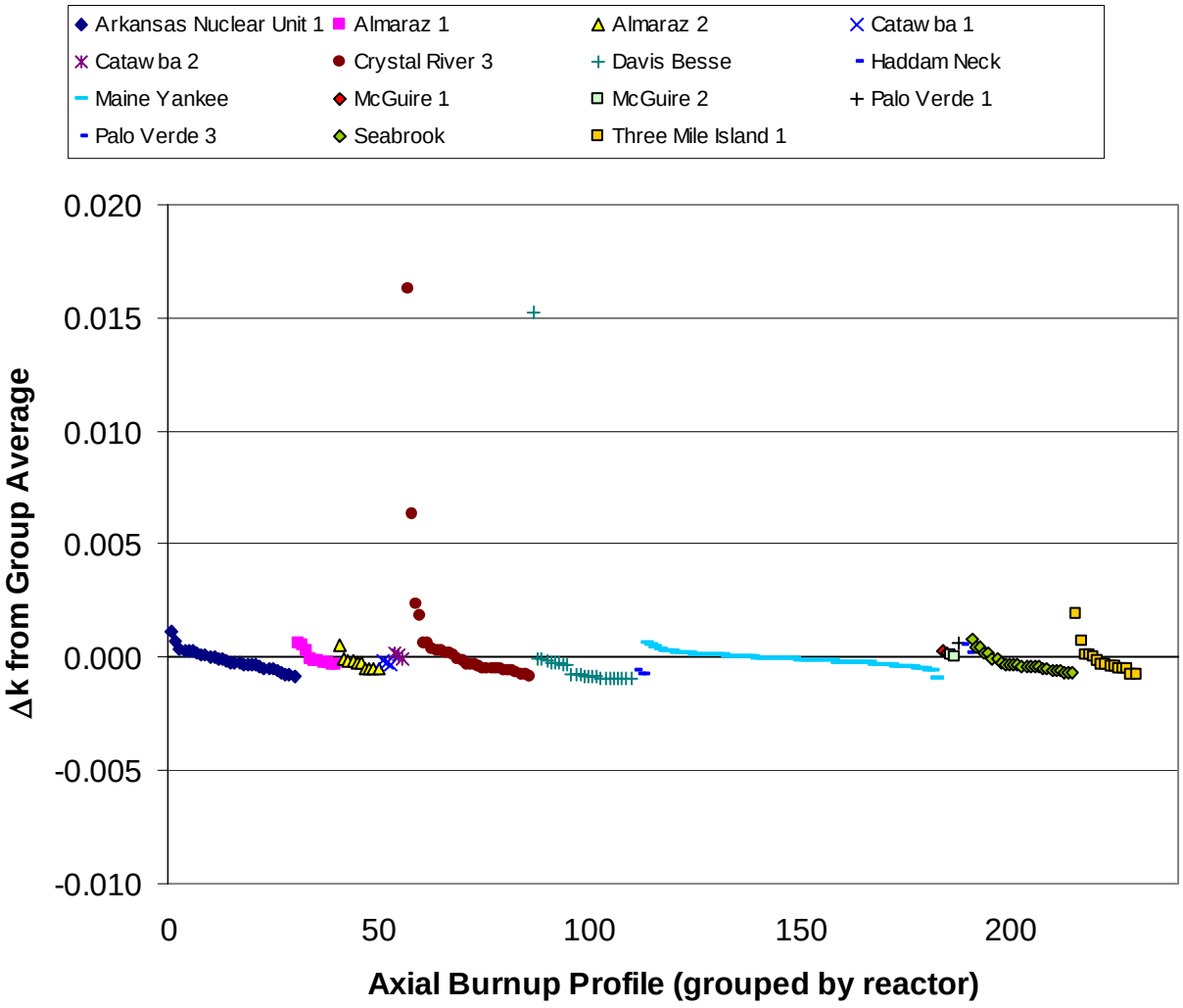

Figure 52 Δ*k* values plotted in terms of reactor for axial-burnup profiles in burnup group 10 (10 < burnup < 14 GWd/MTU)

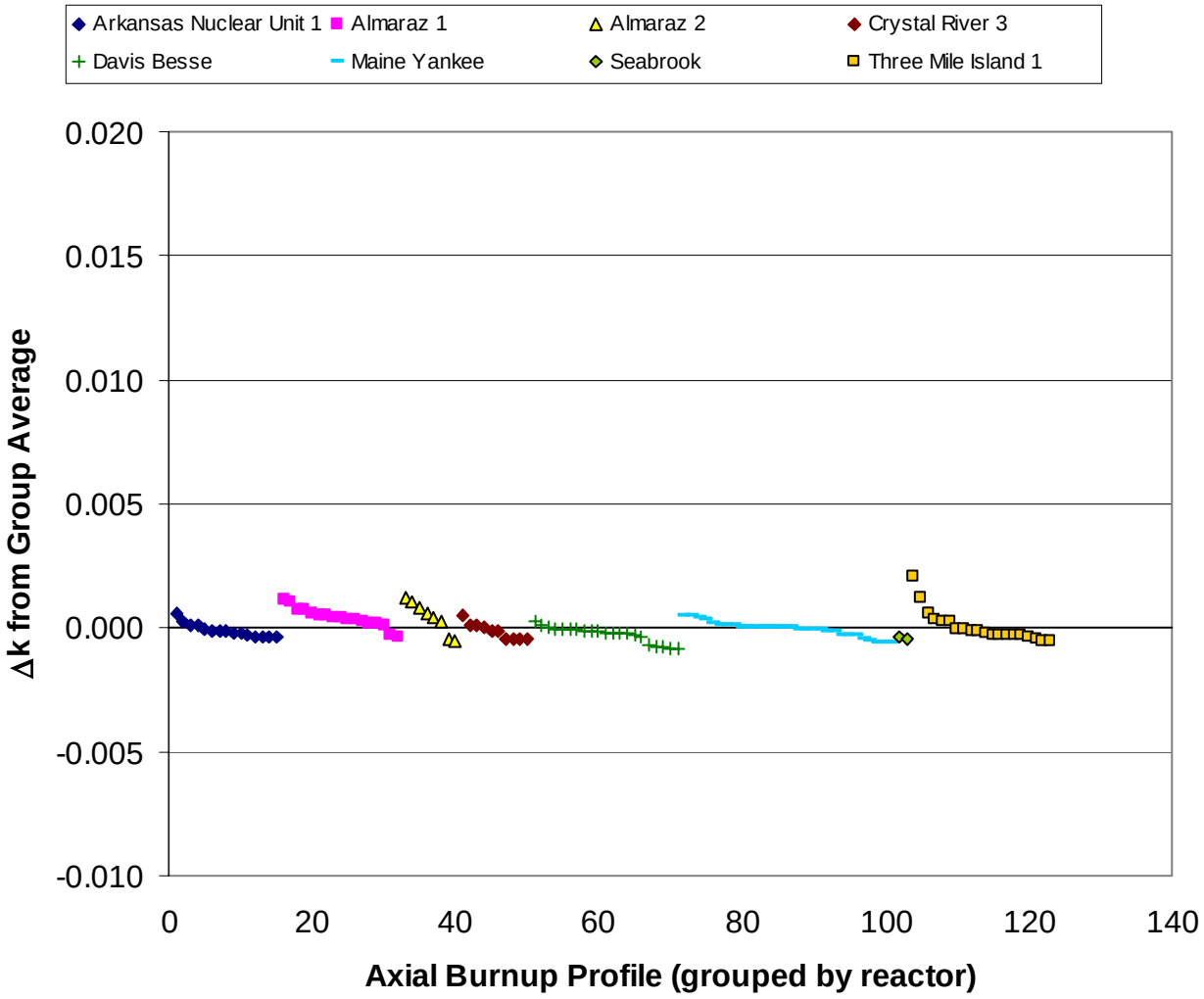

Figure 53 Δ*k* values plotted in terms of reactor for axial-burnup profiles in burnup group 11 (6 < burnup < 10 GWd/MTU)

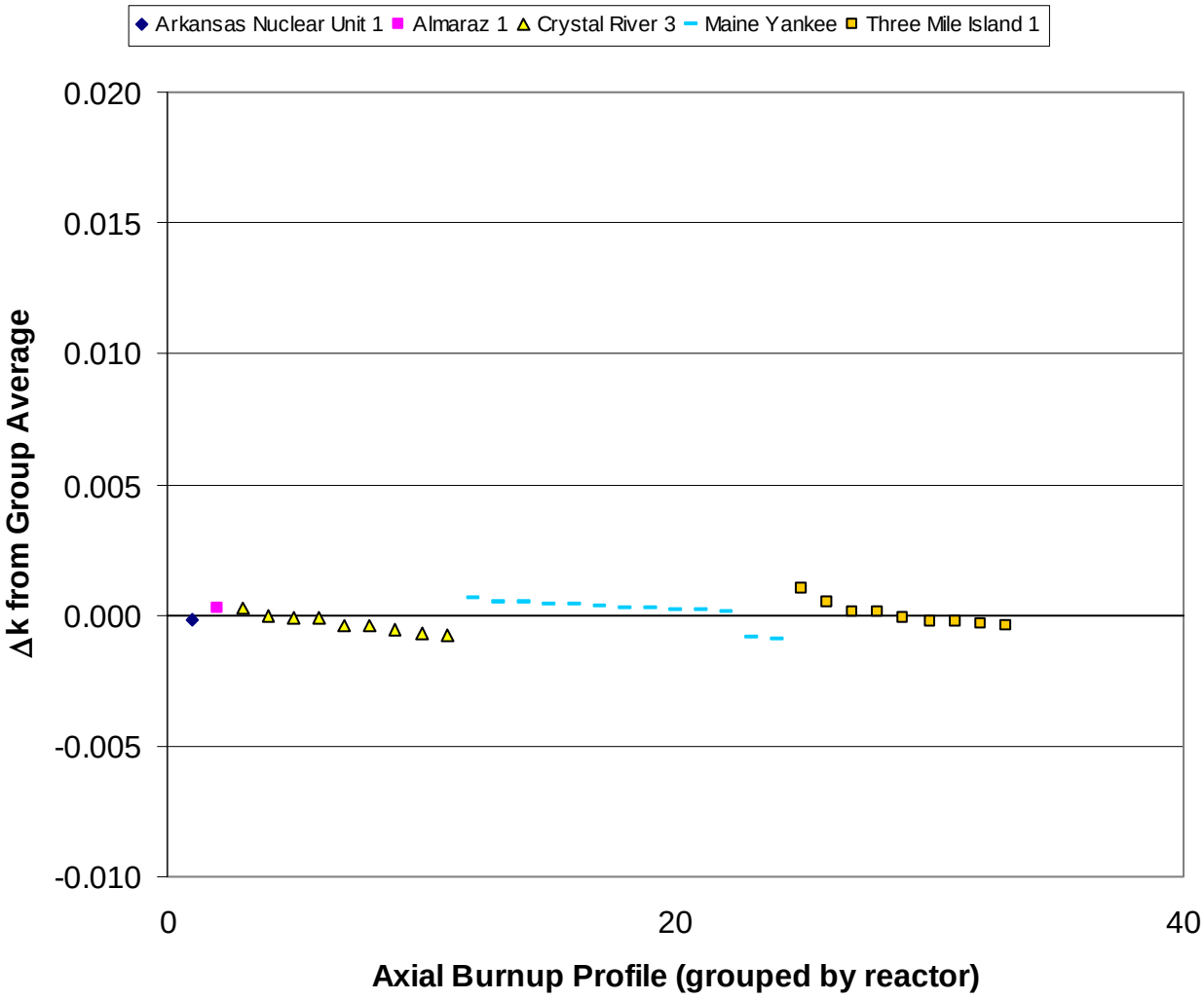

Figure 54 Δ*k* values plotted in terms of reactor for axial-burnup profiles in burnup group 12 (burnup < 6 GWd/MTU)

4.3 END EFFECT IN A BURNUP CASK

Results with the 32-PWR assembly (GBC-32) cask are presented in this section to quantify the effect of axial burnup in a representative burnup-credit cask design. Figure 55 compares the end effect (5-year cooling, fission products present) based on the bounding profiles (from Table 5) with the group-averaged end effect for each of the 12 burnup groups. The burnup value used in the calculations for each group generally corresponds to the group midpoint and is listed in Table 6. The "group-averaged end effect" refers to the mean of the end effects corresponding to each of the profiles within a burnup group. The results in Figure 55 demonstrate that, on average, the end effect increases with burnup and is less than ~1% Δk for these conditions (i.e., 5-year cooling, fission products present). The group-averaged end effect is negative for burnups below approximately 26 GWd/MTU. The use of the bounding profiles results in end effects that are generally between 1 and 4% Δk. Thus, the use of bounding profiles adds considerable margin, as compared with the average.

Figure 56 shows the end effect (5-year cooling) in the GBC-32 cask with only the major actinides included (see Table 4 for specific nuclides). The results in Figure 56 demonstrate that the group-averaged end effect is negative for these conditions (i.e., 5-year cooling, actinide-only). As discussed in greater detail in Ref. 9, for actinide-only models the decrease in reactivity is primarily driven by fuel depletion (net reduction in fissile nuclides). The uniform axial-burnup approximation artificially decreases the fuel depletion at the center where the fission density is greatest and increases the fuel depletion near the ends (away from the peak fission density). The artificial decrease in depletion in the region where the fission density is greatest can cause a net increase in reactivity. As a result, the assumption of uniform axial burnup can be more reactive for actinide-only conditions (similar to the situation for low-burnup values with fission products present, where the fission products have a small effect) and the transition from negative to positive end effects is not observed in the group-averaged end effect values. However, the use of the bounding profiles results in end effects that are generally positive and less than 1.5% Δk. Note that the end effect is known to increase notably with increasing cooling time.[10] Although less than when fission products are included, it is evident from Figure 56 that the use of bounding profiles adds considerable margin (as much as 2.0% Δk), as compared with the average.

For comparison, Figure 56 also shows the end effect resulting from the approach suggested in a DOE topical report on actinide-only burnup credit (Ref. 3), which consists of using bounding profiles over coarser burnup ranges (i.e., a single profile in each of the following three burnup ranges: 0–18, 18–30, and > 30 GWd/MTU). The bounding profiles for the three burnup ranges were determined based on the bounding profiles from Ref. 7. Consequently, the three bounding profiles suggested for use in Ref. 3 correspond to the bounding profiles for burnup groups 5, 8, and 9. Therefore, the end effect associated with the bounding profiles and the suggested approach in Ref. 3 are equivalent for burnup groups 5, 8, and 9. For a given profile, the end effect increases with burnup, and thus the Ref. 3 approach, of using bounding profiles associated with coarse burnup ranges, results in larger end effects, as is apparent in Figure 56.

Since the burnup profile changes with burnup – tending to flatten with increasing burnup, if an axial profile from a lower burnup assembly is used in a calculation involving higher burnup, the end effect is generally over-estimated. Note, however, that this is not true for low burnups (i.e., . 15 GWd/MTU) where the end effect is typically negative. The behavior is illustrated in Figure 56 by comparison of the end effects due to the bounding profiles to those associated with the Ref. 3 approach and even more clearly in Figures 57 and 58, which compare the end effect associated with each of the 12 bounding axial profiles for the same total burnup (i.e., 40 and 60 GWd/MTU, respectively). In these latter figures, it is shown that regardless of cooling time or the inclusion of fission products, within the range of burnup in

which the end effect is positive, axial profiles from lower burnup fuel generally yield larger end effects for a fixed burnup than axial profiles from higher burnup fuel. This trend is the main reason why axial profiles are separated into burnup ranges in analyses for determining bounding profiles. However, the more conservative nature of the Ref. 3 approach may be considered preferable if a simpler analysis method is desired.

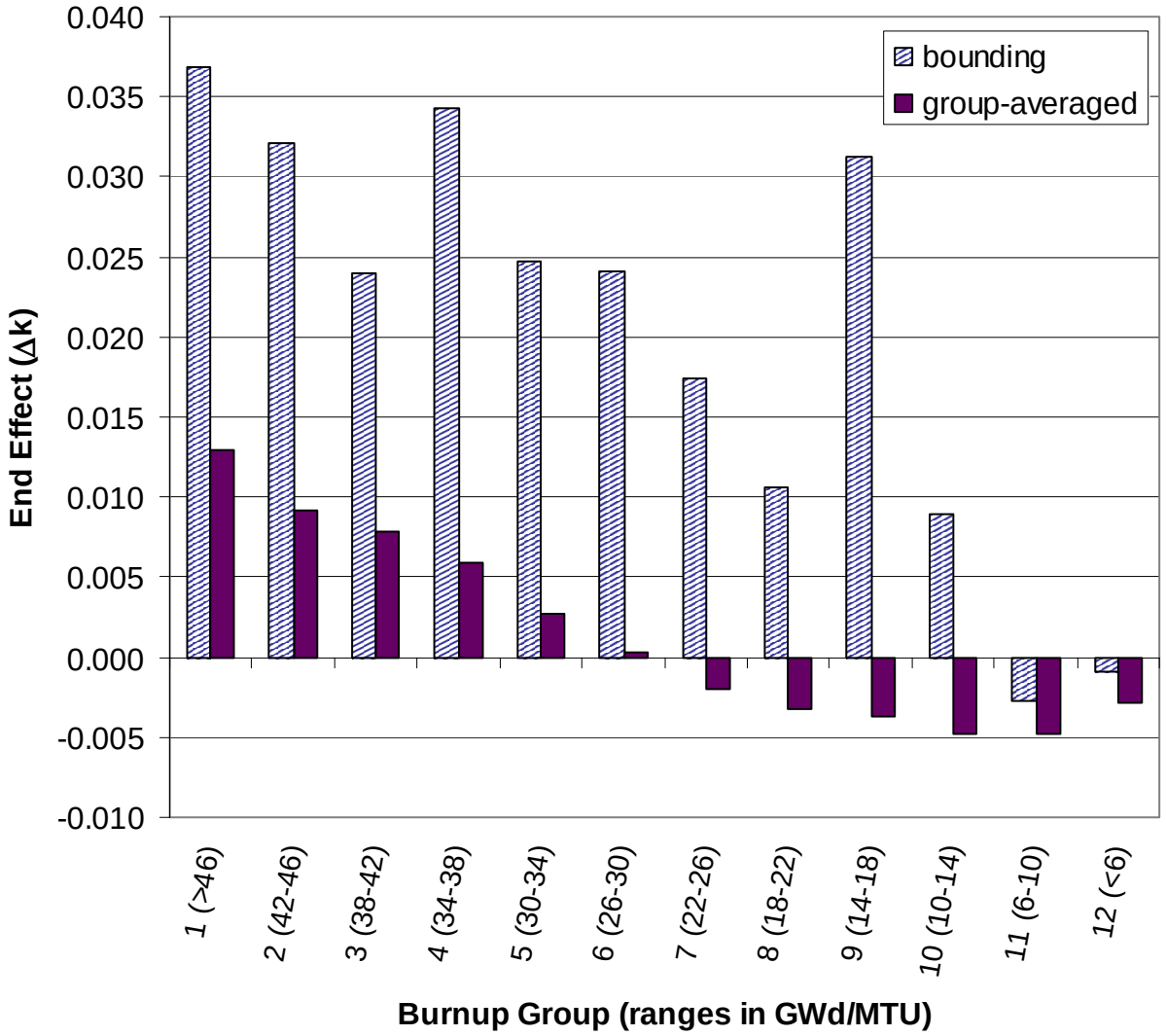

Figure 55 Comparison of the end effect (with fission products, 5-year cooling) based on bounding profiles (from Table 5) and the group-averaged end effect in the GBC-32 cask for each of the 12 burnup groups

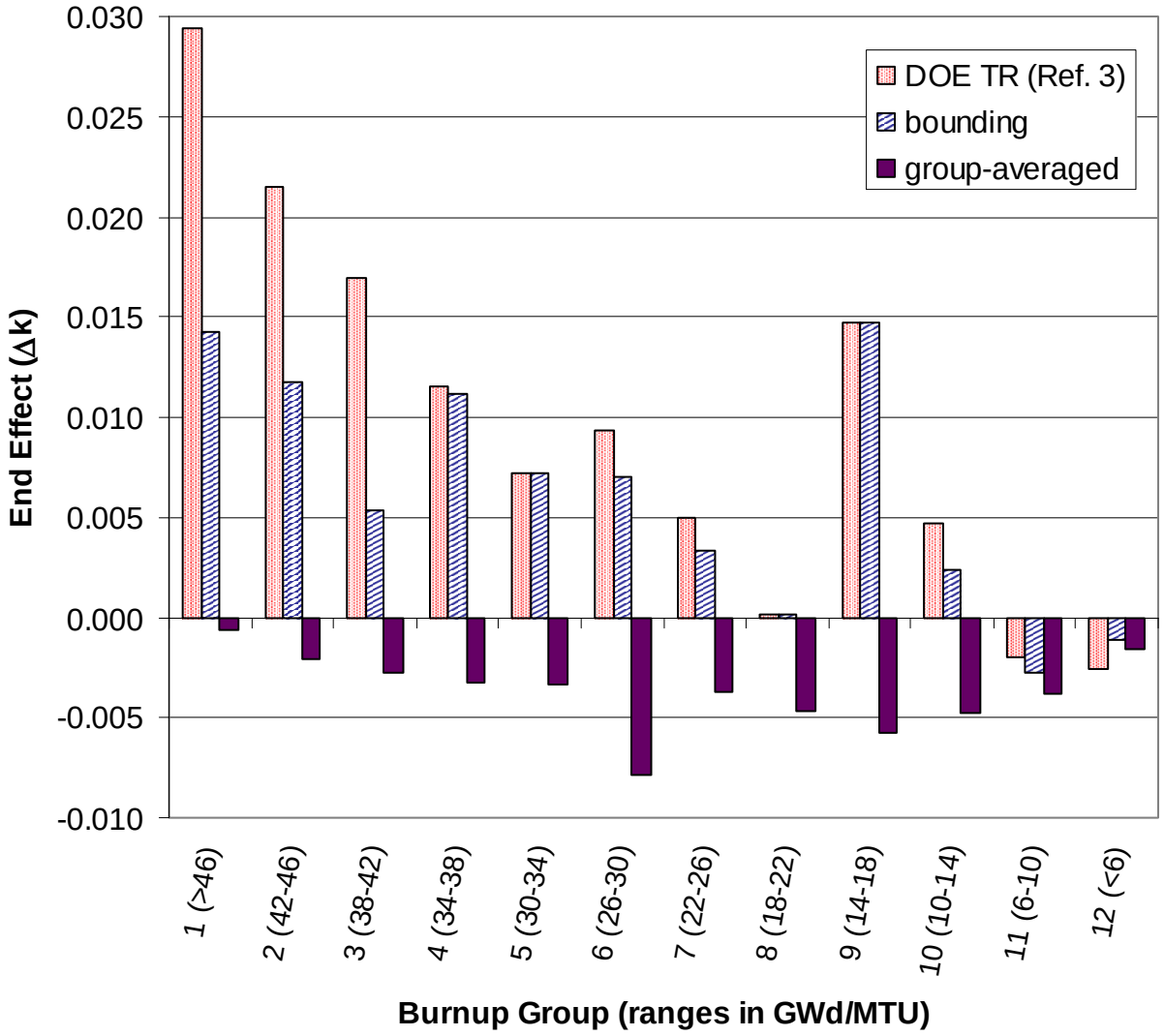

Figure 56 Comparison of end effect for actinide-only calculations in the GBC-32 cask (5-year cooling)

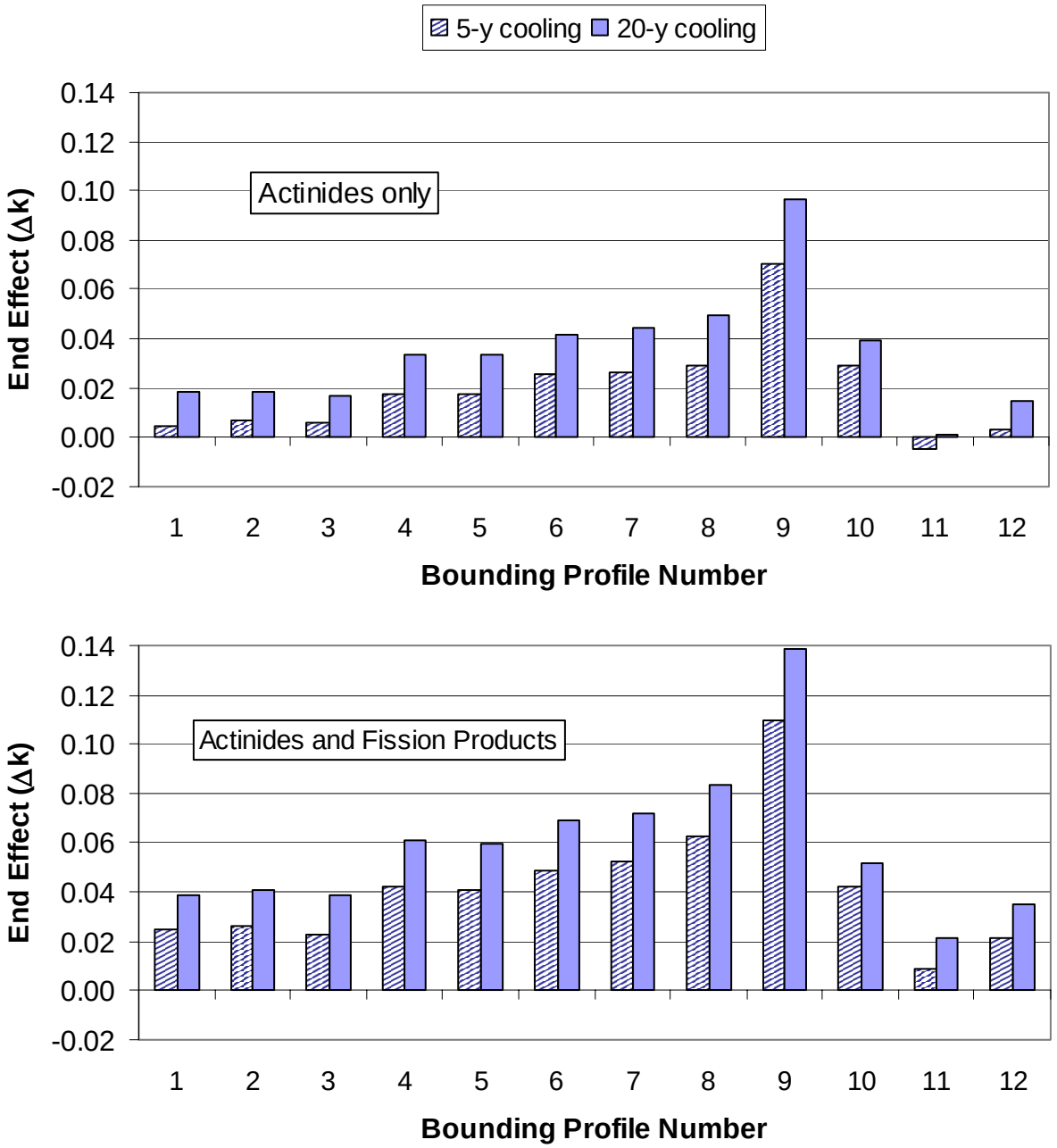

Figure 57 Comparison of end effect values resulting from the use of the 12 bounding profiles (from Table 5) for a fixed burnup of 40 GWd/MTU

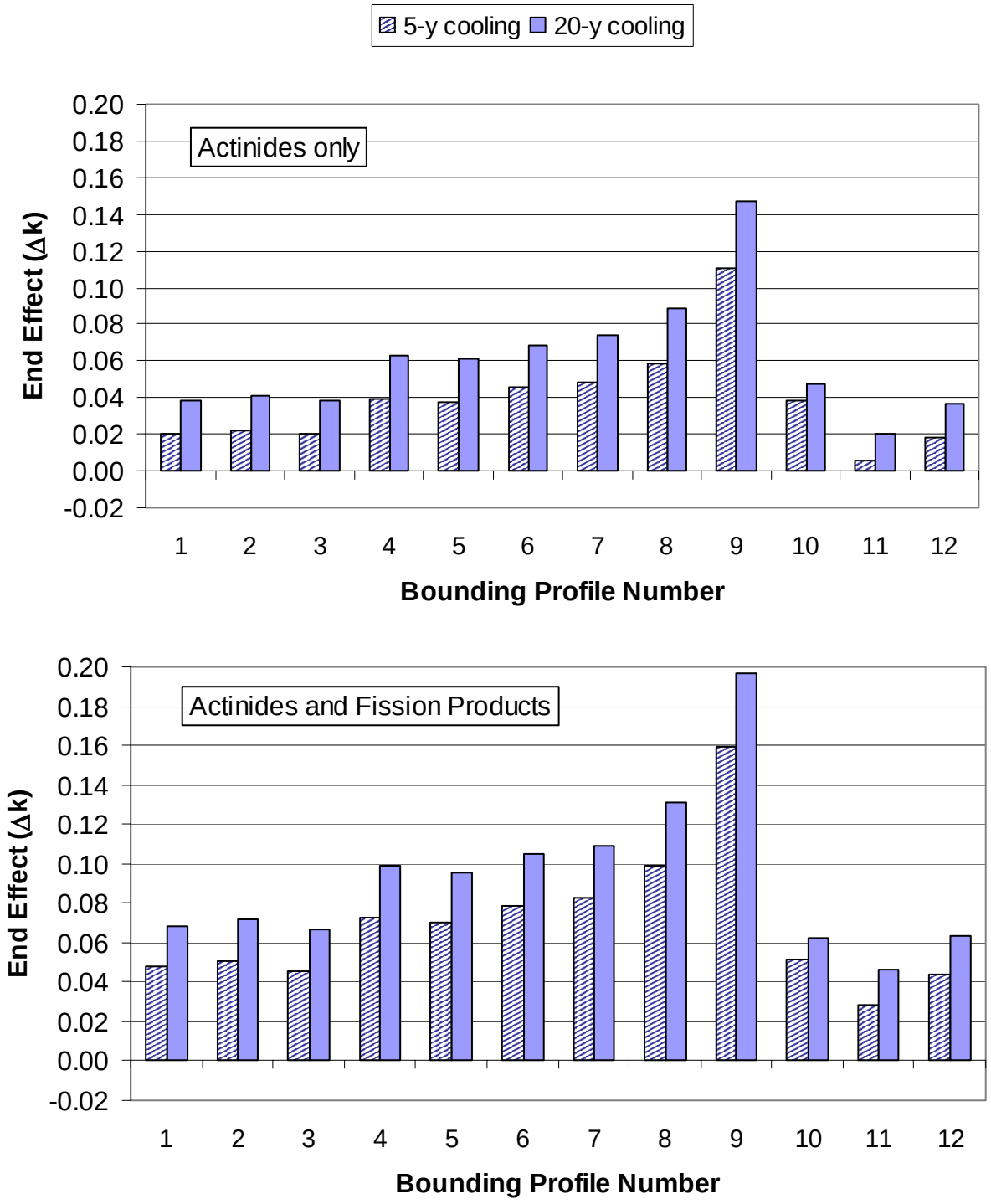

Figure 58 Comparison of end effect values resulting from the use of the 12 bounding profiles (from Table 5) for a fixed burnup of 60 GWd/MTU

4.4 IMPACT OF MORE-REACTIVE PROFILES

Because of the long-standing concern regarding the adequacy of a finite database to completely represent the nearly infinite variety of possible profiles, some[6,7,23] have suggested developing artificial bounding profiles to account for potential unknown, more-reactive profiles. One approach is to develop artificial profiles based on a composite of profiles from a database. For a given set of profiles, the minimum burnup value for each axial region is determined and used to define the burnup in the end regions of the artificial profile. The burnup values for the remaining central regions are estimated based on the maximum burnup values for those regions, and then all of the burnup values are adjusted to yield a normalized profile. In general, this approach does yield more reactive profiles. However, this approach is inherently based on the assumption that the bounding profile has the *typical* axial-burnup profile (i.e., nearly flat in the center with reduced burnup on the ends, see Figure 1), which is not always the case. For example, the bounding profiles for burnup groups 8 though 10 have distinctly different shapes (see Figures 14 through 16), which are apparently due to either control rod or APSR exposure.

Another approach is to developing artificial profiles based on inscribing bounding profiles. For the inscription, the average burnup in each axial region is artificially reduced to the minimum burnup in that region via interpolation between interim regions and extrapolation for the periphery regions. The resulting profile can subsequently be renormalized to conserve total burnup. If the profile is not renormalized, the total burnup is reduced, thereby adding additional conservatism. This approach reduces the burnup in areas where the burnup profile has a significant gradient, and consequently has been found to yield *significantly* larger end effects. The large effect of this inscribing approach on the end effect (5-year cooling) in the GBC-32 cask is illustrated in Figures 59 and 60, with and without fission products present, respectively, and with and without profile renormalization. As can be seen in the figures, this approach results in increases in the end effect of as much as 5% Δk. Considering the fact that this approach more than doubles the end effect, as compared to the bounding case, it is a significant departure from reality.

The inscribing approach does offer a means to assess the impact of loading one or more assemblies into a burnup-credit cask that have an axial profile that is not bounded by the existing database. Therefore, an analysis was performed with the GBC-32 cask to assess the impact of loading one or more assemblies into a burnup-credit cask that have a significantly more-reactive axial profile than found in the existing database.[8] The analyses were performed for 5-year cooling and separately for burnup values of 36 and 50 GWd/MTU, which correspond to burnup groups 4 and 1, respectively. The more reactive profile corresponded to an inscribed bounding profile without renormalization and the calculations assumed that the assemblies with the more reactive profile were loaded from the center outward. The results are shown in Figure 61 for calculations with and without fission products present. They confirm the relatively small reactivity consequence of loading a single assembly with a significantly more reactive profile. Results are shown in Figure 61 for multiple loadings of assemblies with more reactive axial profiles to demonstrate the associated impact on k_{eff}. The reactivity consequence of loading a single assembly with a significantly more reactive profile, as compared to the actual bounding profile, is shown to be less than ~0.5% Δk.

The reactivity consequence of loading an assembly with a more reactive axial profile will depend on the total burnup and the more reactive profile selected. Considering the statistical evaluation of k_{eff} values provided in Section 4.2.1, the likelihood of the existence of axial-burnup profiles that have significantly higher reactivity is very small. Furthermore, the likelihood that these higher reactivity profiles would be significantly more reactive than the bounding profiles is very small. Therefore, the use of the significantly higher reactivity inscribed profile for this analysis leads to an extremely conservative approach to bound the potential impact of more-reactive profiles.

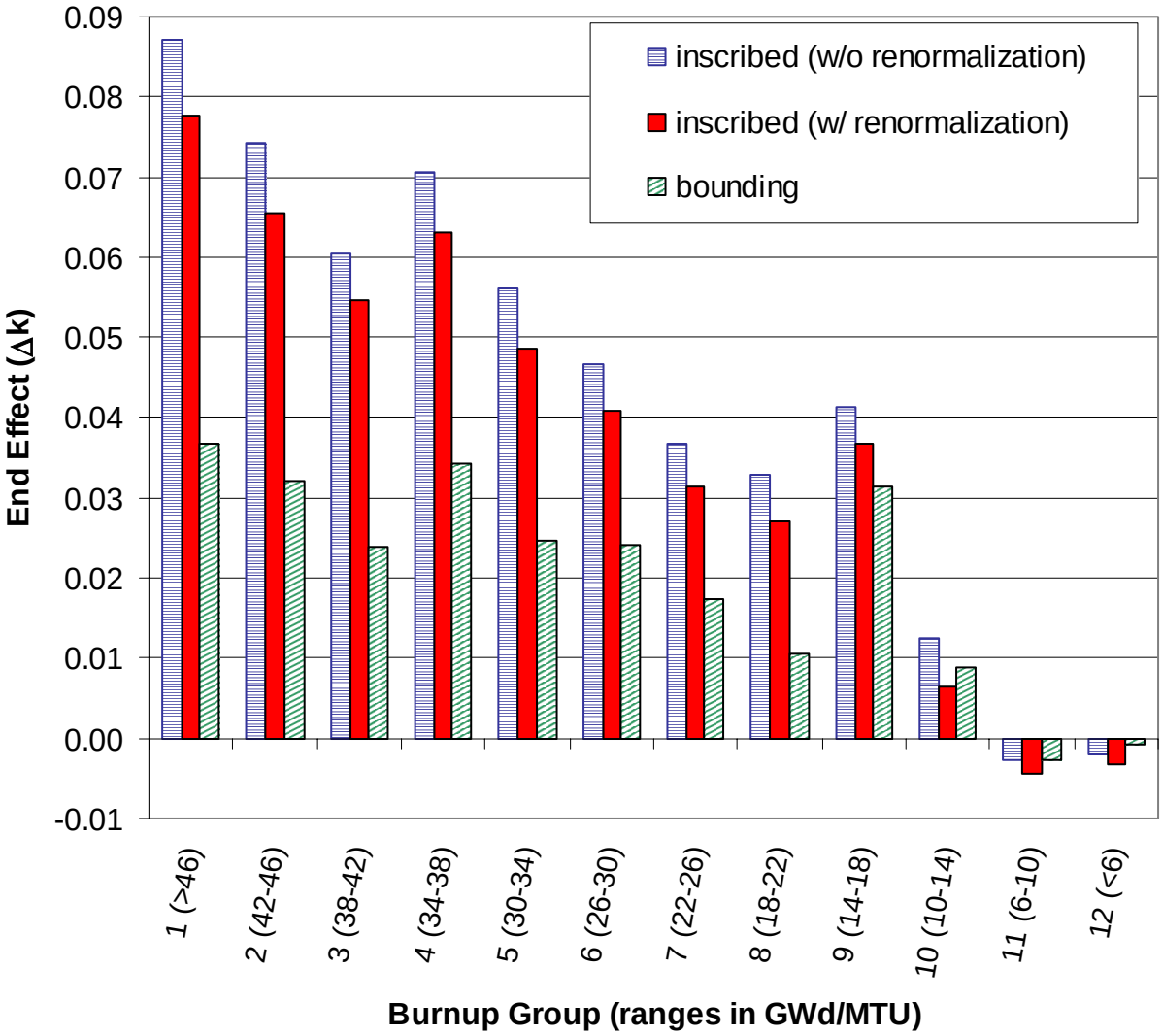

Figure 59 Illustration of the impact of profile inscribing (with and without profile renormalization) on the end effect in the GBC-32 cask with fission products present (5-year cooling)

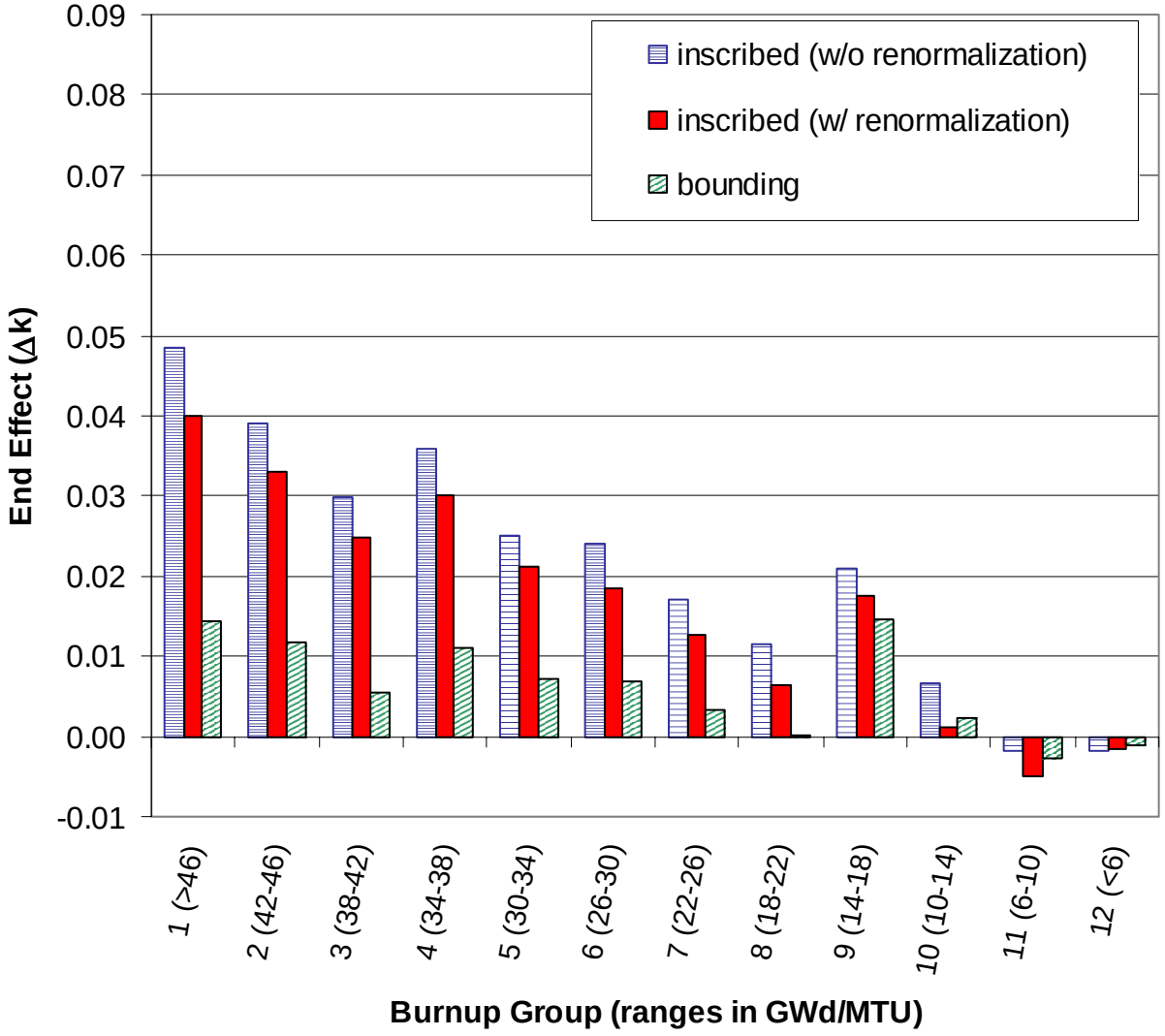

Figure 60 Illustration of the impact of profile inscribing (with and without profile renormalization) on the end effect in the GBC-32 cask without fission products present (5-year cooling)

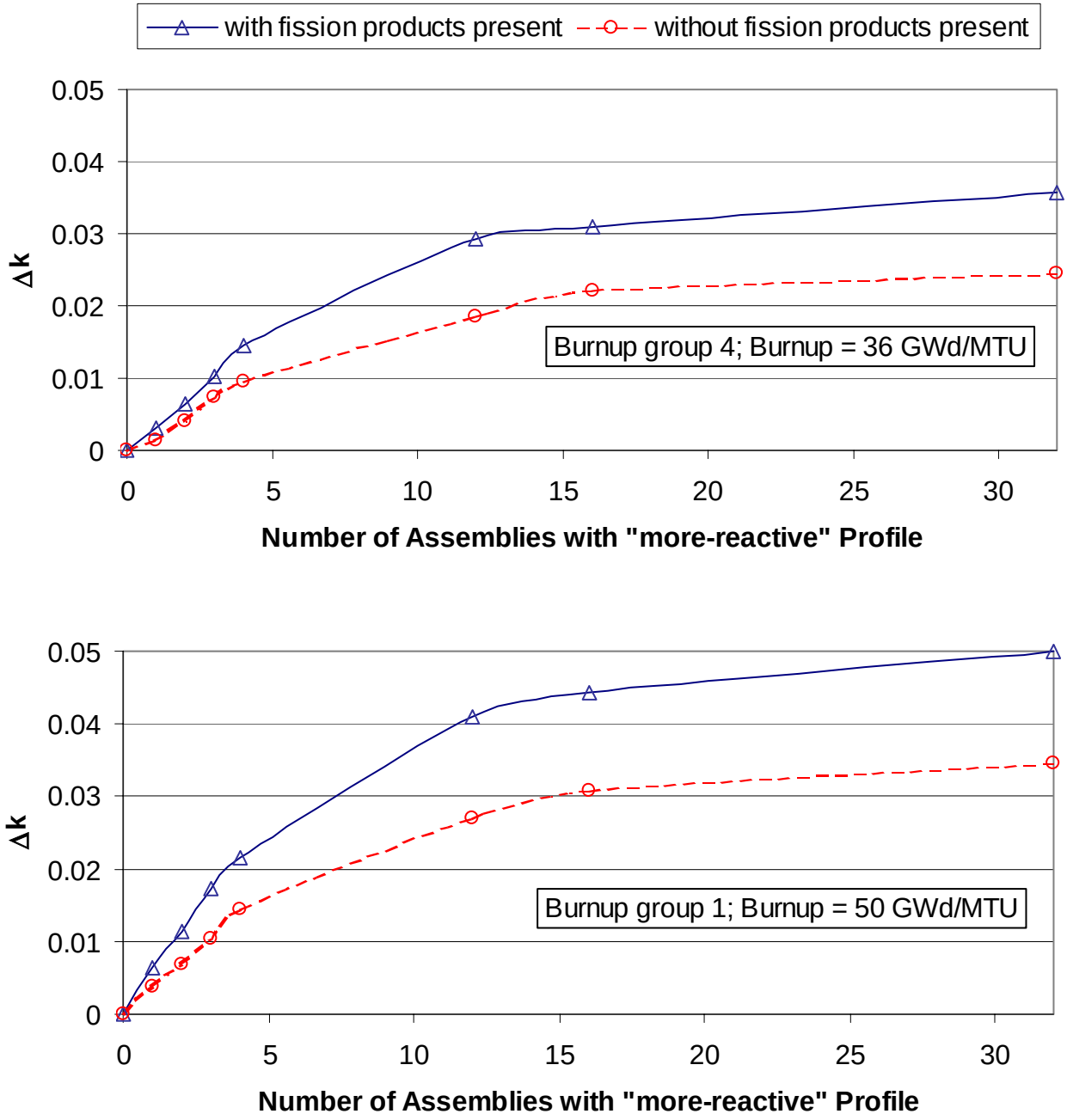

Figure 61 Δk consequence of loading various numbers of assemblies with a "more reactive" axial-burnup profile (based on inscribing) into the GBC-32 cask in which the remaining assemblies have the "actual bounding" axial-burnup profile (5-year cooling)

5 DISCUSSION AND IMPLICATIONS

Previous proposed approaches for addressing axial burnup in a burnup-credit criticality safety analysis have involved the determination of bounding axial profiles from actual burnup profiles; either identifying specific profiles that are bounding or developing "artificial" bounding profiles based on the characteristics of bounding profiles. Therefore, it is essential that the axial profiles considered in the determination of bounding profiles adequately represent the axial-burnup profiles of the SNF to be qualified as acceptable contents. A detailed examination of the available axial-profile database[8] suggests that, in terms of categories, it provides a very good representation of discharged PWR SNF assembly designs through the mid-1990s for the burnup and enrichment range of the current regulatory guidance[1,2] (i.e., $\leq$ 40 GWd/MTU and $\leq$ 4.0 wt % ^{235}U).

Although this evaluation focused on the burnup and enrichment criteria of the regulatory guidance, it is postulated that the Ref. 8 database is also sufficient for extension beyond the current burnup and enrichment limitations. This postulate is based on findings that show that, for a fixed burnup in the range in which the end effect is positive, axial profiles from lower burnup assemblies tend to yield higher end effects than axial profiles from higher burnup assemblies. This finding is illustrated in Figure 57, which demonstrates larger end effects for higher burnups (greater than ~34 GWd/MTU) associated with the use of a bounding profile from a lower burnup group (i.e., 30–34 GWd/MTU). Regarding higher initial enrichments, the bounding profiles tend to be associated with relatively low enrichments, and thus higher initial enrichments are not expected to lead to more reactive profiles. Perhaps more important than the addition of data for higher enrichments and burnups, is the continued addition of profiles from current fuel designs and operations to maintain the applicability of the database. In any case, it is paramount that the bounding axial profiles used in a safety evaluation be appropriate for the anticipated SNF contents. Specifically, the axial-profile database used for the determination of bounding profiles should represent the range of anticipated burnups, enrichments, reactor operations, and fuel designs.

Although the Ref. 8 database has been found to be quite comprehensive, it is not exhaustive. One issue is the adequacy of this (or any) finite database to completely represent the nearly infinite variety of possible profiles resulting from irradiation in U.S. PWRs. To address this issue, a statistical evaluation was performed on the neutron multiplication factors resulting from each of the profiles contained in the database to assess the likelihood of the existence of significantly more reactive profiles and the associated consequence to the neutron multiplication. Based on the Ref. 8 database, the k_{eff} value associated with each of the axial profiles was calculated and the mean and standard deviation for each of 12 burnup groups was determined. The results have generally confirmed the bounding profiles determined in a previous study (Ref. 7), but have shown that the bounding profiles are not representative of the average. For all but one of the 12 burnup groups, the k_{eff} value associated with the bounding axial profile is more than 3 standard deviations above the mean and, in most cases, is more than 4 standard deviations above the mean. In other words, the limiting profiles are statistical outliers, as opposed to being representative of typical SNF profiles. Consequently, one can infer that the probability that other axial profiles exist that are notably more reactive than the bounding profiles (determined from the database) is very small. When one considers ***that the limiting profiles are based on statistical outliers and that these limiting profiles will be applied to all assemblies in a burnup-credit cask***, it appears evident that this approach results in an adequate bounding approach in comparison to reality.

Analyses were also presented to assess the impact of loading an assembly that has an axial profile that is not bounded by the existing database. The analysis confirmed that the reactivity consequence is not significant (less than ~0.5% Δk, but depends on burnup and the specification of the "more reactive" profile). The "more reactive" profiles used for the analysis were artificially developed profiles created by

setting the average axial zone burnup equal to the minimum zone burnup for the actual bounding profiles. Considering that (1) the bounding profiles are based on statistical outliers, (2) the bounding profiles will be applied to all assemblies in a burnup-credit cask, (3) the very small probability that more reactive profiles exist, and (4) the small reactivity consequence of loading one assembly with an artificially-developed "more reactive" profile, the use of bounding profiles from the Ref. 8 database provides an adequate bounding approach for addressing axial burnup.

The use of a bounding profile provides a considerable increase in reactivity over the predominant typical or average profiles. Hence, less bounding approaches may be possible. For example, if axial-profile measurements for each assembly were performed prior to loading, a profile deemed bounding of the typical profiles could be used in the safety analysis and the profile for the as-loaded assembly could be checked for adherence.

Although the recommendations in the following section address burnup-credit criticality safety analyses within the constraints of the actinide-only assumption, the evaluations in this report suggest that the Ref. 8 database is equally adequate for analyses that include fission products. In fact, because the end effect increases with the presence of fission products (as compared to actinide-only analyses that neglect fission products), the margin associated with the use of the bounding profiles, in comparison to the use of typical profiles, is actually larger when fission products are included. Note that, due to the enlarged end effect associated with the presence of fission products, the use of alternative approaches that make use of more typical profiles, as described above, have greater potential benefit for analyses that include fission products.

6 RECOMMENDATIONS

The analyses summarized in this report, provide a technical basis for endorsing the adequacy of the axial-profile database[8] for obtaining bounding profiles for use with actinide-only burnup credit within the currently established burnup and enrichment range (i.e., ≤ 40 GWd/MTU and ≤ 4.0 wt % ^{235}U). The rationale for this recommendation are: (1) the axial-profile database[8] provides an adequate representation of discharged U.S. PWR SNF assembly designs; (2) the bounding profiles, as determined from the database, are statistical outliers, and thus the probability that more reactive profiles exist is very small; (3) the bounding profiles will be applied to all assemblies in a burnup-credit cask; and (4) the small reactivity consequence of loading an assembly with an artificially-developed "more reactive" profile. Because the end effect for assemblies with low enrichment axial blankets is typically very small or negative, this approach will bound those assemblies. For burnup and enrichment values beyond the current limits of 40 GWd/MTU and 4.0 wt % ^{235}U, expansion of the existing database would be desirable to increase the number of profiles representing that regime. However, analysis presented in this report indicates that bounding profiles from intermediate burnup ranges bound the available profiles at higher burnups. Consequently, the existing database may be adequate for burnups beyond 40 GWd/MTU. Future work should address the adequacy of the database for higher burnups and enrichments, and expand the database as additional profiles become available. Additionally, future work should evaluate the measured axial-profile data that has recently become available.[18]

7 REFERENCES

1. *Spent Fuel Project Office Interim Staff Guidance – 8, Rev. 1 – Limited Burnup Credit*, U.S. Nuclear Regulatory Commission, July 30, 1999.

2. *Standard Review Plan for Transportation Packages for Spent Nuclear Fuel – Final Report*, NUREG/1617, U.S. Nuclear Regulatory Commission, March 2000.

3. *Topical Report on Actinide-Only Burnup Credit for PWR Spent Nuclear Fuel Packages*, DOE/RW-0472, Rev. 2, U.S. Department of Energy, Office of Civilian Radioactive Waste Management, September 1998.

4. J. C. Wagner and C. E. Sanders, *Assessment of Reactivity Margins and Loading Curves for PWR Burnup Credit Cask Designs*, NUREG/CR-6800 (ORNL/TM-2002/6), U.S. Nuclear Regulatory Commission, Oak Ridge National Laboratory, March 2003.

5. S. E. Turner, "An Uncertainty Analysis – Axial Burnup Distribution Effects," *Proc. Workshop Use of Burnup Credit in Spent Fuel Transport Casks, Washington D.C., February 21-22, 1988*, SAND89-0018, TTC-0884, UC-820, T. L. Sanders, Ed., Sandia National Laboratories, October 1989.

6. M. D. DeHart, *Sensitivity and Parametric Evaluations of Significant Aspects of Burnup Credit for PWR Spent Fuel Packages*, ORNL/TM-12973, Lockheed Martin Energy Research Corp., Oak Ridge National Laboratory, May 1996.

7. T. A. Parish and C. H. Chen, *Bounding Axial Profile Analysis for the Topical Report Database*, Nuclear Engineering Dept, Texas A&M University, May 1997.

8. R. J. Cacciapouti and S. Van Volkinburg, "Axial Burnup Profile Database for Pressurized Water Reactors," YAEC-1937, Yankee Atomic Electric Company (May 1997). Available from the Radiation Safety Information Computational Center at Oak Ridge National Laboratory as DLC-201.

9. J. C. Wagner and M. D. DeHart, *Review of Axial Burnup Distribution Considerations for Burnup Credit Calculations*, ORNL/TM-1999/246, Lockheed Martin Energy Research Corp., Oak Ridge National Laboratory, February 2000.

10. J. C. Wagner and C. V. Parks, *Recommendations on the Credit for Cooling Time in PWR Burnup Credit Analyses*, NUREG/CR-6781 (ORNL/TM-2001/272), U.S. Nuclear Regulatory Commission, Oak Ridge National Laboratory, January 2003.

11. J. C. Wagner, *Computational Benchmark for Estimation of Reactivity Margin from Fission Products and Minor Actinides in PWR Burnup Credit*, NUREG/CR-6747 (ORNL/TM-2000/306), U.S. Nuclear Regulatory Commission, Oak Ridge National Laboratory, October 2001.

12. M. Takano and H. Okuno, *OECD/NEA Burnup Credit Criticality Benchmark - Result of Phase IIA*, JAERI-Research-96-003 (NEA/NSC/DOC(61)01), Japan Atomic Energy Research Institute, 1996.

13. A. Nouri, *OECD/NEA Burnup Credit Criticality Benchmark - Analysis of Phase II-B Results: Conceptual PWR Spent Fuel Transportation Cask*, IPSN/98-05 (NEA/NSC/DOC(98)1), Institut de Protection et de Surete Nucleaire, May 1998.

14. *Determination of the Accuracy of Utility Spent Fuel Burnup Records – Interim Report*, Electric Power Research Institute, EPRI TR-109929, May 1998.

15. *Spent Nuclear Fuel Discharges from U.S. Reactors 1994*, SR/CNEAF/96-01, Energy Information Administration, U.S. Department of Energy, February 1996.

16. RW-859 Nuclear Fuel Data, Energy Information Administration, December 2000.

17. R. J. Cacciapouti and S. Van Volkinburg, *Axial Burnup Profile Database for the Combustion Engineering 14x14 Fuel Design*, YAEC-1918, September 1995.

18. J. C. Neuber, *Measured Axial Burnup Shapes from Nuclear Power Plants Neckarwestheim 1 and Neckarwestheim 2*, Siemens AG Power Generation Group, NEA-1607, June, 1999. Available from the Radiation Safety Information Computational Center at Oak Ridge National Laboratory as DLC-209.

19. *Disposal Criticality Analysis Methodology Topical Report*, YMP/TR-004Q, Rev. 0, Las Vegas, Nevada: Yucca Mountain Site Characterization Office. ACC: MOL.19990210.0236, November 1998.

20. Summary Report of Commercial Reactor Critical Analyses Performed for the Disposal Criticality Analysis Methodology, BB00000000-01717-5705-00075, Rev. 1, Las Vegas, NV: CRWMS M&O. ACC: MOL.19980825.0001, August 1998.

21. C. H. Kang and D. B. Lancaster, "Actinide-Only Burnup Credit for Pressurized Water Reactor Spent Nuclear Fuel – III: Bounding Treatment of Spatial Burnup Distributions," *Nucl. Technol.* **125**, 292 (1999).

22. *SCALE: A Modular Code System for Performing Standardized Computer Analyses for Licensing Evaluation*, NUREG/CR-0200, Rev. 6 (ORNL/NUREG/CSD-2/R6), Vols. I, II, III, May 2000. Available from Radiation Safety Information Computational Center at Oak Ridge National Laboratory as CCC-545.

23. J. C. Neuber, "Burnup Credit Applications to PWR and BWR Fuel Assembly Wet Storage Systems," *Int. Conf. Physics of Nuclear Science and Technology*, Long Island, New York, October 5–8, 1998.

APPENDIX A

AXIAL DISCRETIZATION AND BOUNDARY CONDITIONS

APPENDIX A

AXIAL DISCRETIZATION AND BOUNDARY CONDITIONS

A.1 INTRODUCTION AND OVERVIEW

A significant concern in the implementation of burnup credit is the effect of axial discretization in a numerical model of spent fuel assemblies. Because of the effects of in-core axial leakage, partial length absorbers, moderator density changes, and other localized effects, the distribution of burnup is non-uniform. Typically, spent fuel burnup profiles are in the form of a flattened cosine, relatively uniform over most of the length of the fuel, but dropping off significantly towards the ends. As was illustrated in the body of this report, the shape of the profile itself has ramifications for the reactivity of the fuel when loaded in a cask.

A study has been performed to assess the impact of both axial discretization and boundary conditions on burnup credit analysis. The goals of this study were (1) to determine if 18-axial-zone discretization is adequate, (2) to identify a conservative boundary condition for a cask model, and (3) to investigate relationships between axial discretization and boundary conditions. (Note that in this usage "boundary condition" refers to the composition of the material at the end of the active fuel length. This is distinguished from the computational boundary condition, with an assumed vacuum beyond the outer ends of the cask, and was unchanged in all models.) Monte Carlo calculations were completed using a prototypical cask model to study trends in discretization and boundary condition effects as a function of burnup and isotopic compositions. Results were judged by plotting k_{eff} values and looking for trends. Because of the statistical uncertainty in the Monte Carlo calculations, it can be difficult to separate random fluctuations from true trends. For this reason, calculations were normalized to a mean for all axial discretizations for each parameter studied, such that enough sets of calculations were available to draw clear distinction between random variations and physical trends. All calculations were performed with sufficient neutron histories such that random variations would be bounded (with a 95% probability) by a $\pm$ 0.1% Δk band. Trends were assumed to exist when calculations showed a consistent deviation from this band.

The results of the study provide two clear findings: (1) assumption of a stainless steel boundary condition beyond the ends of the fuel is more conservative than water or a mixture of steel and water, and (2) the 18 axial-zone model (typical of reactor record burnup discretization) is adequate to capture the effects of a severe burnup profile with a conservative boundary condition.

A.2 BACKGROUND

Given an axially varying burnup profile, axial discretization is necessary to capture this effect. Because burnup corresponds to a change in isotopic composition in the fuel, the axial length in a spent fuel model should be subdivided into different material regions, each with a composition corresponding to the local burnup. If discretization is too coarse, the calculated flux distribution, and hence fuel reactivity, will be incorrect. This limitation is typically not a problem in a reactor calculation, since fluxes are generally more axially centered due to the presence of fresh and/or low-burn fuel at any point of operation, and flux distributions are not severely perturbed by burnup. In a spent fuel cask, however, most if not all fuel is fully burned. This effect is most dramatically indicated by the assumption of a uniform axial burnup,

representing the assembly-averaged burnup. The so-called "end-effect" (studied in the body of this report) is a measure of the error in the prediction of the neutron multiplication factor introduced by this assumption. This error results from an incorrect weighting of fuel reactivity resulting from both the inaccurate isotopic distribution and the corresponding flux that results from the distribution. Although this is an extreme example of the effect of poor axial discretization, more refined discretization can still be inadequate. The rapid change in the burnup profile near the ends of a spent fuel assembly and a concomitant shift in the predicted flux toward the outer ends of the fuel, results in a strong sensitivity to the isotopic distribution near one or both ends of the fuel.

Figure A.1 illustrates the fission density profiles calculated as a function of height using a 100 axial-zone model with both an axially varying and an averaged or uniform axial-burnup distribution, in a cask model with only water between the ends of the fuel and the cask walls. The fission density computed using the axially varying burnup profile shows a peak near the upper end of the fuel assembly. This peak represents a region where the lower burnup fuel is balanced by the loss due to leakage. Fuel burnup decreases further as one approaches the top of the fuel, but at the same time the leakage probability also increases. The cosine-shaped fission density profile computed for a uniform burnup approximation represents a balance between leakage from either end of the assembly, since there is no burnup gradient. This mismatch between reality (top-peaked fission density distribution) and the uniform burnup approximation (cosine-shaped distribution) results in the end effect. Increasing the number of axial zones in the burnup discretization will move the fission density away from a cosine shape and toward a top-peaked profile, providing an improved estimate of the true fission density profile.

Note that often a very small secondary peak is observed at the other end of the fuel rod, due to the reduced burnup at that end as well. In this case, however, the difference in reactivity between the two ends diminishes the effect and no lower peak is seen.

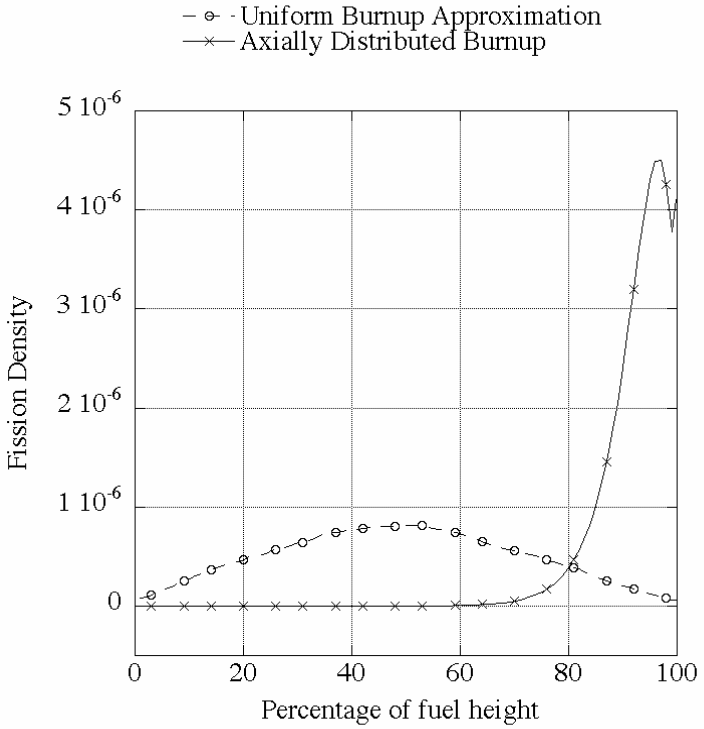

Figure A.1 Comparison of fission densities computed for uniform and axially distributed burnup profiles

A reasonably fine discretization scheme is necessary to capture the effect of the reduced burnup near the ends of a fuel rod. However, because fuel reactivity is highly weighted by the local flux near the ends of a fuel assembly, the boundary condition assumed beyond the ends of the fuel rod is also important, and may influence the amount of discretization needed near the ends of spent fuel. A study of the effects of different axial discretization schemes was performed, investigating the relationship between discretization and boundary conditions, burnup, and isotopic contents (i.e., limited actinides-only, or a limited set of actinides and fission products). This appendix has been provided to document this study, since the topic is very relevant to the subject matter of the body of this report.

A.3 APPROACH

A study of axial effects can be difficult, as there are many parameters known to influence the relative reactivity of spent fuel. These include the shape of the axial profile itself, the design of the cask within which the spent fuel is modeled, the initial enrichment of the fuel, post-irradiation cooling time, and the assumptions on reactor operations leading to a given burnup state. Rather than trying to perform a general study over the range of these many independent variables, this study makes some simplifying assumptions on these parameters so that a focus on discretization and boundary conditions is possible. Calculations were performed based on the GBC-32 cask, Westinghouse 17×17 OFA fuel assemblies with a 4% initial enrichment, assuming a 5-year cooling time, and conservative depletion parameters, consistent with calculations described in Section 4.3 of this report. The same sets of nuclides were used to define actinide-only and actinide plus fission-product calculations. A single axial profile was assumed for all calculations, based on profile 3 from Table 3 of this report. This profile is considered to be bounding for all YAEC database profiles for burnups greater than 30 GWd/MTU. Hence, this single profile was selected as it characterizes high burnup fuel and has been shown to be the most sensitive to the end effect. Because this profile was applied to calculations over a range of burnups, differences in results are known to be due to burnup-dependent isotopics only, and are not clouded by differences in the assumed burnup profile.

The specifications for this profile are available in Table 3, and are based on 18 equal-length axial zones. To be able to apply this profile as a basis for a number of axial discretization models, it was necessary to perform a fit to the data and use this fit to calculate the local burnup at the midpoint of different axial zones. The midpoint burnup was selected to represent the average burnup within that zone. An eighth-order polynomial fit was generated for the original 18 data points for this profile, giving normalized burnup as a function of axial height, *z*, by the equation:

$$B = 0.38252 + 0.031554z - 0.00051706z^2 + 3.7459e\text{-}06z^3 - 7.3721e\text{-}09z^4 - 5.9056e\text{-}11z^5 + 4.0467e\text{-}13z^6 - 9.4578e\text{-}16z^7 + 7.8724e-19z^8$$

where z is in cm ($0 < z < 365.76$), and B is a unitless burnup multiplier.

Figures A.2 – A.6 show the axial discretization relative to the continuous profile for the 10, 18, 50, 100, and 250 uniform-height axial-zone models used in these analyses. For each model, after generating *N* burnup multipliers for the midpoints of *N* axial zones (i.e., $B(Z_n)$, n=1,N), the burnups were renormalized to an average of 1.0. Calculations were performed with each axial discretization model for assembly-averaged burnup states of 20, 40, and 60 GWd/MTU; local burnup in each axial zone was calculated as the product of the assembly average and the value of the normalized profile for that zone. As indicated earlier, calculations were performed using a subset of major actinides-only, and a subset of major actinides plus major fission products.

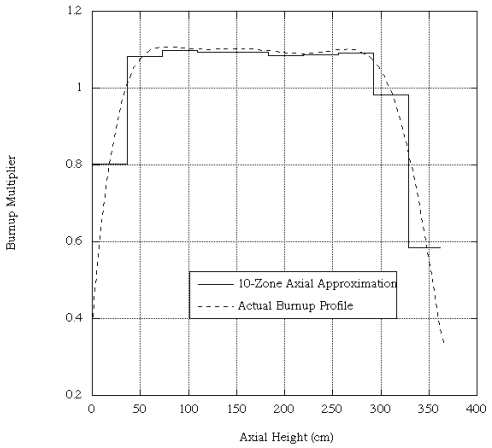

Figure A.2 10-Zone axial-burnup model

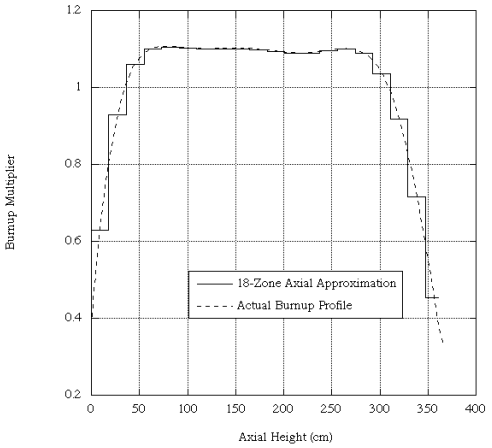

Figure A.3 18-Zone axial-burnup model

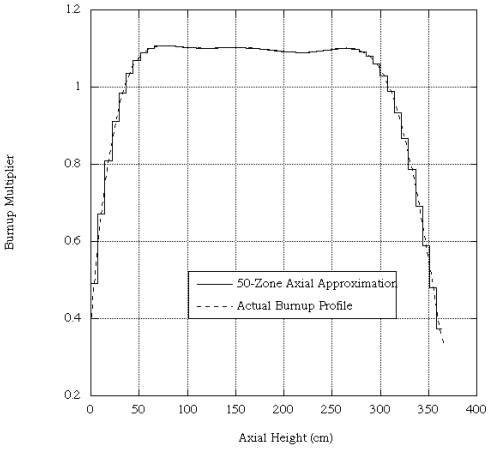

Figure A.4 50-Zone axial-burnup model

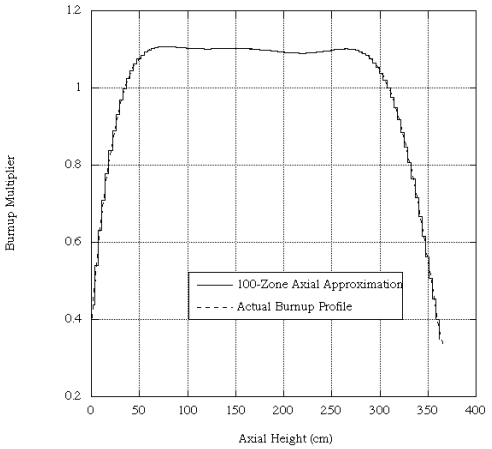

Figure A.5 100-Zone axial-burnup model

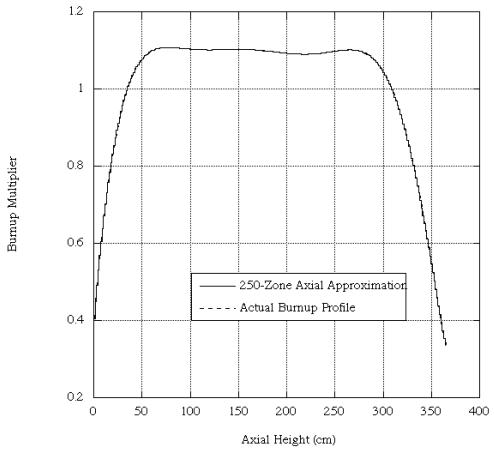

Figure A.6 250-Zone axial-burnup model

The water-filled GBC-32 cask model used in the analyses documented in this report used fuel with a length of 365.76 cm, with a 15 cm region of water below the fuel, and 30 cm of water above the fuel, separating the fuel from the cask. It is the neutronic properties of these zones that are of interest in terms of their effect on axial discretization, because they are immediately adjacent to the low-burnup ends of the fuel, and because modeling simplifications were used in assuming water only beyond the ends of the fuel. In reality, the end regions of fuel assemblies contain non-negligible amounts of stainless steel as support for fuel rods in the assembly. Since it would be difficult to try to model the physical design of the ends of the assembly, the GBC-32 specification assumes water-only to maximize moderation at the ends of the rod. An alternative model could be to assume only stainless steel at the fuel ends, which would decrease local moderation but increase reflection back into the assembly. A third alternative would be to assume a homogenized mixture of both water and stainless steel. For this study, these three models were assumed for the 15 cm region below the fuel and the 30 cm region above the fuel: (1) 100% water, (2) 100% stainless steel, and (3) 50% water and 50% stainless steel (homogenized). Depletion calculations were performed to estimate isotopic concentrations as a function of zone for the three burnup states, and calculations were repeated with each of these three boundary conditions.

A.4 RESULTS

With three burnup states, three fuel boundary conditions, and two sets of isotopics, 18 different calculations were performed for each of the five axial discretizations. Combined results for all 90 calculations are illustrated in Figure A.7. In order to do a relative comparison, all calculated k_{eff} values were normalized to the mean calculated k_{eff} values of all five axial discretization models computed for each burnup/boundary/nuclide set. With such normalization, results should be clustered around 1.0, with a distribution characterized by the standard deviation associated with the Monte Carlo calculations, i.e., approximately 95% of the calculated and normalized values should lie within the range of $1.0 +/- 2\sigma$. Clear, non-random deviations from this band would indicate a trend with respect to the independent variable.

To help visually distinguish between the models, conventions were used in the selection of plotting symbols and line types, as can be seen from the plot legend of Figure A.7.

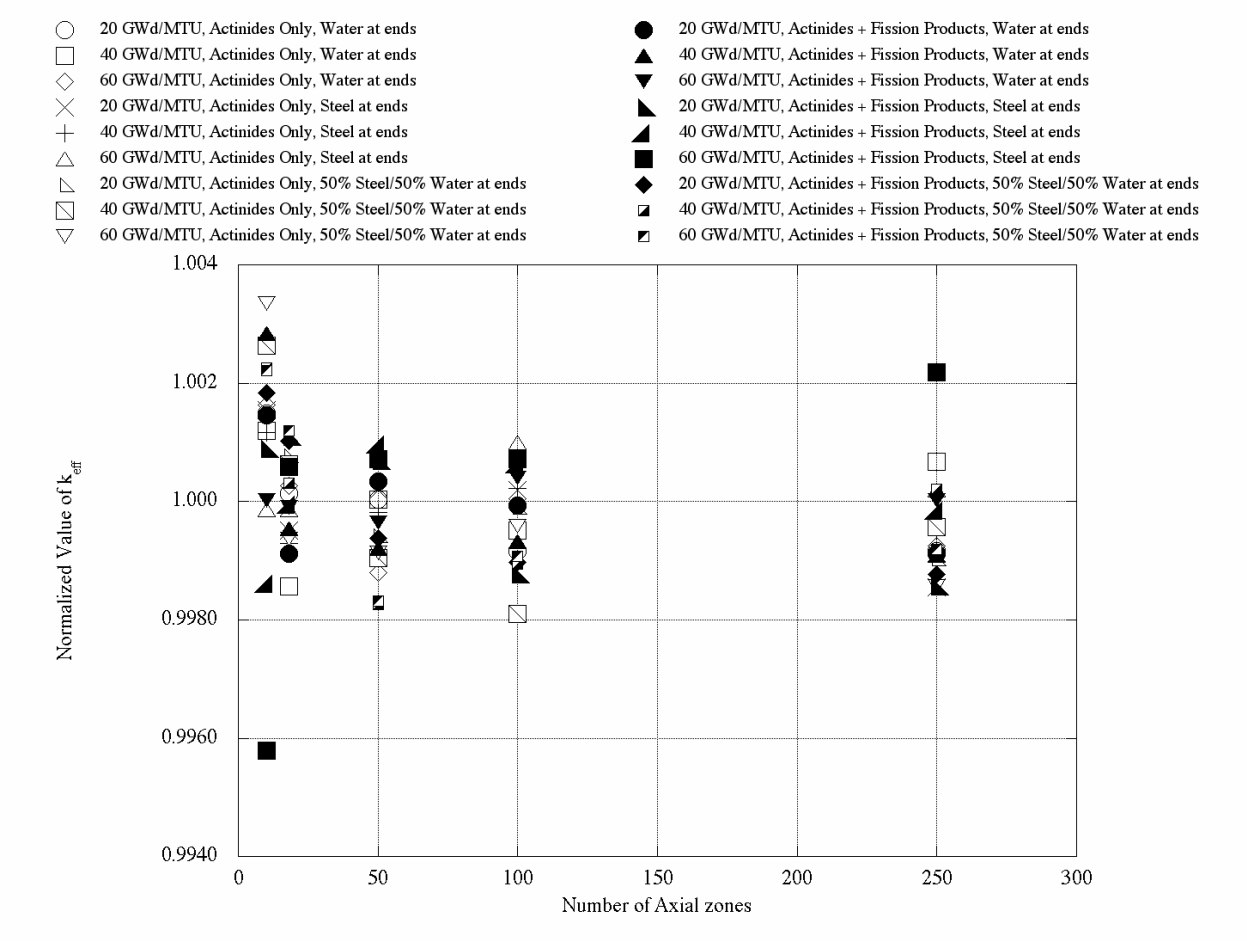

Figure A.7 Summary of normalized results all calculations

Several observations can be made from this gross collection of all results:

1) Since the standard deviation on each individual calculation was on the order of 0.0005 for all calculations, the scatter around 1.0 is consistent with a 2σ spread in data, which should capture 95% of a normal distribution. With the exception of the 10-axial-zone models, results are clustered within $\pm$ 0.001.

2) Results for 10 axial zones have roughly the same spread, but are shifted above a mean of 1.0. This indicates that the 10 axial-zone model is inadequate for this axial-burnup profile.

3) Overall, the results of the 60 GWd/MTU, steel-ends cases with fission products present (solid square symbol) appear to be generally higher than the other cases (the solid square symbols are at the upper end of the 18–250 zone sets of results). In fact, the opposite is true. The single 10-zone case gives a much lower result than that of the other axial models; normalization tends to raise the other results (for the 60 GWd/MTU, steel ends cases) to maintain an average. However, the low 10-zone result is not a statistical outlier. The calculation has been rerun with a different random

number seed and with twice as many histories, with essentially the same result. Apparently, the nuclides present in highly burned fuel are more sensitive to the presence of steel at the end of the fuel when a coarse axial model is used.

4) No clear trends are seen as a function of nuclides, burnup, or boundary conditions with 18 or more axial zones. However, it will be instructive to look at subsets of data to simplify the picture.

Figures A.8 – A.10 show trends in discretization modeling for each burnup state. There are no clear trends with nuclide set or with boundary conditions in these plots; however, Figure A.8 indicates that for low-burnup (20 GWd/MTU for 4 wt % enrichment) fuel, a very large number of axial zones is necessary to capture the effects associated with this axial-burnup profile. The trend is very small and could be a statistical fluke resulting from the randomness of Monte Carlo calculations; however, the trend does appear to lie outside the band of randomness characterizing these calculations. The effect is probably the result of using a burnup profile that is typical of more highly burned fuel. Because the fuel is underburned, the assumed profile artificially puts more reactive fuel near the ends of the assembly, giving a stronger sensitivity to the axial profile. No similar trends are seen for the 40 and 60 GWd/MTU burnup cases (Figures A.9 and A.10); both appear to show spatial convergence with 18 axial zones. Further study would be necessary to positively identify the reason for the apparent slope in Figure A.8. However, the magnitude of the trend is on the order of statistical uncertainty, and does not appear to warrant further investigation.

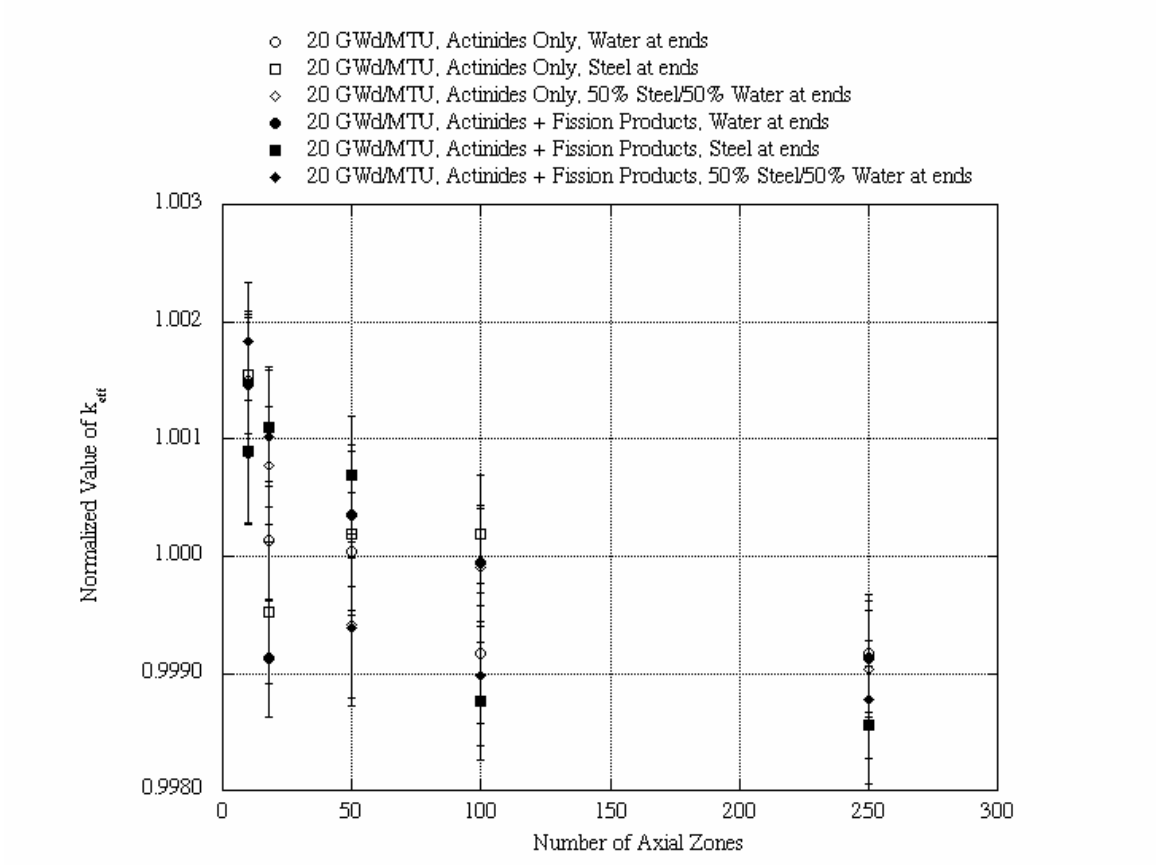

Figure A.8 Normalized results for 20 GWd/MTU burnup fuel

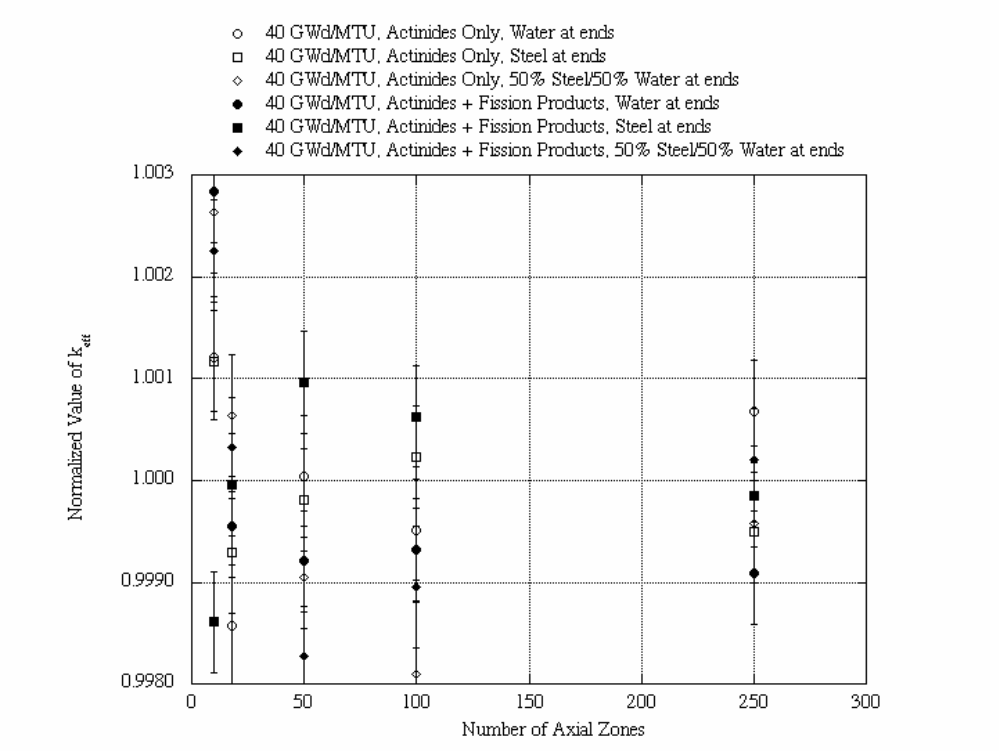

Figure A.9 Normalized results for 40 GWd/MTU burnup fuel

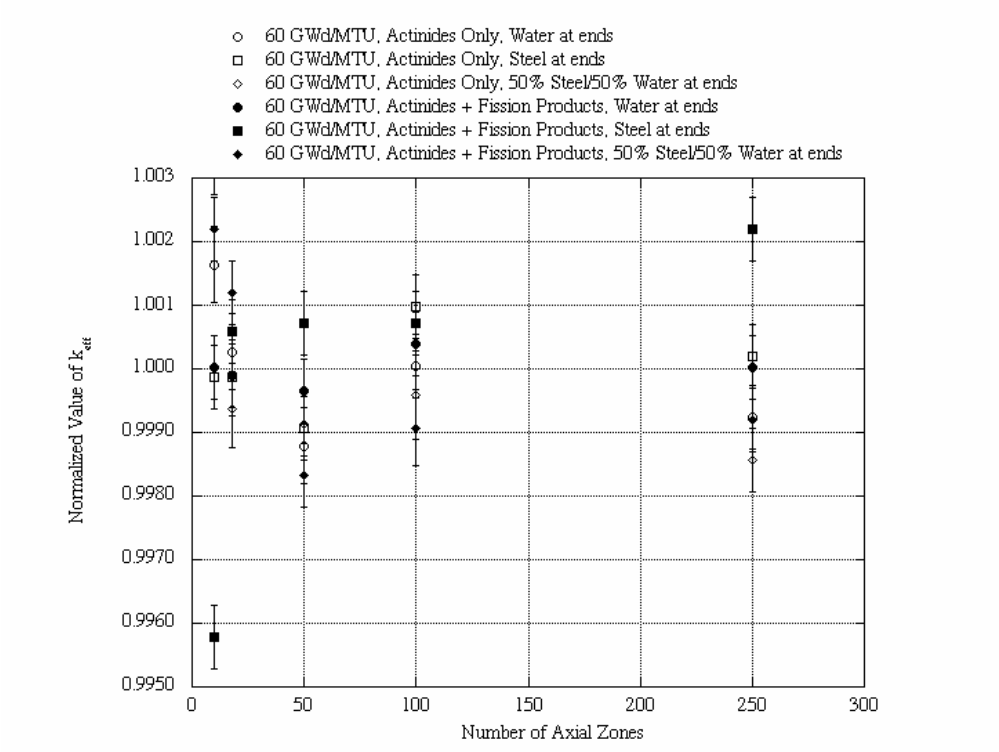

Figure A.10 Normalized results for 60 GWd/MTU burnup fuel

Figures A.11 – A.16 illustrate the raw, non-normalized results for cases with and without fission products, and for burnups of 20, 40, and 60 GWd/MTU. These results show clearly that for all burnups and for both sets of fuel nuclides, steel placed at the ends of the fuel is slightly more reactive than water in the same region, for the assumed burnup profile. The magnitude of the effect is roughly 0.5 to 1% in k, and appears to increase with burnup. It is also clear that use of more than 18 axial zones does not alter the estimate of k_{eff}, i.e., 18 axial zones is adequate to capture the effect of the variation in boundary conditions.

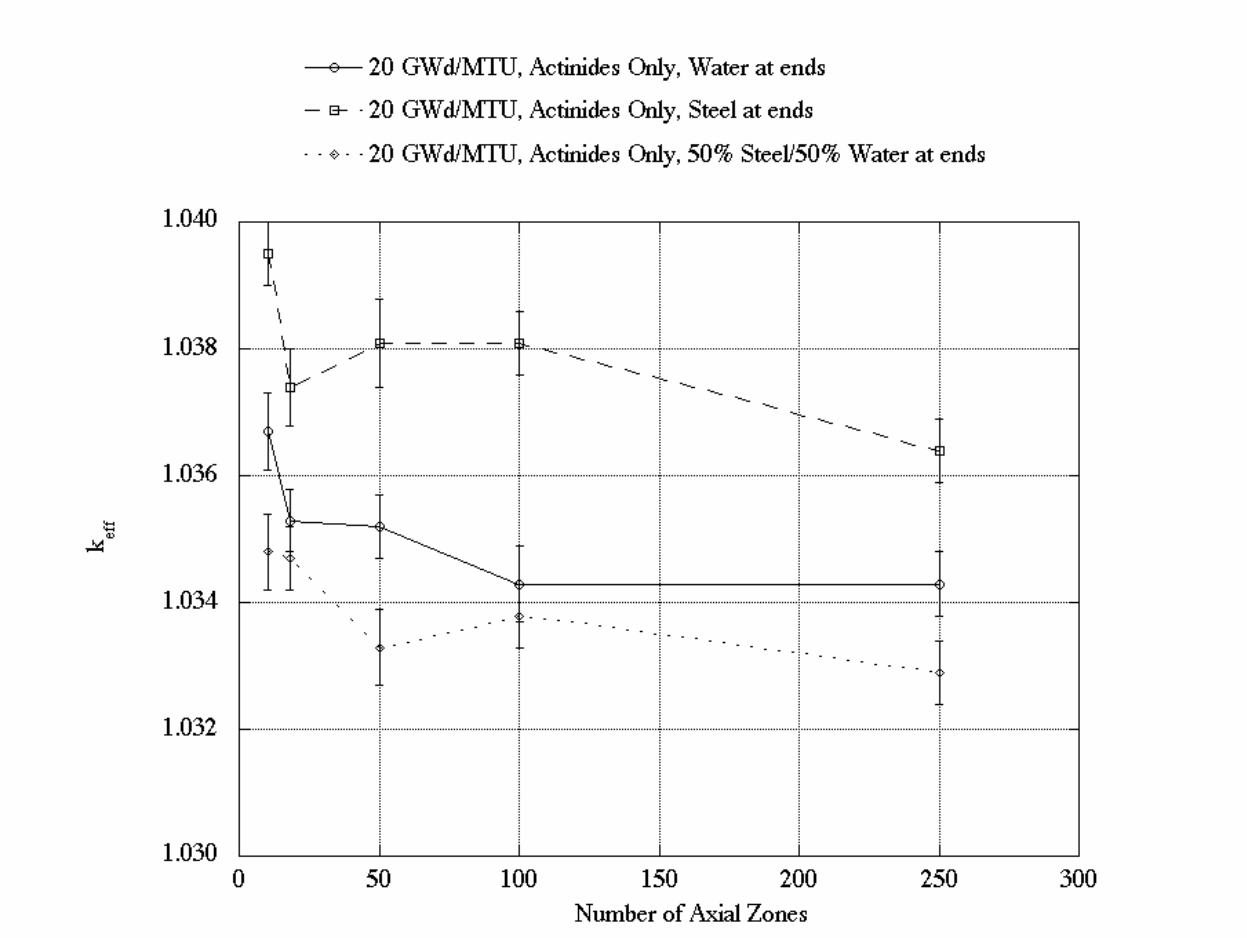

Figure A.11 Computed results for 20 GWd/MTU burnup fuel, actinides-only

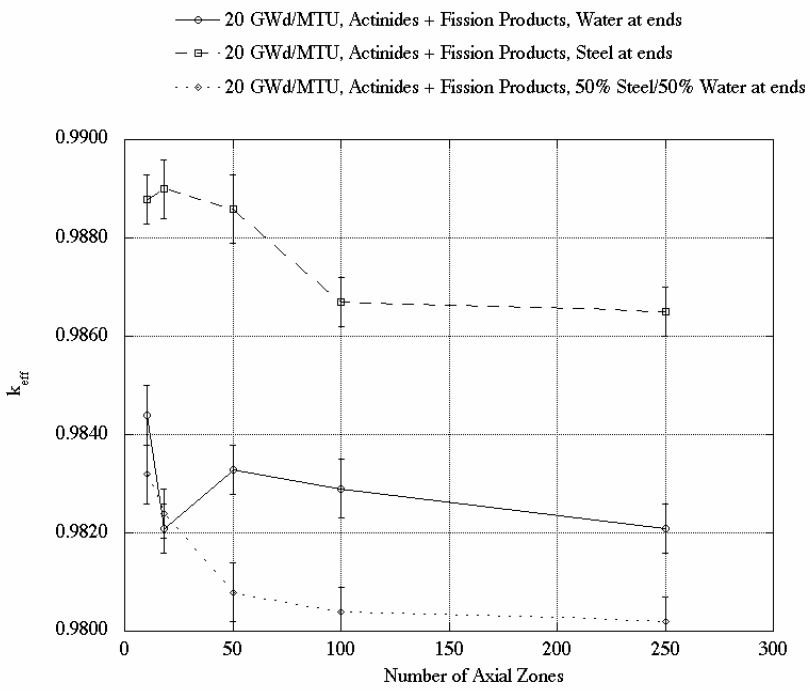

Figure A.12 Computed results for 20 GWd/MTU burnup fuel, actinides and fission products

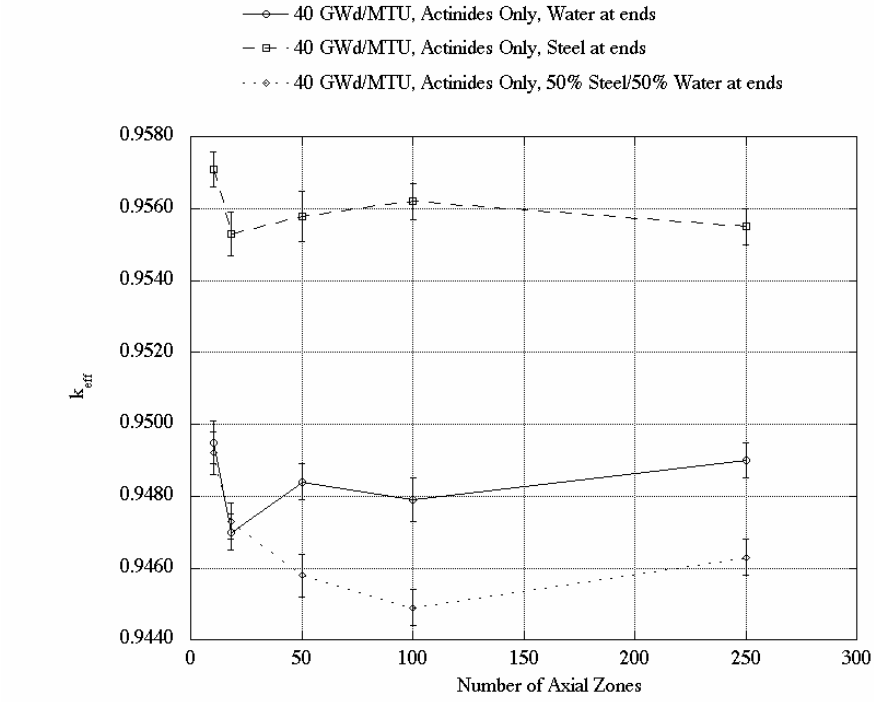

Figure A.13 Computed results for 40 GWd/MTU burnup fuel, actinides-only

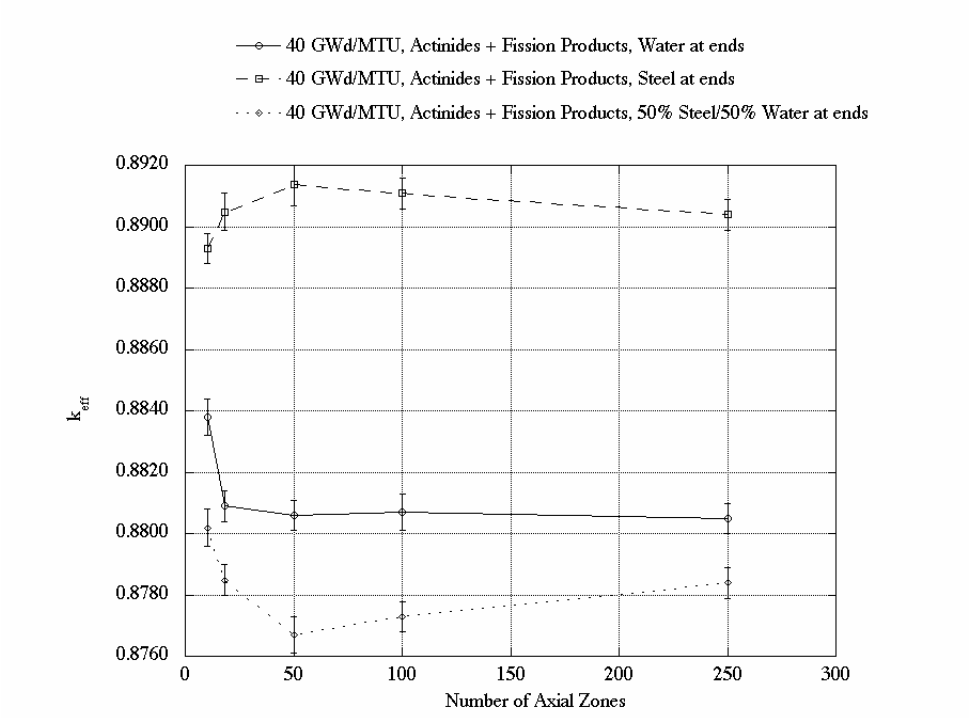

Figure A.14 Computed results for 40 GWd/MTU burnup fuel, actinides and fission products

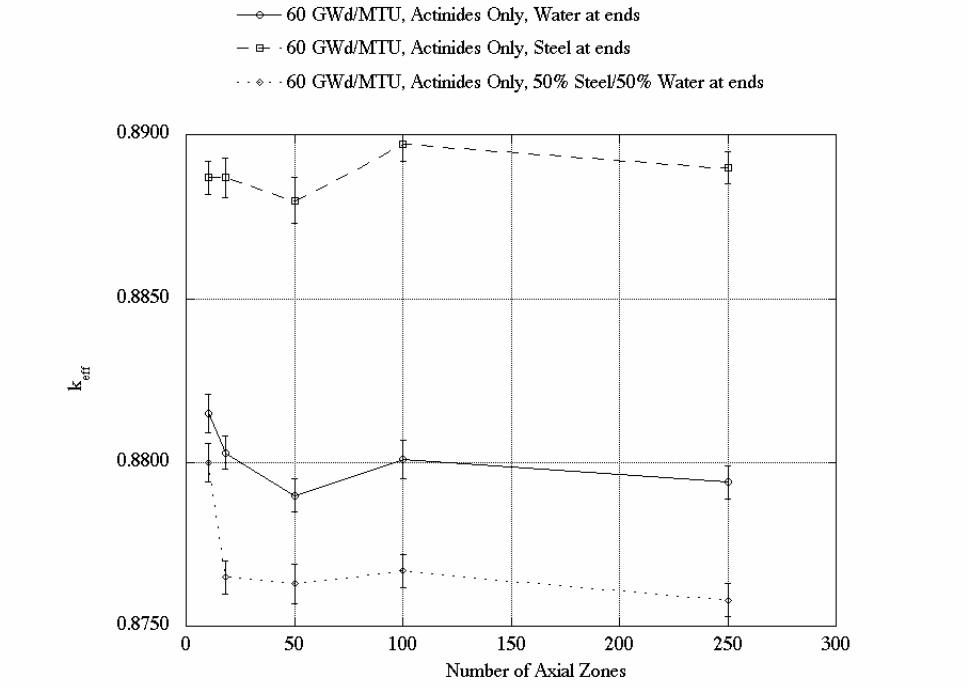

Figure A.15 Computed results for 60 GWd/MTU burnup fuel, actinides-only

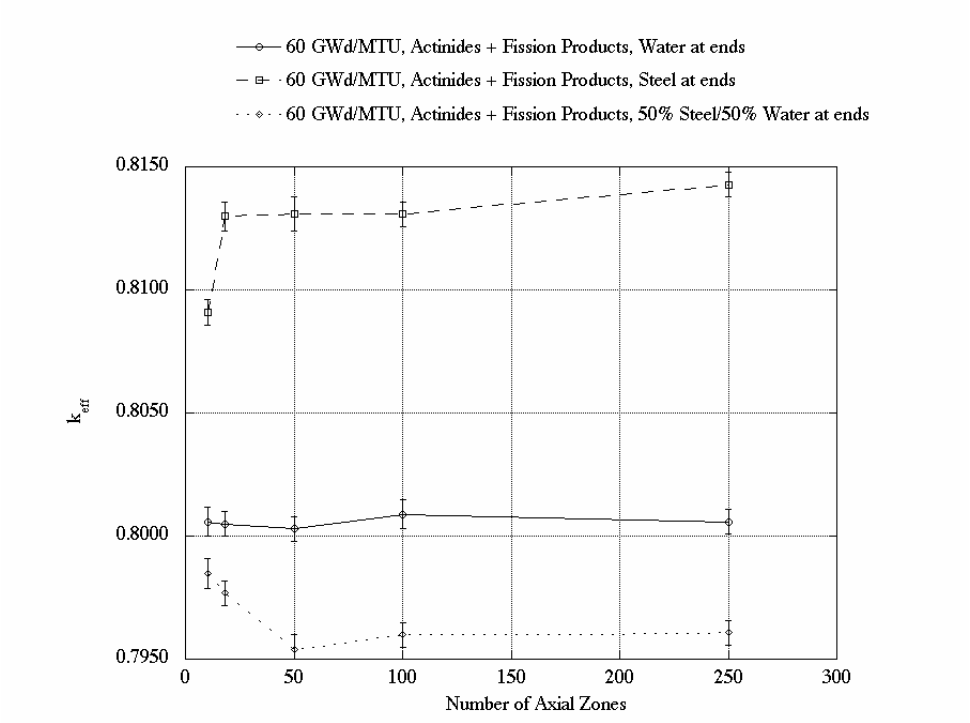

Figure A.16 Computed results for 60 GWd/MTU burnup fuel, actinides and fission products

Interestingly, both steel and water, by themselves, are more conservative (yield a higher value of k_{eff}) than a 50/50 mixture of the two materials. To study this phenomenon further, fission densities were plotted as a function of axial position in the fuel. In this calculation, the fission density peaks in the most reactive region of the fuel assembly, which for this burnup profile and cask model is near the upper end of the fuel assembly. Figure A.17 illustrates the fission densities calculated using the 250 axial-zone model for 60 GWd/MTU burnup with fission products present, for all three boundary conditions studied; only the upper end is plotted. Although there is statistical error associated with the fission density calculated for each zone, the error is very small, and error bars are not plotted, for clarity. This figure clearly indicates that a 100% steel boundary condition is a significantly better reflector than the other two models, resulting in a greater fission density and thus a greater reactivity for the fuel. Note that the fission peak also shifts somewhat toward the upper end, into a region with lower burnup. Because of this shift and the increased fission density, net leakage is also substantially greater in the steel-only model; however, the net effect is a reactivity gain.

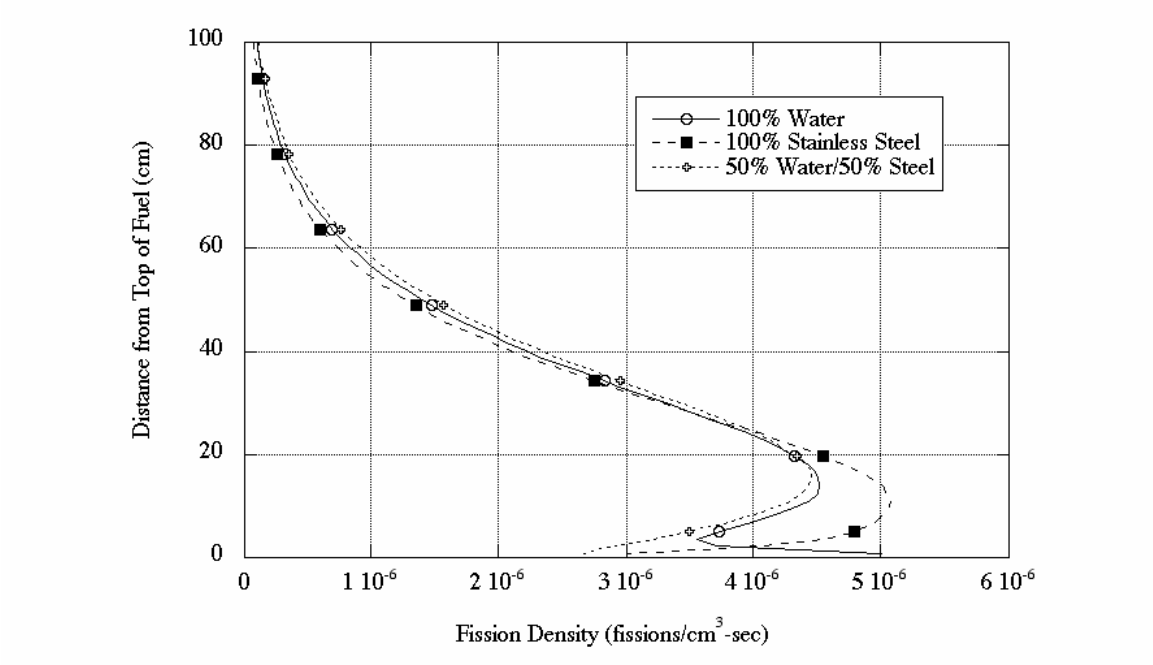

Figure A.17 Fission density profiles for different fuel boundary conditions

For the water-only boundary condition, a thermal peak is seen at the very end of the fuel, where neutrons thermalized in the water and scattered back into the fuel are causing fissions in the ultra-low-burnup fuel at the very top of the fuel assembly. However, neutrons born at the very end of the fuel have a high escape probability and, therefore, do not significantly alter the reactivity of the fuel.

The homogenized steel/water mixture at the end of the fuel is the closest representation of reality (the ratio of steel and water in this region varies with assembly design and was not explicitly determined). This case does not show a thermal peak – the amount of steel present is sufficient to reduce moderation. However, the amount of water is sufficient to prevent significant reflection by the steel. Thus, this case has a slightly lower fission density than either of the other two cases. The relative fission densities for the three cases studied are consistent with Figures A.11 – A.16; those figures seem to indicate that this fission density behavior is consistent for all discretization models ($N \geq 18$) for all burnups and nuclide set combinations.

All calculations performed in this study indicate that for the axial-burnup profile assumed, an 18-axial-zone burnup distribution model is sufficient. As was discussed earlier, and illustrated in Figure A.1, inadequate discretization results in an incorrect fission density distribution. One can conclude that as more axial zones are added in approximating the burnup distribution, the closer the fission density distribution gets to the top-peaked distribution. This behavior converges fairly rapidly, and for the burnup distribution assumed in these analyses 18 axial zones is sufficient to converge to the correct fission density profile. Even though the burnup profile is discretized in a computational model, the fission density profile that characterizes the reactivity of the fuel is still a continuous function. It is conjectured that the 18-axial-zone model for the burnup distribution results in a closely converged fission density profile, whereas the 10-zone model does not. To test this hypothesis, fission densities were extracted from models with 1, 2, 4, 10, 18, and 100 axial burnup zones. Assuming 100 axial zones is a very close approximation to a continuous burnup profile, this profile is used as a basis for comparison in determining a converged profile. Figure A.18 illustrates the results of these calculations. The strong agreement

between the 18 zone model and the 100 zone model indicates that the 18 zone model is sufficient to capture the effects of the burnup distribution, and explains why higher order discretization shows no significant improvement.

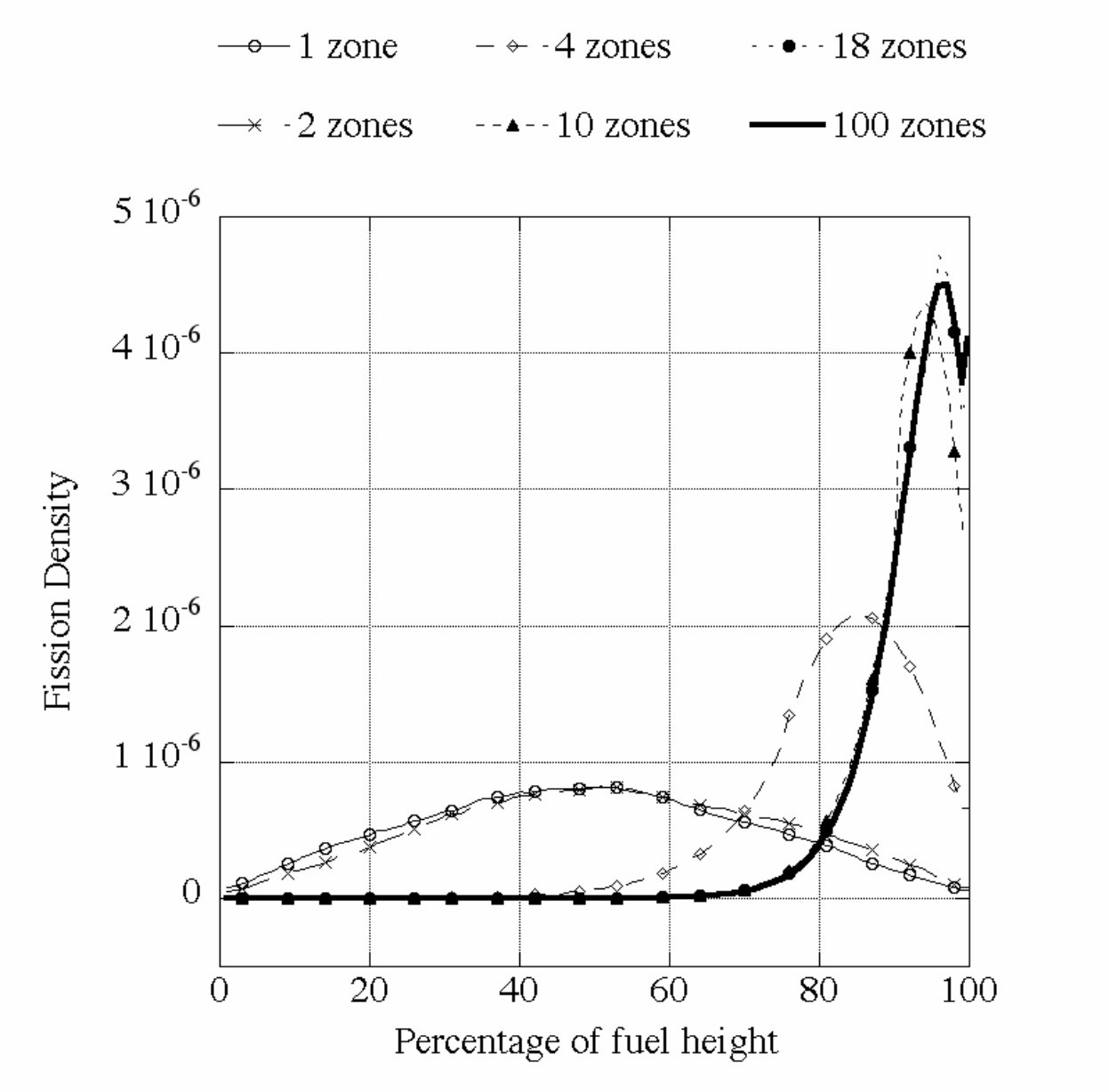

Figure A.18 Fission density profiles for different burnup discretization approximations

A.5 CONCLUSIONS

This study was performed to assess the effect of discretization and boundary conditions on the calculation of k_{eff} for spent fuel in a cask for a burnup-credit analysis. In this study, the term "boundary condition" was used to describe the material assumed at the end of the fuel assemblies, separating the ends of fuel assemblies from the cask walls; the mathematical boundary conditions applied on the outer boundaries of the cask were unchanged in this work.

Results of variations in the size of axial zones in fuel assembly models indicated that for the most part, use of 18 uniform-height axial zones is sufficient to capture burnup distribution effects, even for the "limiting" axial burnup profile assumed in this study. This is fortuitous, because axial-burnup data available from reactor records are typically based on 18–20 axial zones. Furthermore, because refined data is not available for spent fuel, this study used a numerical fit to 18-zone data. Conclusions drawn from differences in finer discretization must be balanced with the realization that the actual burnup profile is not well known in the last 10 cm of the fuel, however the spent fuel reactivity appears to be driven by the fuel compositions lying more than 10 cm away from the end of the fuel, as indicated in Figure A.17.

The study of the effect of the representation of structure immediately beyond the ends of the fuel showed more significance. Because of the complexity of assembly hardware beyond the active fuel region, various approaches can be taken to represent the hardware structure. The study in the main body of this document ignored all structure and assumed water-only beyond the ends of the active fuel regions. The studies described in this appendix looked at the effect of other assumptions for the material in this region. No attempt was made to mock up the actual hardware design for assembly endfittings; rather, two conditions expected to represent the two extremes in structure approximation were assumed, along with an intermediate representation. The all-water approximation is considered one extreme, and would be expected to increase moderation near the end of the fuel. Replacing this water with steel represents the other extreme, in which the extra moderation is removed and replaced with a better reflector. The intermediate case is a 50/50 combination of steel and water, homogenized into one material.

Both full steel and full water were found to be more conservative than the mixture of the two. The homogenized mixture tended to dilute both the reflection and moderation effects, although the behavior more closely resembled water-only. Models based on full steel content, excluding all water beyond the ends of the fuel, were more conservative than the water-only model by as much as 1% in k_{eff}. However, it must be recognized that this is an extreme model, and that water would almost always be present within the endfitting regions in a flooded cask, albeit in a discrete rather than homogenized volume. Nevertheless, these results indicate that some attention should be paid to the hardware design in a burnup-credit analysis. A simple approach would be to assume solid hardware (e.g., 100% steel) beyond the ends of the fuel.

APPENDIX B

COMPARISON OF PROFILES WITH 3-D CASK CALCULATIONS

APPENDIX B

COMPARISON OF PROFILES WITH 3-D CASK CALCULATIONS

In addition to the statistical comparison of profiles with 1-D calculations, as described in Section 4.2.1 of this report, a comparison was also performed on the k_{eff} values from 3-D calculations with the GBC-32 cask (actinides and fission products included; 5-year cooling time assumed). The results are completely consistent with those described in Section 4.2.1, but are provided in this appendix for comparison purposes.

Figures B.1–B.12 show the spread of k_{eff} values that result from the set of profiles in each of the 12 burnup groups. In addition to the individual calculated k_{eff} values, the figures show the mean k_{eff} value and indicators for 1, 2, and 3 standard deviations. For all but two of the 12 burnup groups, the k_{eff} value associated with the bounding axial profile, is more than 3 standard deviations above the mean and, in most cases, is more than 4 standard deviations above the mean. The results are summarized in Table B.1, which lists the mean, standard deviation, maximum, minimum, number of standard deviations that the maximum k_{eff} value is above the mean, and the maximum and average end effect for each burnup group. The results confirm the 1-D results for determining bounding profiles and for demonstrating that the bounding profiles can be considered statistical outliers, as opposed to representative of typical SNF profiles.

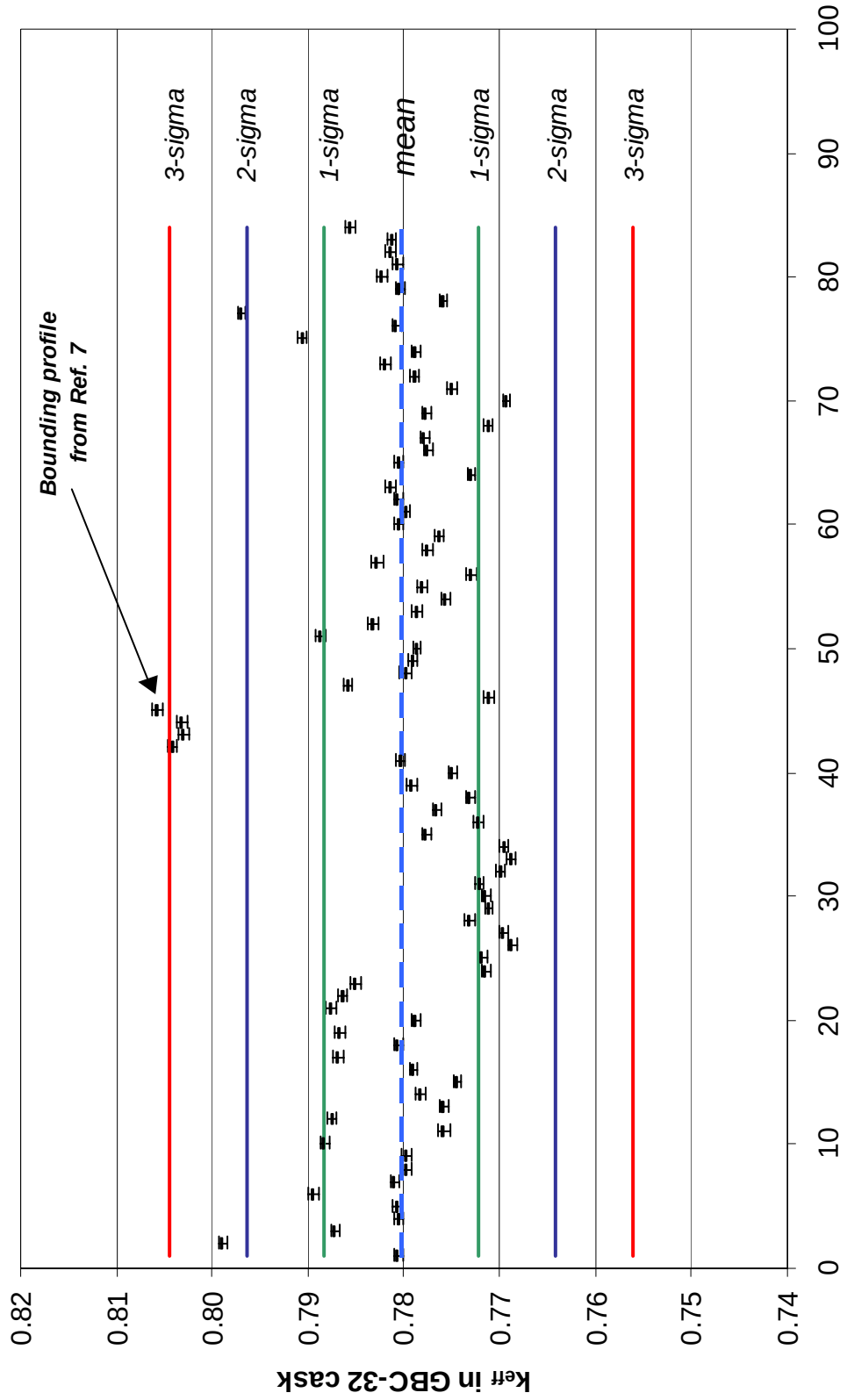

Figure B.1 Plot of k_{eff} values for axial burnup profiles in burnup group 1 (burnup > 46 GWd/MTU). Total number of profiles in this burnup group is 84.

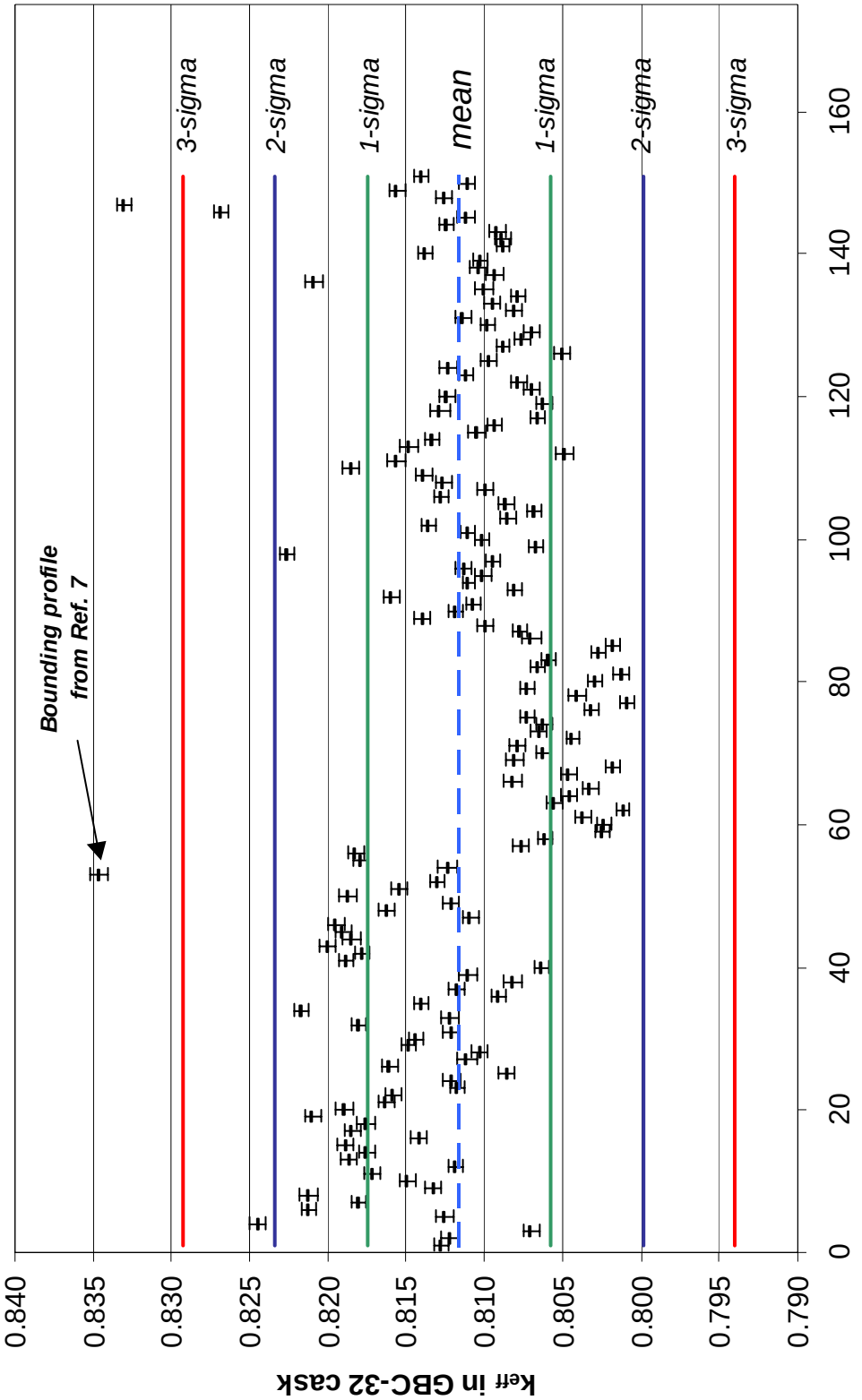

Figure B.2 Plot of k_{eff} values for axial burnup profiles in burnup group 2 (42 < burnup < 46 GWd/MTU). Total number of profiles in this burnup group is 151.

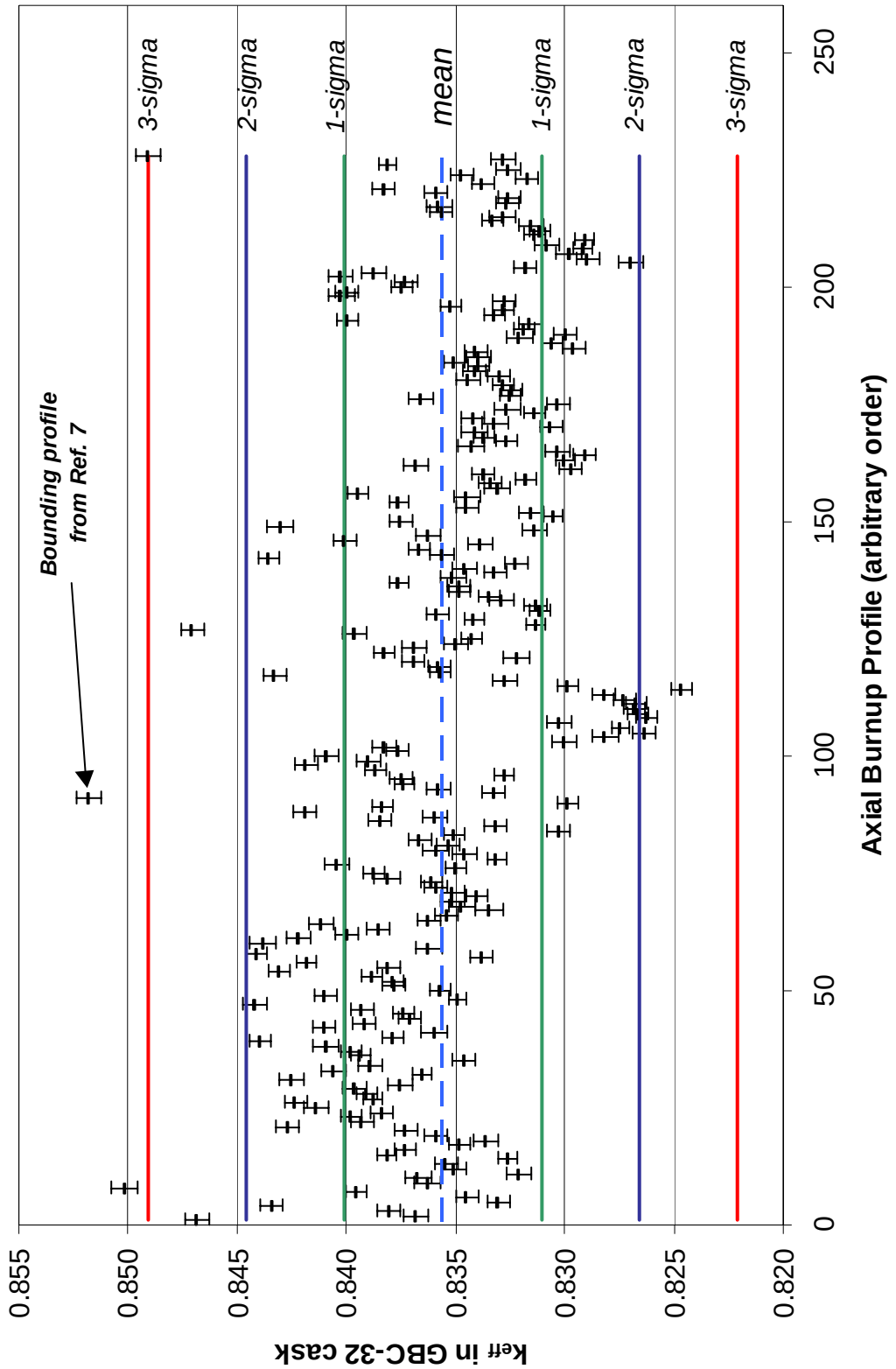

Figure B.3 Plot of k_{eff} values for axial burnup profiles in burnup group 3 (38 < burnup < 42 GWd/MTU). Total number of profiles in this burnup group is 228.

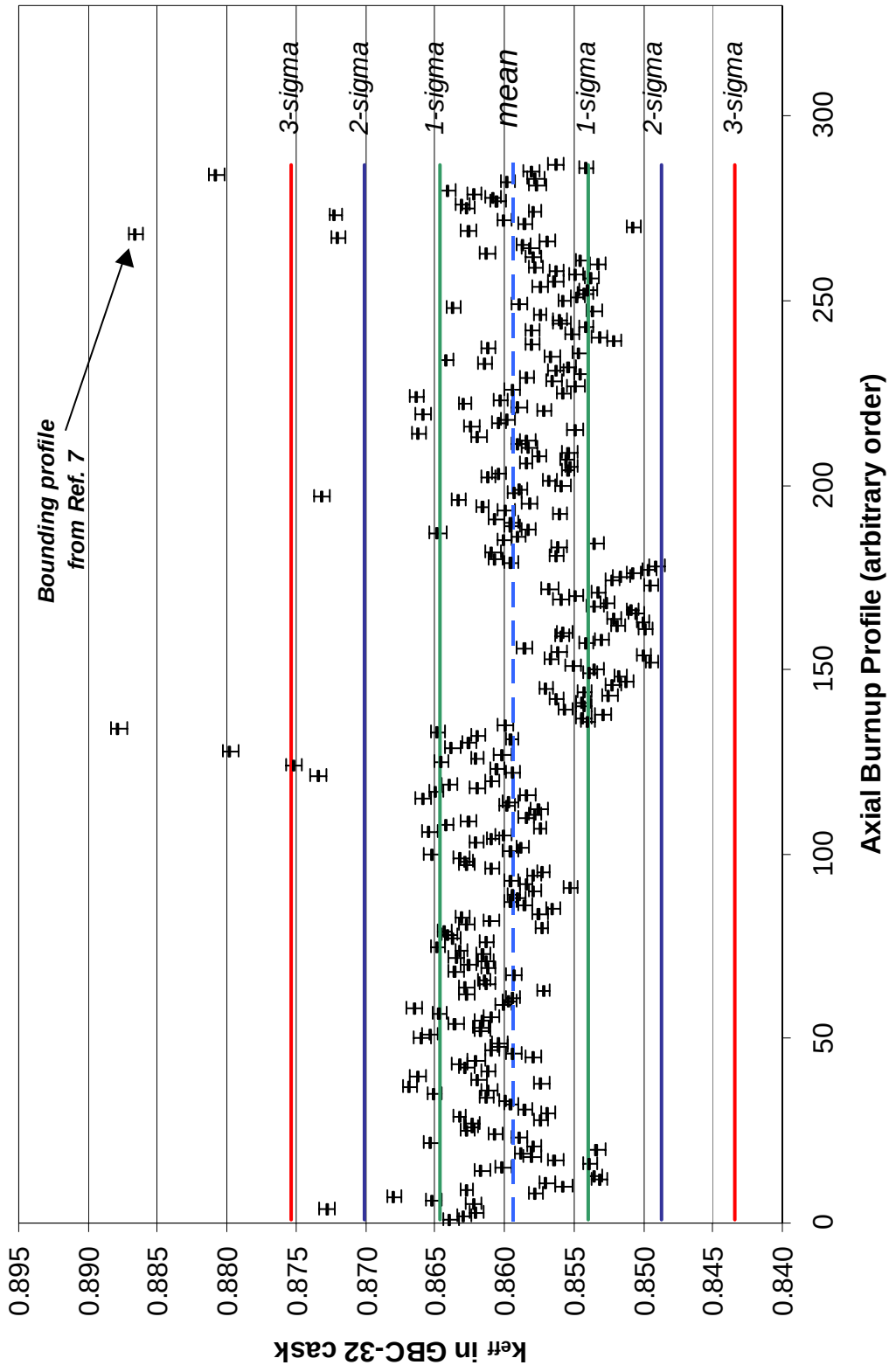

Figure B.4 Plot of k_{eff} values for axial burnup profiles in burnup group 4 (34 < burnup < 38 GWd/MTU). Total number of profiles in this burnup group is 287.

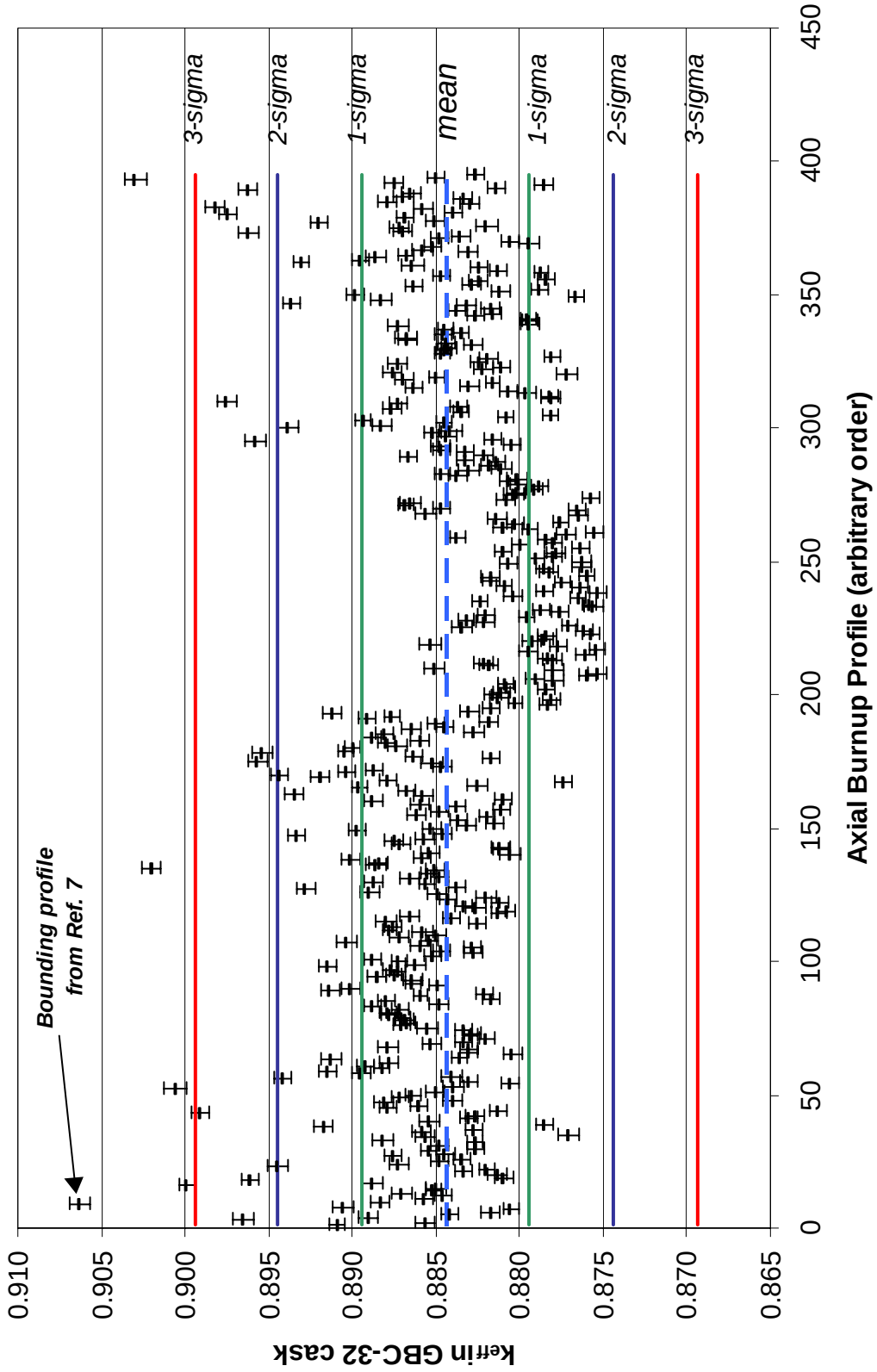

Figure B.5 Plot of k_{eff} values for axial burnup profiles in burnup group 5 (30 < burnup < 34 GWd/MTU). Total number of profiles in this burnup group is 395.

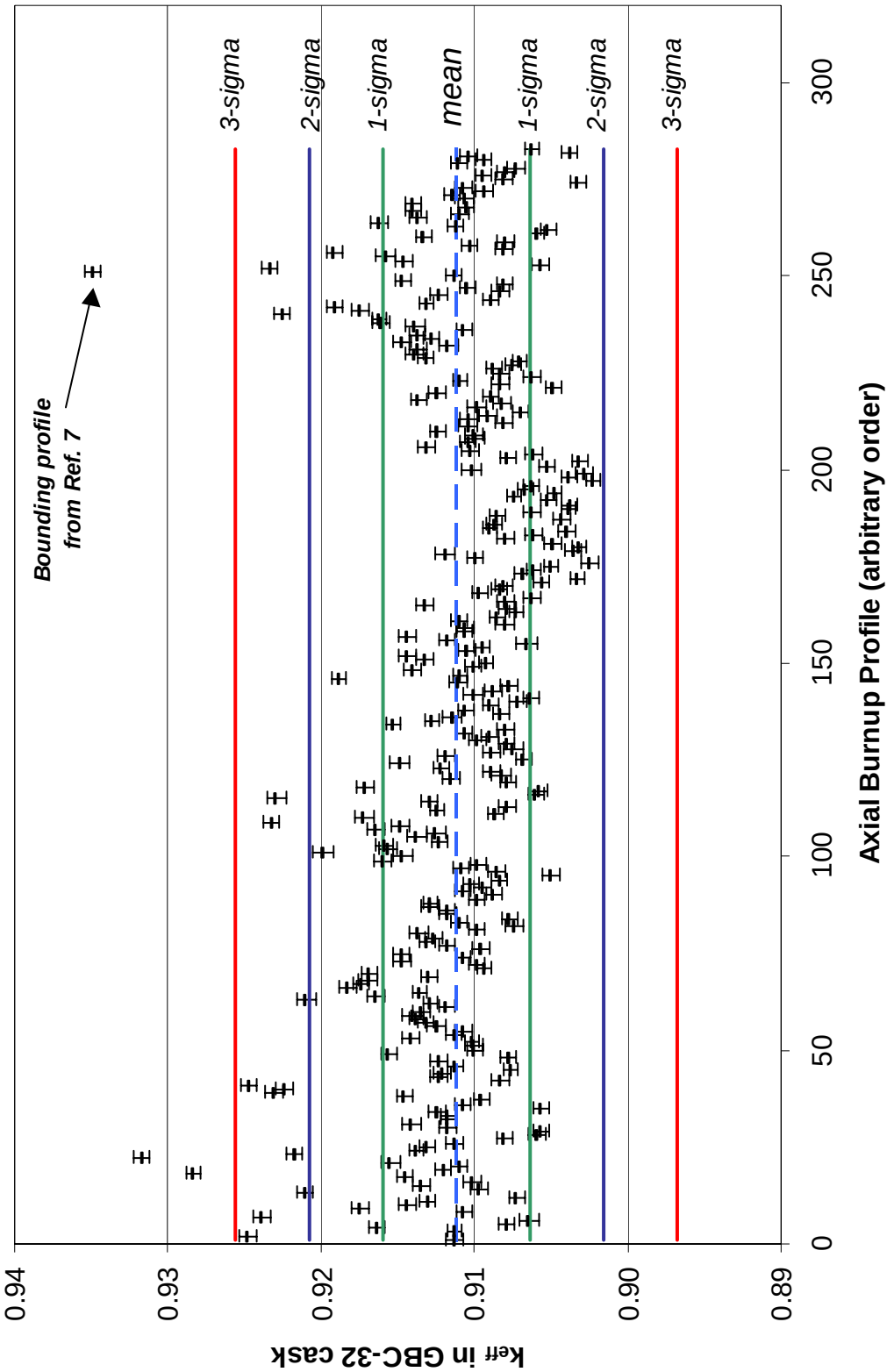

Figure B.6 Plot of k_{eff} values for axial burnup profiles in burnup group 6 (26 < burnup < 30 GWd/MTU). Total number of profiles in this burnup group is 283.

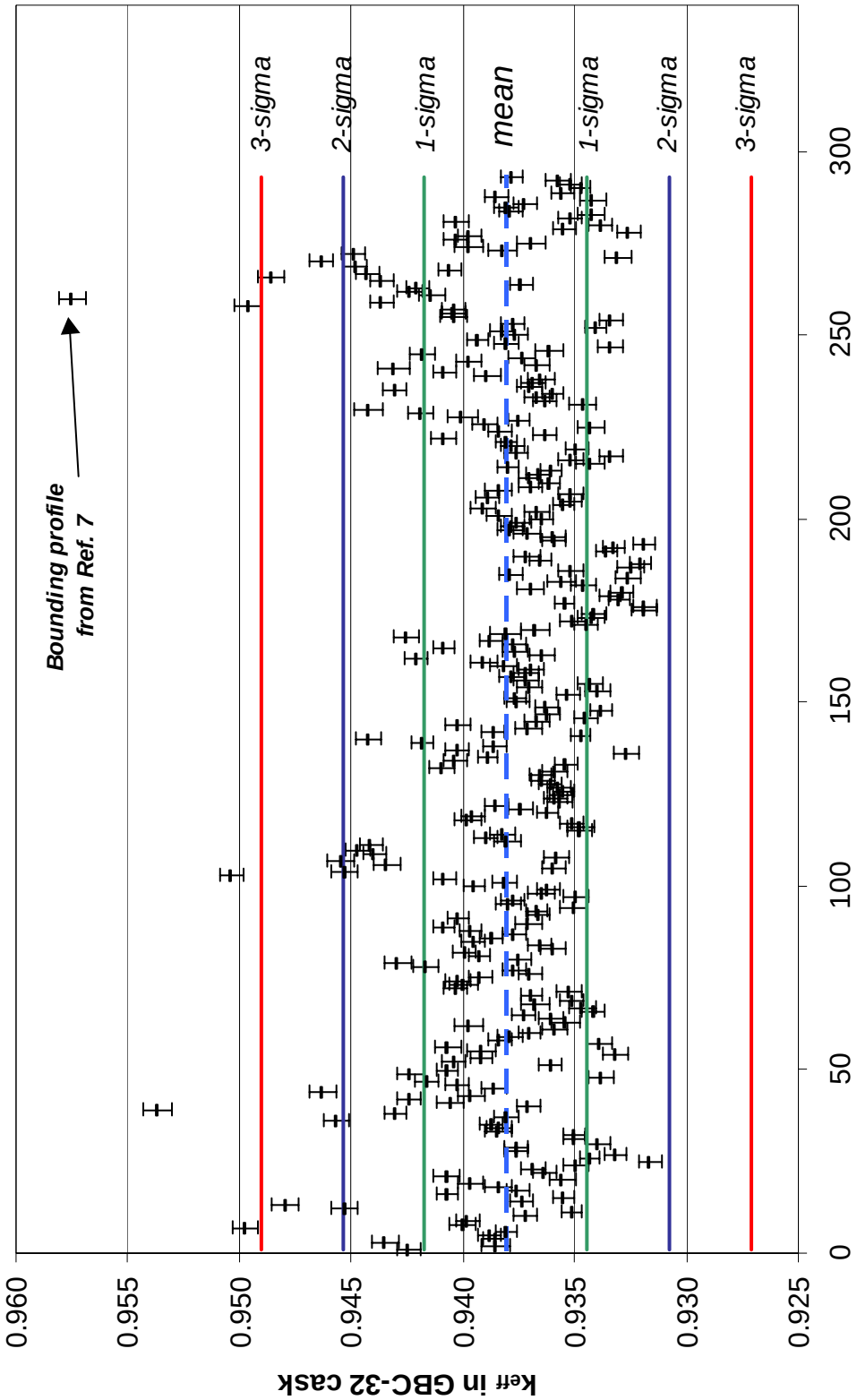

Figure B.7 Plot of k_{eff} values for axial burnup profiles in burnup group 7 (22 < burnup < 26 GWd/MTU). Total number of profiles in this burnup group is 293.

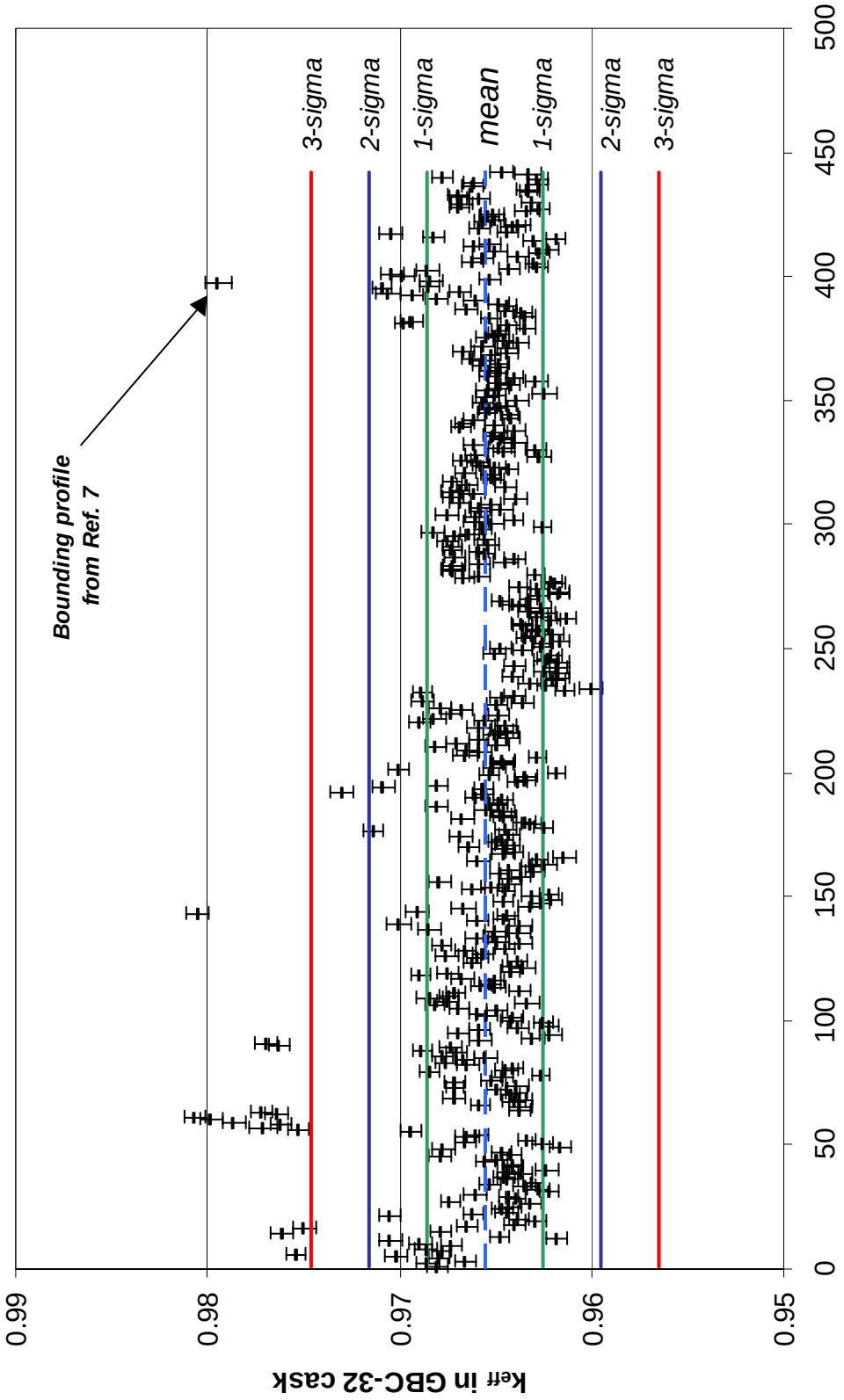

Figure B.8 Plot of k_{eff} values for axial burnup profiles in burnup group 8 (18 < burnup < 22 GWd/MTU). Total number of profiles in this burnup group is 442.

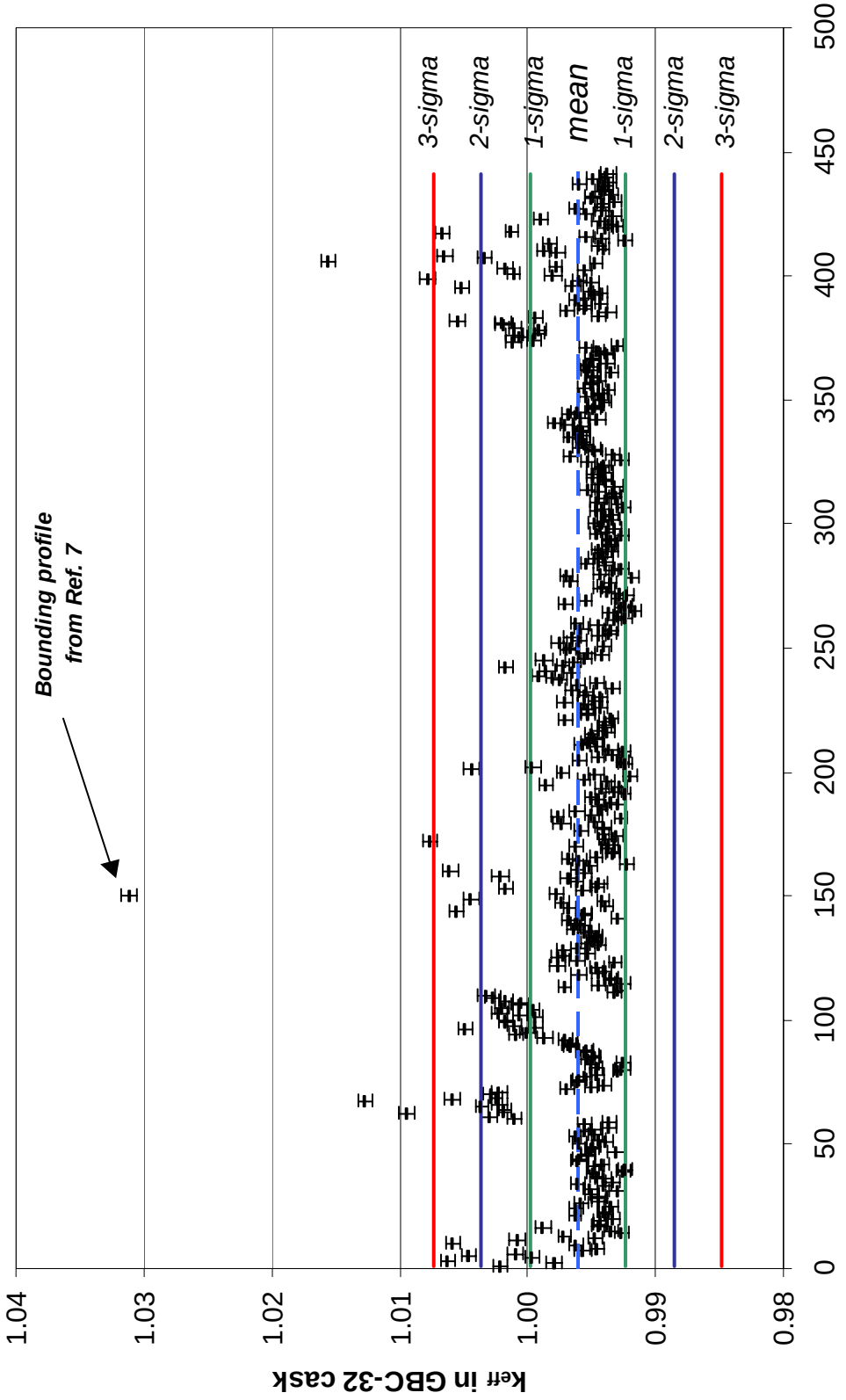

Figure B.9 Plot of k_{eff} values for axial burnup profiles in burnup group 9 (14 < burnup < 18 GWd/MTU). Total number of profiles in this burnup group is 441.

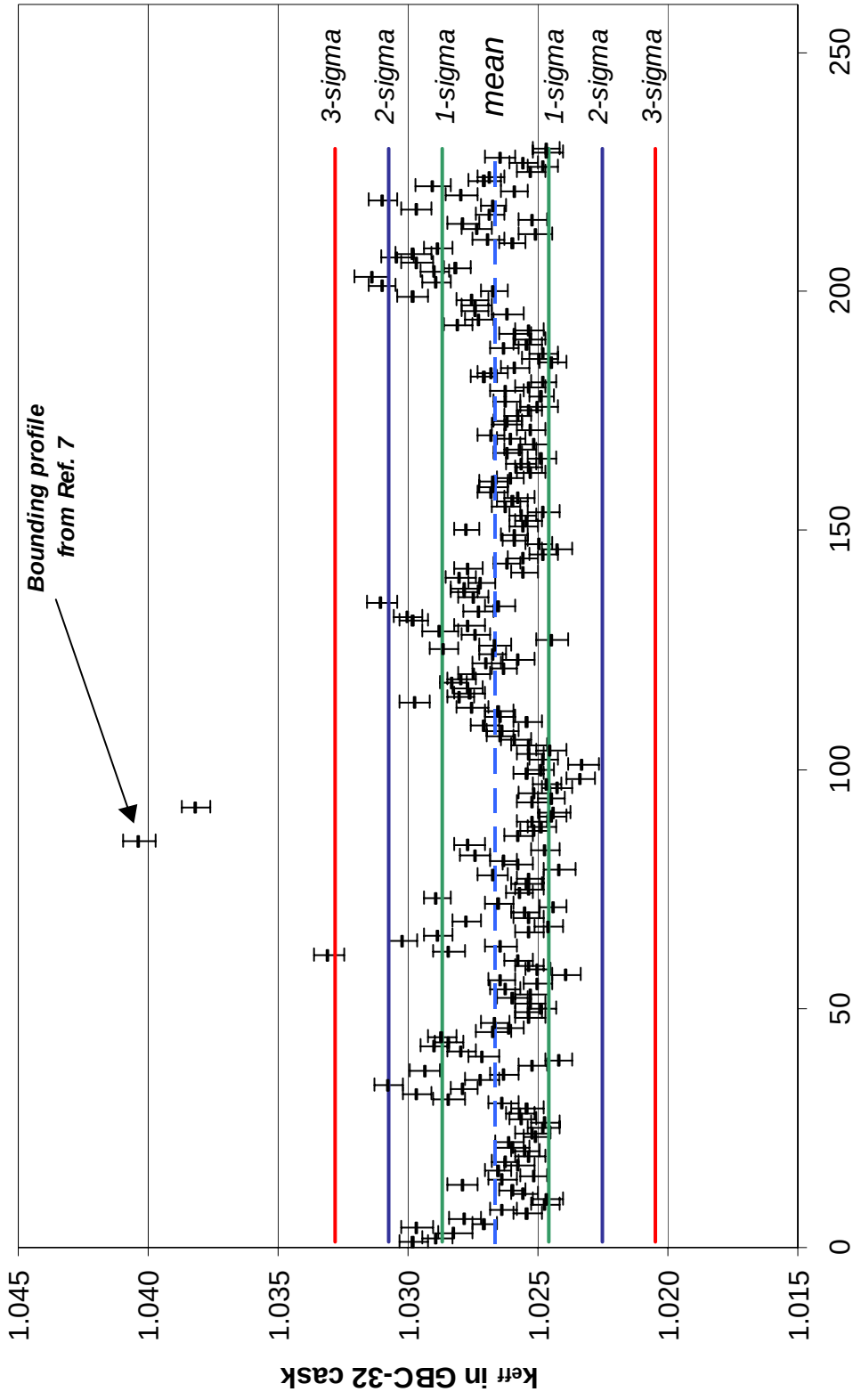

Figure B.10 Plot of k_{eff} values for axial burnup profiles in burnup group 10 (10 < burnup < 14 GWd/MTU). Total number of profiles in this burnup group is 230.

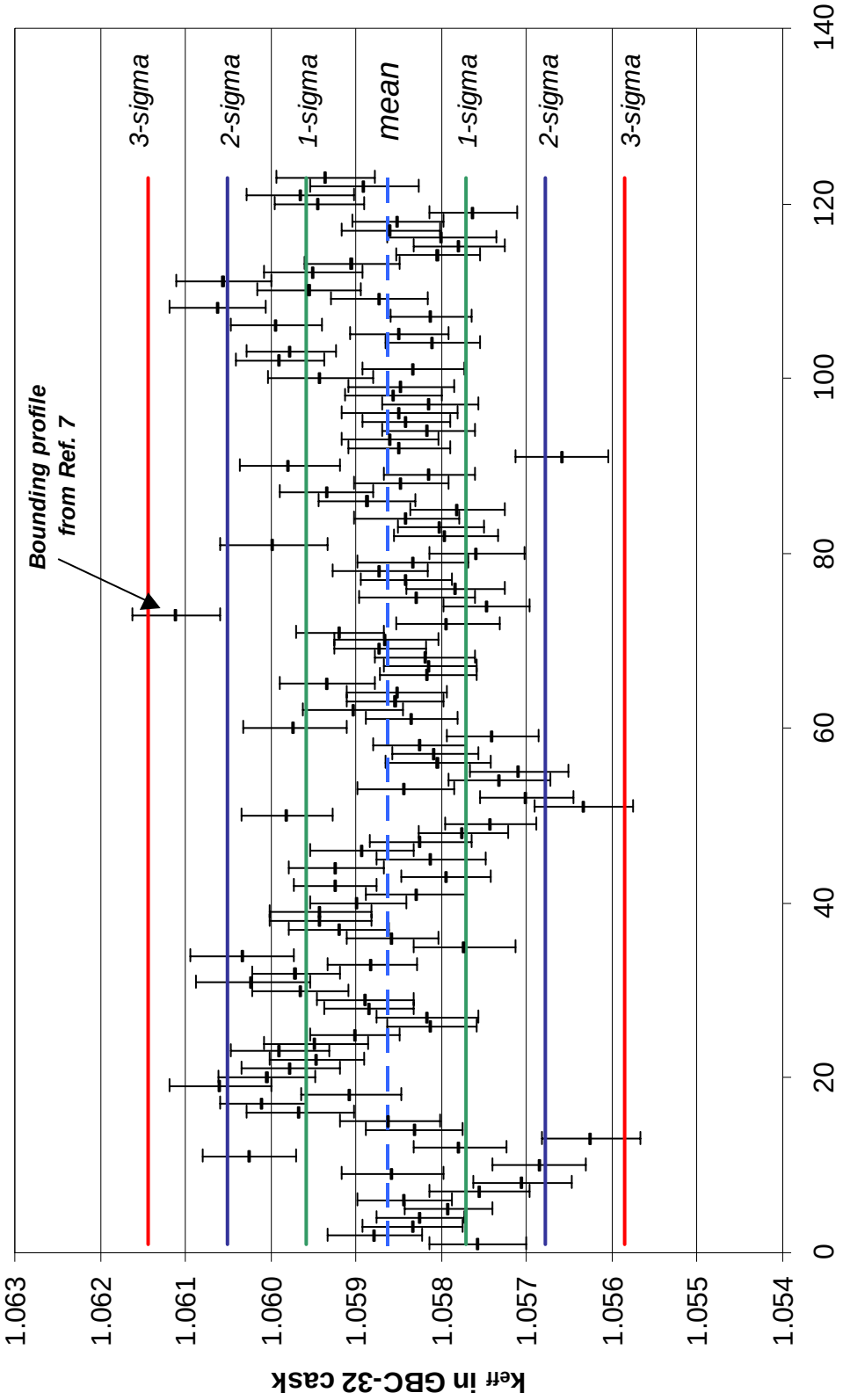

Figure B.11 Plot of k_{eff} values for axial burnup profiles in burnup group 11 (6 < burnup < 10 GWd/MTU). Total number of profiles in this burnup group is 123.

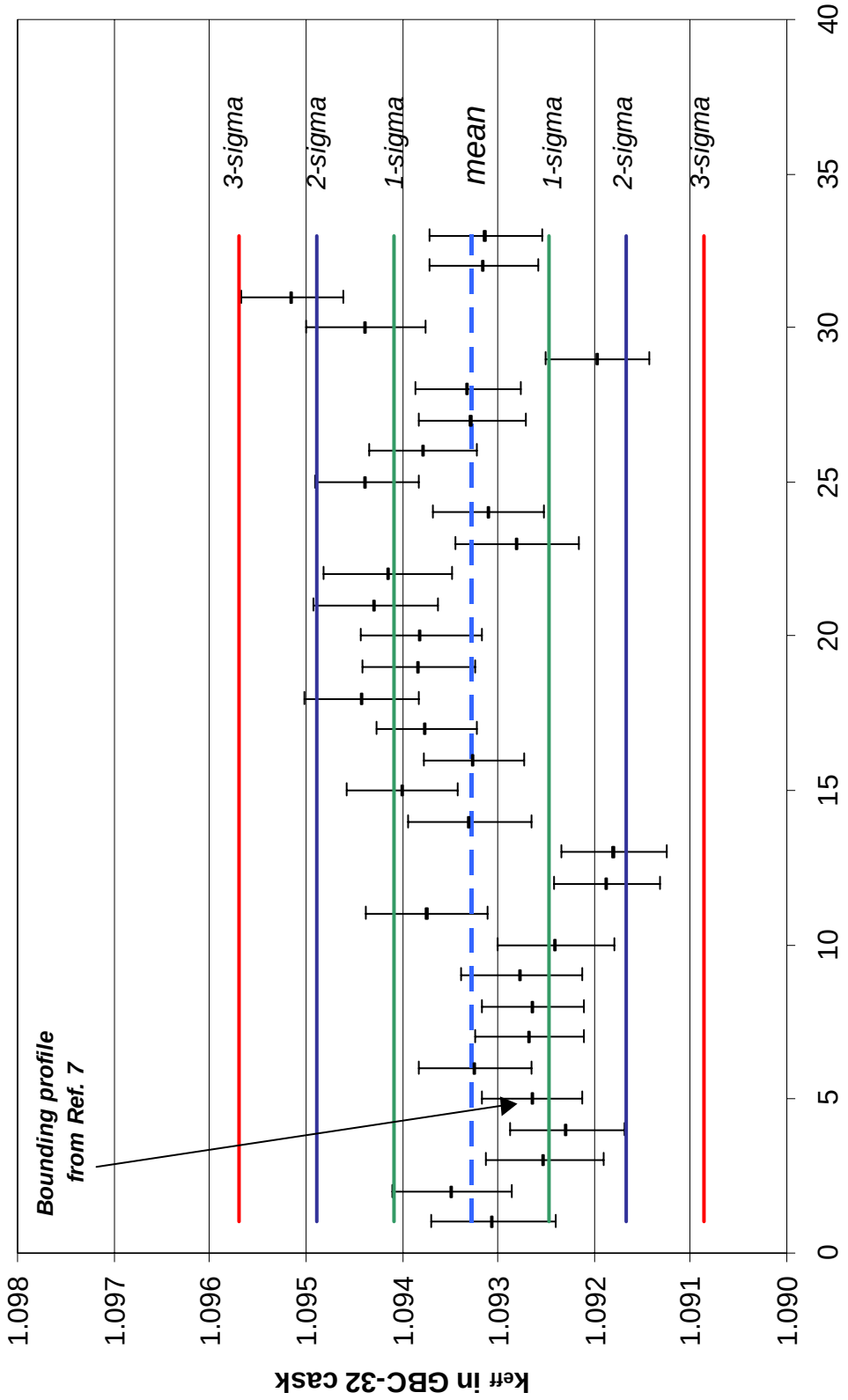

Figure B.12 Plot of k_{eff} values for axial burnup profiles in burnup group 12 (burnup < 6 GWd/MTU). Total number of profiles in this burnup group is 33.

Table B.1 Summary of k_{eff} values (GBC-32 cask) with the axial profile database (Ref. 8)

Burnup group	Analysis burnup (GWd/MTU)	k_{eff} values				Number of standard deviations that the maximum k_{eff} value is above the mean	End effect	
		Mean	Standard deviation	Minimum	Maximum		Maximum	Mean
1	50	0.78028	0.00806	0.76865	0.80577	3.2	0.03846	0.01297
2	44	0.81163	0.00587	0.80085	0.83462	3.9	0.03212	0.00913
3	40	0.83558	0.00449	0.82466	0.85178	3.6	0.02399	0.00779
4	36	0.85936	0.00534	0.84900	0.88781	5.3	0.03433	0.00588
5	32	0.88438	0.00501	0.87531	0.90631	4.4	0.02470	0.00277
6	28	0.91117	0.00480	0.90225	0.93490	4.9	0.02405	0.00032
7	24	0.93806	0.00365	0.93163	0.95748	5.3	0.01740	! 0.00202
8	20	0.96557	0.00302	0.96001	0.98068	5.0	0.01185	! 0.00326
9	16	0.99607	0.00375	0.99159	1.03111	9.3	0.03130	! 0.00374
10	12	1.02662	0.00205	1.02327	1.04036	6.7	0.00893	! 0.00481
11	8	1.05864	0.00093	1.05624	1.06110	2.6	! 0.00227	! 0.00473
12	4	1.09328	0.00081	1.09179	1.09515	2.3	! 0.00091	! 0.00278

NUREG/CR-6801
ORNL/TM-2001/273

INTERNAL DISTRIBUTION

1. S. M. Bowman, 6011, MS-6370
2. B. L. Broadhead, 6011, MS-6370
3. W. C. Carter, 6011, MS-6370
4. M. D. DeHart, 6011, MS-6370
5. M. E. Dunn, 6011, MS-6370
6. K. R. Elam, 6011, MS-6370
7. R. J. Ellis, 6025, MS-6363
8. I. C. Gauld, 6011, MS-6370
9. J. C. Gehin, 6025, MS-6363
10. S. Goluoglu, 6011, MS-6370
11. J. N. Herndon, 4500N, MS-6228
12. D. J. Hill, 4500N, MS-6228
13. D. F. Hollenbach, 6011, MS-6370
14. B. L. Kirk, 6025, MS-6362
15. S. B. Ludwig, NTRC, MS-6472
16. G. E. Michaels, 4500N, MS-6210
17. C. V. Parks, 6011, MS-6370
18. L. M. Petrie, 6011, MS-6370
19. R. T. Primm, III, 7917, MS-6399
20. B. T. Rearden, 6011, MS-6370
21. J. J. Simpson, 4500N, MS-6210
22. J. C. Wagner, 6011, MS-6370
23. R. M. Westfall, 6011, MS-6370
24. Laboratory Records-RC
    4500N, MS-6285
25. Central Research Library
    4500N, MS-6191

26–50. Return extra ORNL copies to:
W. C. Carter, 6011, MS-6370

EXTERNAL DISTRIBUTION

51. M. L. Anderson, Bechtel SAIC Company, LLC, 1261 Town Center Drive, Las Vegas, NV 89134
52. S. Anton, Holtec International, 555 Lincoln Drive West, Marlton, NJ 08053
53. A. C. Attard, U.S. Nuclear Regulatory Commission, NRR/DSSA/SRXB, MS O10-B1, Washington, DC 20555-0001
54. M. G. Bailey, U.S. Nuclear Regulatory Commission, NMSS, MS T8-A23, Washington, DC 20555-0001
55. A. B. Barto, U.S. Nuclear Regulatory Commission, NMSS/SFPO/TRA, MS O13-D13, Washington, DC 20555-0001
56. C. J. Benson, Bettis Atomic Power Laboratory, PO Box 79, West Mifflin, PA 15122
57. G. H. Bidinger, NUMEC, 17016 Cashell Road, Rockville, MD 20853
58. J. Boshoven, Transnuclear West, Inc., 39300 Civic Center Drive, Suite 280, Fremont, CA 94538
59. M. C. Brady Raap, Battelle, Pacific Northwest National Laboratory, PO Box 999 / MS K8-34, Richland, WA 99352
60. R. J. Cacciapouti, Duke Engineering and Services, 400 Donald Lynch Boulevard, Marlborough, MA 01752
61. D. E. Carlson, U.S. Nuclear Regulatory Commission, RES/DSARE/REAHFB, MS T10-F13A, Washington, DC 20555-0001

62. J. M. Conde López, Consejo de Seguridad Nuclear, Jefe de Area de Ingeniería Nuclear, Subdirección General de Technologia Nuclear, Justo Dorado, 11, 28040 Madrid, SPAIN
63. D. R. Conners, Bettis Atomic Power Laboratory, PO Box 79, West Mifflin, PA 15122
64. P. Cousinou, Institut de Protection et de Sûreté Nucleaire, Départment de Recherches en Sécurité, CECI B.P. 6 - 92265 Fontenzy-Aux-Roses, Cedex, FRANCE
65. T. W. Doering, Bechtel SAIC Company, LLC, 1261 Town Center Drive, Las Vegas, NV 89134
66. E. P. Easton, U.S. Nuclear Regulatory Commission, NMSS/SFPO/TRD, MS O13-D13, Washington, DC 20555-0001
67. F. Eltawila, U.S. Nuclear Regulatory Commission, RES/DSARE, MS T10-E32, Washington, DC 20555-0001
68. K. T. Erwin, U.S. Nuclear Regulatory Commission, NMSS/SFPO/TRB, MS O13-D14, Washington, DC 20555-0001
69. A. S. Giantelli, U.S. Nuclear Regulatory Commission, NMSS/SFPO/TRA, MS O13-D13, Washington, DC 20555-0001
70. R. N. B. Gmal, Gesellschaft für Anlagen-und Reaktorsicherheit (GRS) mbH, Leiter der Gruppe Kritikalität, Forschungsgelände, 85748 Garching b. München
71. P. Grimm, Paul Scherrer Institute, CH-5232 Villigen Psi, SWITZERLAND
72. J. N. Gulliford, BNFL, R101, Rutherford House, Risley, Warrington, Cheshire WA3 6AS
73. J. Guttmann, U.S. Nuclear Regulatory Commission, NMSS/SFPO/TRD, MS O13-D13, Washington, DC 20555-0001
74. L. A. Hassler, Framatome ANP, 3315 Old Forest Road, PO Box 10935, Lynchburg, VA 24506-0935
75. D. Henderson, Framatome ANP, 3315 Old Forest Road, PO Box 10935, Lynchburg, VA 24506-0935
76. M. W. Hodges, U.S. Nuclear Regulatory Commission, NMSS/SFPO/TRD, MS O13-D13, Washington, DC 20555-0001
77. Hae Ryong Hwang, Radiation Safety Analysis Group, KOPEC, 150, Duckjin Dong, Taejon, SOUTH KOREA 305-600
78. H. Kühl, Wissenschaftlich-Technische Ingenieurberatung GMBH, Karl-Heinz-Beckurts-Strasse 8, 52428 Jülich
79. W. H. Lake, Office of Civilian Radioactive Waste Management, U.S. Department of Energy, RW-46, Washington, DC 20585
80. D. B. Lancaster, Nuclear Consultants.com, 320 South Corl Street, State College, PA 16801
81. C. Lavarenne, Institut de Protection et de Sûreté Nucléaire, Department of Prevention and Studies of Accidents, Criticality Studies Division, CEA - 60-68, avenue de Général Leclerc, B.P. 6 - 92265, Fontenay - Aux - Roses, Cedex, FRANCE

82–86. R. Y. Lee, U.S. Nuclear Regulatory Commission, RES/DSARE/SMSAB, MS T10-K8, Washington, DC 20555-0001

87. Willington J. Lee, NAC International, 655 Engineering Drive, Norcross, GA 30092
88. M. Mason, Transnuclear, Two Skyline Drive, Hawthorne, NY 10532-2120
89. A. J. Machiels, Electric Power Research Institute, Advanced Nuclear Technology, Energy Convervation Division, 3412 Hillview Ave., Palo Alto, CA 94304-1395
90. L. Markova, Ustav jaderneho vyzkumu Rez, Theoretical Reactor Physics, Nuclear Research Institute, Czech Republic, 25068 REZ
91. Daniel Marloye, Belgonucléaire, Av. Ariane 4, B-1200, Brussels, BELGIUM
92. C. W. Mays, Framatome ANP, 3315 Old Forest Road, PO Box 10935, Lynchburg, VA 24506-0935

93. J. N. McKamy, U.S. Department of Energy, Office of Engineering Assistance and Site Interface, EH-34, 19901 Germantown Rd., Germantown, MD 20874
94. N. B. McLeod, JAI Corporation, 4103 Chain Bridge Road, Suite 200, Fairfax, VA 22030
95. D. Mennerdahl, E. Mennerdahl Systems, Starvägen 12, S-183 57 Täby, SWEDEN
96. Dr. Raymond L. Murray, 8701 Murray Hill Drive, Raleigh, NC 27615
97. K. A. Neimer, Duke Engineering & Services, 400 S. Tyron St., WC26B, PO Box 1004, Charlotte, NC 28201-1004
98. P. Noel, Bechtel SAIC Company, LLC, 1261 Town Center Drive, Las Vegas, NV 89134
99. I. Nojiri, Japan Nuclear Cycle Development Institute, Environment and Safety Division, Tokai Works, Muramatsu Tokai-mura, Naka-gun Ibaraki-ken 319-1194, JAPAN
100. J. C. Neuber, SIEMENS AG, KWU NS-B, Berliner Str. 295-303, D-63067 OFFENBACH AM MAIN, GERMANY
101. A. Nouri, OECD/NEA Data Bank, Le Seine-Saint Germain, 12 Boulevard des Iles, F-92130 Issy-les-Moulineaux, FRANCE
102. Office of the Assistant Manager for Energy Research and Development, Department of Energy Oak Ridge Operations (DOE-ORO), PO Box 2008, Oak Ridge, TN 37831
103. H. Okuno, Japan Atomic Energy Research Institute, Department of Fuel Cycle, Safety Research, 2-4 Shirakata-Shirane, 319-1195 Tokai-mura, Naka-Gun, Ibaraki-ken, JAPAN
104. N. L. Osgood, U.S. Nuclear Regulatory Commission, NMSS/SFPO/SLID, MS O13-D13, Washington, DC 20555-0001
105. V. A. Perin, U.S. Nuclear Regulatory Commission, NMSS/FCSS/SPB, MS T8-A33, Washington, DC 20555-0001
106. B. Petrovic, Westinghouse Electric Company, Science and Technology Department, 1344 Beulah Road, Pittsburgh, PA 15235
107. J. S. Philbin, Sandia National Laboratory, PO Box 5800, Mail Stop 1143, Albuquerque, NM 87185-1143
108. M. Rahimi, U.S. Nuclear Regulatory Commission, NMSS/DWM/HLWB, MS T7-F3, Washington, DC 20555-0001
109. E. L. Redmond II, Holtec International, 555 Lincoln Drive West, Marlton, NJ 08053
110. I. Reiche, Bundesamt fuer Strahlenschutz, Willi Brandt Str. 5, D-38226 SALZGITTER, GERMANY
111. C. Rombough, CTR Technical Services, Inc., 5619 Misty Crest Dr., Arlington, TX 76017-4147
112. J. E. Rosenthal, U.S. Nuclear Regulatory Commission, RES/DSARE/SMSAB, MS T10-K8, Washington, DC 20555-0001
113. C. E. Sanders, Bechtel SAIC Company, 1930 Village Center Cir 3-256, Las Vegas, NV 89134
114. A. Santamarina, Commissariat A L'Energie Atomique, Nuclear Reactor Division, Reactor Studies Department, Reactor and Cycle Physics Service, CEA/CADARACHE/DRN/DER/SPRC Bat. 230, 13108 Saint-Paul-Lez-Durance, Cedex, FRANCE
115. E. Sartori, OECD/NEA Data Bank, Le Seine-Saint Germain, 12 Boulevard des Iles, F-92130 Issy-les-Moulineaux, FRANCE
116. J. J. Sapyta, Framatome Cogema Fuels, 3315 Old Forest Road, PO Box 10935, Lynchburg, VA 24506-0935
117. M. Smith, Virginia Power Co., PO Box 2666, Richmond, VA 23261
118. N. R. Smith, AEA Technology, A32 Winfrith, Dorchester, Dorset DT2 8DH, United Kingdom
119. J. T. Stewart, Department of Environment, Transport, and Re, RMTD, 4/18, GMH, 76 Marsham Street, London SW1P 4DR, United Kingdom

120. T. Suto, Power Reactor and Nuclear Fuel Development Corporation, Technical Service Division, Tokai Reprocessing Plant, Tokai Works, Tokai-Mura, Naka-gun, Ibaraki-ken, JAPAN
121. H. Taniuchi, Kobe Steel, Ltd., 2-3-1 Shinhama, Arai-Cho, Takasago, 676 JAPAN
122. D. A. Thomas, Bechtel SAIC Company, LLC, 1261 Town Center Drive, Las Vegas, NV 89134
123. P. R. Thorne, British Nuclear Fuels plc (BNFL), Nuclear and Radiological Safety, R101 Rutherford House, Risley Warrington WA3 6AS, United Kingdom
124. J. R. Thornton, Duke Engineering & Services, 230 S. Tyron St., PO Box 1004, Charlotte, NC 28201-1004
125. S. E. Turner, Holtec International, 230 Normandy Circle East, Palm Harbor, FL 34683
126. A. P. Ulses, U.S. Nuclear Regulatory Commission, RES, MS T10-K8, Washington, DC 20555-0001
127. M. D. Waters, U.S. Nuclear Regulatory Commission, NMSS/SFPO/SLID, MS O13-D13, Washington, DC 20555-0001
128. A. Wells, 2846 Peachtree Walk, Duluth, GA 30136
129. B. H. White IV, U.S. Nuclear Regulatory Commission, NMSS/SFPO/TRD, MS O13-D13, Washington, DC 20555-0001
130. Robert Wilson, Rocky Flats Field Office, USDOE, 10808 Highway 93, Golden, CO 80403-8200
131. C. J. Withee, U.S. Nuclear Regulatory Commission, NMSS/SFPO/TRD, MS O13-D13, Washington, DC 20555-0001

NRC FORM 335 (2-89) NRCM 1102 3201, 3202

U.S. NUCLEAR REGULATORY COMMISSION

BIBLIOGRAPHIC DATA SHEET

(See instructions on the reverse)

1. REPORT NUMBER (Assigned by NRC, Add Vol., Supp., Rev., and Addendum Numbers, if any.)

NUREG/CR-6801
ORNL/TM-2001/273

2. TITLE AND SUBTITLE

Recommendations for Addressing Axial Burnup in PWR Burnup Credit Analyses

3. DATE REPORT PUBLISHED

MONTH	YEAR
March	2003

4. FIN OR GRANT NUMBER

W6479

5. AUTHOR(S)

J. C. Wagner, M. D. DeHart, and C. V. Parks

6. TYPE OF REPORT

Technical

7. PERIOD COVERED *(Inclusive Dates)*

8. PERFORMING ORGANIZATION — NAME AND ADDRESS *(If NRC, provide Division, Office or Region, U.S. Nuclear Regulatory Commission, and mailing address; if contractor, provide name and mailing address.)*

Oak Ridge National Laboratory, Managed by UT-Battelle, LLC
PO Box 2008, Bldg. 6011, MS-6370
Oak Ridge, TN 37831-6370 USA

9. SPONSORING ORGANIZATION — NAME AND ADDRESS *(If NRC, type "Same as above"; if contractor, provide NRC Division, Office or Region, U.S. Regulatory Commission, and mailing address.)*

Division of Systems Analysis and Regulatory Effectiveness
Office of Nuclear Regulatory Research
U.S. Nuclear Regulatory Commission
Washington, DC 20555-0001

10. SUPPLEMENTARY NOTES

R. Y. Lee, NRC Project Manager

11. ABSTRACT *(200 words or less)*

This report presents studies performed to support the development of a technically justifiable approach for addressing the axial burnup distribution in pressurized-water reactor (PWR) burnup-credit criticality safety analyses. The effect of the axial burnup distribution on reactivity and proposed approaches for addressing the axial burnup distribution are briefly reviewed. A publicly available database of profiles is examined in detail to identify profiles that maximize the neutron multiplication factor, k_{eff}, assess its adequacy for PWR burnup credit analyses, and investigate the existence of trends with fuel type and/or reactor operations. A statistical evaluation of the k_{eff} values associated with the profiles in the axial burnup profile database was performed, and the most reactive (bounding) profiles were identified as statistical outliers that are not representative of typical discharged spent fuel assemblies. The impact of these bounding profiles on k_{eff} is quantified for a high-density burnup credit cask. Analyses are also presented to quantify the potential reactivity consequence of loading assemblies with axial burnup profiles that are not bounded by the database. The report concludes with a discussion on the issues for consideration and recommendations for addressing axial burnup in criticality safety analyses using burnup credit for dry cask storage and transportation.

12. KEY WORDS/DESCRIPTORS *(List words or phrases that will assist researchers in locating the report.)*

burnup credit, criticality safety, spent fuel, storage, transportation

13. AVAILABILITY STATEMENT

unlimited

14. SECURITY CLASSIFICATION

(This Page) unclassified

(This Report) unclassified

15. NUMBER OF PAGES

16. PRICE